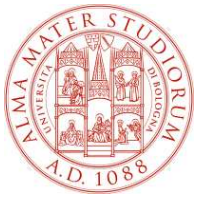

Bologna University

Ph.D. in Geophysics

XXI Cycle

Scientific Sector: GEO/10

STUDY OF THE CIRCULATION PROCESSES IN THE NORTHERN ADRIATIC SEA - COASTAL AREA AND VENICE LAGOON INLETS

Debora Bellafiore

Ph.D. Coordinator:
Prof. Michele Dragoni

Tutor:
Dr. Georg Umgiesser

Final Exam Year 2009

Contents

Abstract **viii**

Introduction **3**

1 Phenomenology of the Northern Adriatic Sea **5**
1.1 Adriatic Sea Morphological Characteristics 5
1.2 Rivers 7
1.3 Meteorological Characteristics 9
1.4 Tides, Surge and Seiches in the Adriatic Sea 10
1.4.1 Tides 10
1.4.2 Storm Surges 11
1.4.3 Seiches 12
1.5 General Circulation 13
1.6 North Adriatic Coastal Circulation 14

2 Numerical Modeling in the Northern Adriatic Sea **17**
2.1 Numerical models description 17
2.1.1 POM 18
2.1.2 ROMS 20
2.1.3 COHERENS 22
2.1.4 NCOM 22
2.1.5 DieCAST 23
2.1.6 SYSTEM3 24
2.1.7 MITgcm 25
2.1.8 SHYFEM 25
2.2 Setup Comparison 26

2.2.1 Numerical Grid 26
2.2.2 2D and 3D Model Implementations 29
2.2.3 Boundary Conditions 29
2.2.4 Initial Conditions 32
2.2.5 Forcings 32

3 SHYFEM Model **35**
3.1 The equations 36
3.2 Boundary and Initial Conditions 37
3.3 Discretization in time and space 38

4 Test Cases - Process Study in ideal basins **41**
4.1 Baroclinic Module 41
4.1.1 Estuarine Outflow Test Cases 41
4.2 Turbulence Module 51
4.2.1 Kato-Phillips Test Case 51
4.2.2 Deardorff Test Case 54

5 Data Treatment and Model Input Preparation **57**
5.1 Wind 57
5.1.1 Historical wind dataset analysis 58
5.1.2 Wind database used as model input 66
5.2 Tides and Currents 67
5.2.1 Tidal data 67
5.2.2 The flow rate ADCP data 68
5.3 HF Radar 69
5.4 Temperature and Salinity 70

6 Modeling Barotropic Processes **71**
6.1 The 2D Simulation Setup 71
6.2 Barotropic Simulation Results 74
6.2.1 Calibration of harmonic constants 75
6.2.2 Water level validation 76
6.2.3 Flux data validation 80
6.2.4 Residual Levels and Fluxes 85

6.2.5 Extreme wind events 88

7 Modeling Baroclinic Processes 93
7.1 The 3D Simulation Setup 93
7.1.1 Idealized Forcing Simulations 93
7.1.2 Sensitivity Simulations 94
7.1.3 Realistic Simulation of the year 2004 94
7.2 Baroclinic Simulation Results 95
7.2.1 Idealized forcing impact 95
7.2.2 Sensitivity Analysis 98
7.2.3 Run of the year 2004 100

8 Summary and Conclusions 109

A The Arakawa Grids 113

B Turbulence Closure Models 117
B.1 Equations 117
B.2 Turbulence parameterization 119
B.2.1 Algebraic approach 119
B.2.2 1 equation models 119
B.2.3 2 equation models 120

Bibliography 124

Abstract

This work is a detailed study of hydrodynamic processes in a defined area, the littoral in front of the Venice Lagoon and its inlets, which are complex morphological areas of interconnection.

A finite element hydrodynamic model of the Venice Lagoon and the Adriatic Sea has been developed in order to study the coastal current patterns and the exchanges at the inlets of the Venice Lagoon. This is the first work in this area that tries to model the interaction dynamics, running together a model for the lagoon and the Adriatic Sea.

First the barotropic processes near the inlets of the Venice Lagoon have been studied. Data from more than ten tide gauges displaced in the Adriatic Sea have been used in the calibration of the simulated water levels. To validate the model results, empirical flux data measured by ADCP probes installed inside the inlets of Lido and Malamocco have been used and the exchanges through the three inlets of the Venice Lagoon have been analyzed. The comparison between modelled and measured fluxes at the inlets outlined the efficiency of the model to reproduce both tide and wind induced water exchanges between the sea and the lagoon.

As a second step, also small scale processes around the inlets that connect the Venice lagoon with the Northern Adriatic Sea have been investigated by means of 3D simulations. Maps of vorticity have been produced, considering the influence of tidal flows and wind stress in the area. A sensitivity analysis has been carried out to define the importance of the advection and of the baroclinic pressure gradients in the development of vortical processes seen along the littoral close to the inlets. Finally a comparison with real data measurements, surface velocity data from HF Radar near the Venice inlets, has been performed, which allows for a better understanding of the processes and their seasonal dynamics.

The results outline the predominance of wind and tidal forcing in the coastal area. Wind forcing acts mainly on the mean coastal current inducing its detachment offshore during Sirocco events and an increase of littoral currents

during Bora events. The Bora action is more homogeneous on the whole coastal area whereas the Sirocco strengthens its impact in the South, near Chioggia inlet. Tidal forcing at the inlets is mainly barotropic. The sensitivity analysis shows how advection is the main physical process responsible for the persistent vortical structures present along the littoral between the Venice Lagoon inlets. The comparison with measurements from HF Radar not only permitted a validation of the model results, but also a description of different patterns in specific periods of the year.

The success of the 2D and the 3D simulations on the reproduction both of the SSE, inside and outside the Venice Lagoon, of the tidal flow, through the lagoon inlets, and of the small scale phenomena, occurring along the littoral, indicates that the finite element approach is the most suitable tool for the investigation of coastal processes. For the first time, as shown by the flux modeling, the physical processes that drive the interaction between the two basins were reproduced.

Introduction

The work presented in this PhD Thesis is a detailed study of hydrodynamic processes in the littoral area in front of the Venice Lagoon and its inlets.

The lagoon of Venice is a complex and unique environment both because of the internal hydrodynamics and the high variety in its morphological characteristics. Because of the presence of channels, shallow flats and multiple connections with the open sea the lagoon is continuously changing. For these aspects the Venice Lagoon and the coastal areas in front of it can be seen as a big laboratory for the study of hydrodynamic processes.

On the other hand, the area deserves its main importance from the presence of the city of Venice inside the lagoon. Many studies are driven by the need to preserve this natural environment. In the last decades, due to the increased frequency of the flooding events and to the deterioration of the water quality, the ongoing research has been focused to control and preserve the hydrological, morphological and bio-geo-chemical characteristics of the lagoon. Its connections with the open sea play a central role and the study of the mass balance through the inlets is fundamental in order to monitor the conservation of the lagoon itself.

The city of Venice is an island situated approximately in the center of the lagoon with other important islands in the southern and in the northern part. The lagoon is connected to the Adriatic Sea through three inlets that guarantee the water exchange with the open sea. The southern and the central inlets (Chioggia and Malamocco, respectively) are about 500 m wide, whereas the northernmost inlet (Lido) is nearly 1000 m wide. The average depth is around 8 m for Chioggia and 14 m for Malamocco and Lido.

The inlets have undergone major changes in the second part of the 19th and the first part of the 20th century. Due to silting up of the entrances only small boats could pass in this period. Therefore jetties have been constructed that reach 2-3 km into the Adriatic Sea and that gave the inlets the shape and morphology that can nowadays be observed.

To my knowledge, in the past no major studies have been carried out that

try to measure or describe the exchange and its mechanisms through the inlets. This might be surprising, considering the importance of the inlets for the maintenance of the lagoon. Only recently a major effort in this direction has been undertaken, investigating the exchange mechanism between the lagoon and the Adriatic Sea, both by measurements of fluxes and biochemical parameters at the inlets (Bianchi et al., 2004). Bottom mounted Acoustic Doppler Current Profilers (ADCPs) have been installed at the three inlets and data have been analyzed (Gačić et al., 2002). With the data of these field campaigns a hydrodynamic model could be validated. The modeling effort is presented in this work.

In the recent past, few modeling studies have been carried out to investigate the Sea-Lagoon water exchange mechanisms. In particular in Umgiesser (2000) a first attempt to understand the residual currents due to the most prominent wind regimes present in the Northern Adriatic can be found. A finite element model (Umgiesser and Bergamasco, 1993, 1995) to simulate the residual currents of a complete year (1987) is used there. The other study (Bergamasco et al., 1998) applied the Princeton Ocean Model (POM) (Blumberg and Mellor, 1987; Mellor, 1991) to the lagoon and the coastal area of the Adriatic Sea to simulate both hydrodynamics and primary production.

Both approaches suffered from main deficiencies. Both models could not be validated with data because flux measurements were not available at the inlets. Moreover, the second study applied the POM model with a 1200 m grid size, too coarse to resolve the important hydrodynamic features of the Venice Lagoon. On the other hand, the first study used a calibrated model for the water levels inside the lagoon with good resolution of the channel system (due to its finite element method), but failed to describe well the interface dynamics, since the model domain ended exactly at the inlets.

The study of the internal dynamics of the interaction channels connecting the lagoon to the open sea is not the only objective of this work. The investigation is also concerned with the Venetian littoral, identifying the main processes that can be found and their interaction with the inlets. To widen the study area to the North-East Italian coast needs to consider additional forcings and to put the local dynamics in relation with the general Adriatic Sea currents. Even if the tidal effects over the inlets can be considered barotropic (Gačić et al., 2002), the presence of many freshwater sources along the coast and the changing bathymetry lead to investigate both the horizontal and the vertical scales. If baroclinic processes are studied, as here, river discharge must be considered because the temperature and salinity gradient created by the river discharge starts to become an important forcing in the general termohaline circulation. The idea is to characterize the coastal hy-

drodynamics, considering even the forcings that act baroclinically. A 3D model formulation has been identified as the suitable tool to perform this study. The small scale horizontal structures that can form and persist along the venetian littoral will be studied in their dynamics.

As a first step, a description of the phenomenology of the Adriatic Sea, with a dedicated section for the nothern coastal area, is provided in the first chapter. This is meant to explain and contextualize the processes that will be studied in this work. The second chapter will deal with the choice of numerical modeling as the suitable tool to inquire the hydrodynamics and a state of the art of model applications in the whole Adriatic basin is drawn. SHYFEM (Shallow water HYdrodynamical Finite Element Model) will be described in chapter 3, providing the numerical characteristics and the advantages that lead to the choice of this tool as the most suitable in the coastal and interaction hydrodynamic processes. Before the implementation in the study area, two modules, the baroclinic and the turbulence closure, will be checked on a idealized basin performing some test cases (Chao and Boicourt, 1986; Luyten et al., 1996; Burchard, 2002) to certify them. They are described in chapter 4. The last three chapters deal with the model preparation and implementation: chapter 5 describes the forcings chosen for the model setup; chapter 6 is devoted to treat the 2D model implementation to simulate the barotropic lagoon-open sea interaction processes, while chapter 7 presents the 3D model runs to identify the vortical small scale structures that occur along the venetian littoral. Conclusions are drawn at the end.

Chapter 1

Phenomenology of the Northern Adriatic Sea

The Northern Adriatic is a very interesting environment for hydrodynamic studies and a number of physical processes, widely ranging both the spatial and the temporal scale, can be seen. To get to the heart the objectives of this work, a more general overview on the whole Adriatic Sea phenomenology is needed: the studied local scale is influenced in different ways by the more general topographical, meteorological and hydrodynamic characteristics of the basin. All the following evidences are the results of campaigns and measurements, also compared with modeling investigations, done in the last twenty years to define the state of the art of knowledge in the Adriatic Sea.

1.1 Adriatic Sea Morphological Characteristics

The Adriatic Sea is a semi enclosed basin, connected with the Mediterranean Sea by the Otranto Strait (Fig. 1.1). It extends latitudinally from 40 to 46 degrees North. It can be divided, topographically, into three main areas: the northern part is characterized by a shelf shallower than 40 m; the Jabuka Pit, 280 m deep is present in the central part of the basin, beeing detached from the deepest part of the Adriatic Sea by the Palagruza Sill. The Southern area reaches a depth of 1200 m in the so called South Adriatic Pit (Orlić et al., 1992). The section drawn along the Otranto Strait, defined as the Adriatic

Sea border, has an average depth of 325 m but it reaches 780 m in its central part (Fig. 1.1).

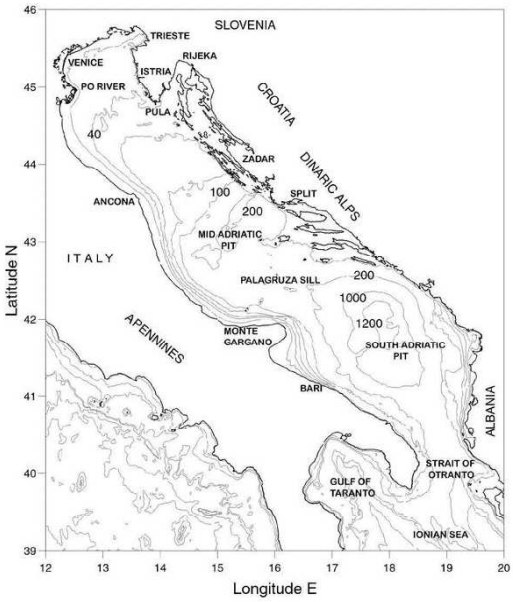

Figure 1.1: Adriatic Sea Map - Bathymetry, ridges and important morphological areas are shown. Harvard University Image.

Two different typologies of coasts characterize the eastern and western sides of the Adriatic Sea: several topographical structures, like small islands, bays, estuaries and segmented rocky coastlines, forms the ex Yugoslavia littoral. In this area, the bathymetry reaches big depths, with an almost complete absence of the shelf. On the other hand, the western italian side is sandy and the depth increases smoothly, particularly in the northern part of the Adriatic (Fig. 1.1).

The morphological configuration continues to change there and focused monitoring has been done, particularly in the Adriatic Northwestern coast, to study thoroughly its evolution: the creation and development of the so called venetian littoral has been historically reconstructed by Gatto (1984). Centuries ago the configuration of the venetian drain basin was really different from now; many rivers, that nowadays flow directly into the Adriatic Sea (Adige, Brenta, Piave), gave their contribution to the water balance of the Venice Lagoon, flowing into it. During the centuries the trajectory of these rivers were anthropogenically changed to the present situation. The main rivers, that are present in the North West coast of the Adriatic Sea, influence

and modify its coastal morphology, bringing high quantities of sediments to the open sea (Gatto, 1984). The Po river, which is the most important source of both sediments and freshwater in the North Adriatic Sea, deserves some more information. It contributes to the coastline variation, particularly in the Sacca di Goro, with the main action of the southern of its branches. Because of the seasonal variations of its discharge, discussed in the next section, it can bring sediments not only along the coast but also straight in the open sea in front of its estuary.

1.2 Rivers

Along the whole Adriatic Sea coastline a number of rivers are present, with different estuarine structure and dimensions.

Because of the interest in the hydrodynamics along the venetian coasts, as a primary step, a description of rivers in the North-West littoral of the basin is given. The local impact of freshwater inflow into the basin starts to become meaningful when the baroclinic processes are studied. The temperature and salinity gradient, created by the river discharge, contributes to the general thermohaline circulation. The main rivers of this area are, following the littoral from North, Isonzo, Tagliamento, Piave, Livenza and Sile; just South of the Venice Lagoon other two rivers, the Brenta and the Adige, flow into the sea (Fig. 1.2).

Even if these are all medium size rivers (average discharge ranging from 40 to 100 m^3s^{-1}), their contribution to the coastal current cannot be neglected. The combined effect of these rivers and of the Po river induces a cyclonic circulation in the northwestern shelves (Kourafalou, 2001).

If the whole basin is considered, a complete overview on the main rivers discharges, both on the western and on the eastern coast, is given by Raicich (1994).

Raicich (1994) provides a sum of both the estimates of the freshwater discharge into the sea and of the hydrometric station measurements, on a seasonal timescale. Even if Raicich (1994) does not give precise error bars, it is useful to define the general trend: as an annual average the eastern rivers contribute for the 45% of the total inflow, while, on the western coast, the Po river alone covers the 28% of the discharge. 19% comes from the several rivers along the North-western littoral, our area of interest and the remaining 8% flows from the western littoral, South of the Po river (Raicich, 1994). These values are variable during the year, with an increase of the western

contribution during winter (January and February) and of the Po river in the early autumn (September 39%) (Raicich, 1994). Also in springtime Po can reach peaks over 4000 m^3s^{-1} (Kourafalou, 1999).

The Po river water outflows during wintertime beeing confined in a coastal strip of stratified freshwater, 10-20 km large (Kourafalou, 2001). As a consequence, the area near the estuary is stratified during winter (Malanotte Rizzoli and Bergamasco, 1983). During summer, the Po river water becomes warmer than the basin water and it produces a surface jet into the open sea. Two plumes develop, one to the Istrian coast and the other to the South. The latter sometimes creates an anticyclonic surface gyre (Malanotte Rizzoli and Bergamasco, 1983; Zavatarelli et al., 2002).

Models applications give some more detail on the principal driving forces connected with the Po plume development: Kourafalou (2001) notes that the N-E winds confine the bulk of low salinity in the coastal band, reducing stratification, while S-E winds increases it, spreading freshwater offshore.

Figure 1.2: North Adriatic rivers location - the image is taken from Raicich (1994).

1.3 Meteorological Characteristics

The geographical position of the Adriatic Sea, in the Southern border of the Middle Europe, and the fact that it is mainly surrounded by mountains in the North-East border, influence the behaviour of wind and atmospheric pressure fields. The combined effect of the large scale atmospheric processes and the local effects can be detected on each part of the basin.

Globally there is a seasonally changing influence of the Westerlies Belt and of the Sub Tropical High Pressure Core: although the effects of the former are seen throughout all the year, forming cyclonic and anticyclonic disturbances, these structures tend to be strongly weakened by the action of the Sub Tropical High during the summer season. Also the coupled action of the Iceland pressure low and the Eurasian pressure high, in winter, and the Azores high and the Karachi low, in summer, affect the dynamics of the area (Orlić et al., 1992).

The presence of planetary wave effects and long-term meteorological preconditioning contribute in the extreme events formation: even if synoptic and smaller scale disturbances, combined with tides, are responsible for a high percentage of water level peaks in the Northern Adriatic, it has been demonstrated that the simple action of planetary waves, that causes the lower-frequency disturbances of the air pressure field, is responsible of one third of the sea level variability. This can be quantified in a sea level variation of 70 cm, that occurs in flood events (Pasarić and Orlić, 2001).

Two main winds act on the meso and local scale: the Bora, proper of wintertime, is a mainly dry wind that blows from North-East and it is created and directed by the big mountain chains of Caucasian Area. It deeply influences the North Adriatic dynamics (Orlić et al., 1992). The second wind is Sirocco, a wet warm wind coming from South-East. It blows over the whole Adriatic Sea, bringing humidity, taken from the sea, to the northern part. In summer, also the land-sea breeze along the coasts becomes important in the local dynamics (Orlić et al., 1992).

The last aspect necessary to characterize the meteorological behaviour of the Adriatic Sea concerns with the solar radiation. Globally, the sea receives 400-500 $\mathrm{Jcm^{-2}day^{-1}}$ in winter and 2200-2600 $\mathrm{Jcm^{-2}day^{-1}}$ in summer (Orlić et al., 1992). The temperature is generally warmer in winter in the North-West area, because of the shallower characteristics of the bathymetry.

1.4 Tides, Surge and Seiches in the Adriatic Sea

Tides, seiches and surges are important processes in the Adriatic Sea because the particular shape of the basin and the shallow bottom of its northern end enhances their effects. Before studying thoroughly the specific condition of our study area, a small overview on these three processes has to be made.

1.4.1 Tides

The Mediterranean Sea is a microtidal environment, usually with tides less than 50 cm. Their action starts to become more important into the semi enclosed basin of the Adriatic Sea, where 1 m of water displacement can be recorded in the northern part (Tomasin and Pirazzoli, 1999). The behaviour of tidal currents in the Adriatic Sea has been investigated during the last century: Polli (1960) stated that there are seven major harmonic components that describe the majority of the tidal signal. Three of them are diurnal (K1, O1, P1) and four are semidiurnal (M2, S2, N2, K2). More info in Tab.1.1 The components M2, S2 and K1 are the more energetic in the Northern

Harmonic Components	Origin	Period [h]
M2	lunar principal semidiurnal	12.42
S2	solar principal semidiurnal	12.00
N2	lunar elliptic semidiurnal	12.66
K2	lunar-solar declinational semidiurnal	11.97
K1	lunar-solar declinational diurnal	23.93
O1	lunar declinational diurnal	25.82
P1	solar declinational diurnal	24.07

Table 1.1: Name, origin and period of the seven major harmonic components in the Adriatic Sea.

Adriatic. These three sinusoidal signals develop differently in the basin. K1 shows cotidal lines (lines where the tidal wave has the same amplitude), perpendicular to the main basin axis. The K1 develops latitudinally, while M2 and S2 have circular cotidal lines around the amphidromic point in front

of Ancona (Fig. 1.3). The M2 and S2 amplitude increases approaching the coast.

The combined action of the three main harmonic components produces waves that develop along the coast as Kelvin waves (Malačić et al., 2000).

The first model application of this work has precisely the aim of reconstructing the tidal currents of the Adriatic Sea, in particular in the study area in front of the Venice Lagoon.

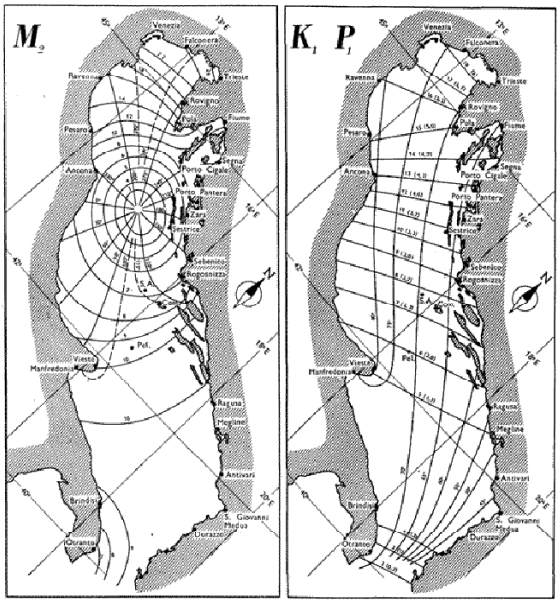

Figure 1.3: Harmonic constants maps. The two main semidiurnal (M2, S2) and the diurnal (K1) components of the Adriatic Sea are shown.

1.4.2 Storm Surges

Following the definition given by Franco et al. (1982), in this work the term "storm surges" is used to define the sum of forced oscillations and water disturbances mainly driven by wind events. Surges are typical phenomena connected with the Adriatic Sea, no external surges or earthquakes effects, like tsunamis, have been recorded in the last century (Tomasin and Pirazzoli, 1999). Surges are strongly connected with the shape of the basin and this aspect enhances the effect of South-Easterlies winds like Sirocco.

The combined action of surges and astronomical tides contributes to the high

water displacement that causes floodings along the northern coast and in the venetian area.

The storm surges tends to break the equilibrium status of the basin and they are strictly connected with the meteorological events. On the basis of the Franco et al. (1982) definition, even long term oscillations (more than 10 days), that are detected in the Adriatic and that are due to the planetary atmospheric oscillation over the sea, can be considered "surges".

1.4.3 Seiches

The seiches, on the other hand, are free stationary oscillations, progressively dumped by the external radiative energy and the internal friction (Tomasin and Pirazzoli, 1999).

The seiches act bringing back the basin to ordinary conditions of equilibrium: they form as a reaction to unstable conditions like a horizontal difference in water level heights, due to the wind. In this case periodic oscillations occur and the period is determined by the topography, the horizontal dimensions, the basin depth and the number of nodes of the stationary wave (Tomasin and Pirazzoli, 1999). On the other hand, the amplitude is connected with the speed and the direction of the wind.

Seiches are stronger in wintertime and in the Northern Adriatic and lower in summertime and in the Southern Adriatic (Franco et al., 1982).

The two major seiches in the Adriatic sea have periods of 21.2 and 10.8 hours and they are generally connected with the presence of Sirocco wind or of frontal systems (Franco et al., 1982). The first seiche is the principal one in the basin and can be considered a uninodal oscillation with the main node at the meridional extreme of the sea and the antinode at the opposite end to the North (Tomasin and Pirazzoli, 1999). The second seiche is binodal, it cuts the basin into two areas with opposite phases and it propagates counterclockwise in the basin, as a semi diurnal tide (Tomasin and Pirazzoli, 1999). In the central and northern part of the basin there are two more seiches of period 8.2 and 6 hours. Seiches produce an average level displacement of 20-30 cm but can reach 60-80 cm and they have a quite long decaying time, around 10-15 days (Franco et al., 1982).

1.5 General Circulation

The study of coastal hydrodynamics cannot neglect the importance of large-small scale processes interaction, so an overview of the general circulation can help in understanding the phenomena present in the area of interest of this work.

A stable surface cyclonic circulation is seen, with a northward flow along the eastern coast and a southward, summer strengthened, flow along the western littoral. The average velocity is of 10 cms^{-1} but interaction with coastal structure can enhance it in some periods (Orlić et al., 1992).

The net transport into the basin is of 0.1 Sv and the thermohaline forcing is seasonally driving part of the circulation: dividing seasonally the analysis of the Adriatic Sea circulation, a general vertically mixed pattern, in terms of temperature, salinity and density, is seen during autumn and winter, North to the Palagruza Sill (Fig. 1.1). The vertical homogeneity is driven mainly by the surface heat in the Northern shallower areas (Malanotte Rizzoli and Bergamasco, 1983; Orlić et al., 1992). The water column is homogeneous during winter and stratified in summer, causing the thermo-halo-pycno seasonal cycles (Franco et al., 1982). In wintertime the surface circulation shows a cyclonic circulation both in the southern and central areas of the basin with a strengthen Western Adriatic Coastal Current (WACC). The North Adriatic cyclonic gyre is wind driven during winter as well as the WACC, which flows southward because of the coastal generated Kelvin waves propagation (Zavatarelli et al., 2002). During summer the baroclinic action is predominant, producing meanders in the WACC and influencing the North Adriatic gyre (Zavatarelli et al., 2002; Artegiani et al., 1997b).

In the Northern end, near the Gulf of Trieste there is the area of deep water formation during the wintertime, caused by the cold dry winds blowing from North East (Bora wind). This water flows along the bottom, in a tongue that follows the western littoral, to the South. The combined action of the dense water and of the freshwater coming from the Po river, drives the formation of the Winter North Adriatic gyre (Malanotte Rizzoli and Bergamasco, 1983; Artegiani et al., 1997b).

Dealing with the dense water formation, and the Adriatic Sea is one of the major sources of it in the Mediterranean Sea, three kind of water masses can be defined: the North Adriatic Water (NAW), the Middle Adriatic Water (MAW) and the Southern Adriatic Water (SAW) (Orlić et al., 1992). The winter formation of NAW fills the Jabuka Pit and only a portion of it gets through the Palagruza Sill, reaching the southern areas. In the Jabuka Pitt the MAW forms mixing with the NAW. This water is warmer and saltier and

tends to stay longer in its origin area (Orlić et al., 1992). In the gyre present in the South Adriatic Pit the SAW can be detected after the winter cooling and it interacts with the western coast NAW vein, along the isobaths, being enriched of oxygen (Orlić et al., 1992).

Moreover, in the same area also the Modified Intermediate Levantine Water (MILW) is present. It is produced in the levantine basin and it is warmer and saltier than the SAW. It enters through the eastern part of the Otranto Strait and it mixes with the denser water found there. The interaction between these different water masses changes not only seasonally but even interannually (Orlić et al., 1992; Oddo et al., 2005).

1.6 North Adriatic Coastal Circulation

The complex hydrodynamic system described embeds a small scale series of phenomena along the coastline and here the focus is on what happens in the North Western area, in the proximity of the Venice Lagoon.

Once more the influence of the Po river has to be considered because, in a way, its action influences the North entrapped circulation (Oddo et al., 2005). From modeling studies (Umgiesser and Bergamasco, 1998), the Po river estuarine dynamics has been described: the freshwater outflow can have a deflection to the North and then to South, in clockwise direction, following the rules of potential vorticity conservation. This phenomenon can interact with the littoral circulation South of the Venice Lagoon and there can be interactions with the other two rivers present in the area, the Brenta and the Adige. The big introduction of freshwater injected by the Po river does not influence directly the venetian littoral hydrodynamics but can enhance the open sea North Adriatic gyre (Kourafalou, 2001). In summer a quite significant northward coastal flow can be seen (Orlić et al., 1992).

Near the Venice Lagoon, the main large scale pattern is the geostrophic southern current, which interacts with the action of the three inlets of lagoon (Fig. 1.4). In fact, the amount of water coming from the lagoon-open sea exchange is bigger than that coming from the Po river: at the Malamocco inlet (Fig. 1.4) a flow rate of 10000 m^3s^{-1} is measured and, summing the contribution of the three inlets, the total flow rate can reach 24000 m^3s^{-1}, while the Po river shows an average discharge rate of 1500 m^3s^{-1} (Gačić et al., 2002). Additionally the combined action of tides and meteorological forcings produces interesting patterns which deviates the mean coastal current, creating meanders (Kovačević et al., 2004).

Figure 1.4: Satellite image of the Venice Lagoon and the coastal area in front of it. The three inlets of the lagoon, Lido, Malamocco and Chioggia, are shown.

There is a crest in these meanders in the proximity of the Malamocco inlet (Paduan et al., 2003). The mean current tends to approach the littoral North to the inlet and then deviates offshore because of the shallow bathymetry (Gatto, 1984). The inlets tidal cycles are typically of barotropic nature while, from HF Radar measurements, there is some indication that the surface current tends to be affected weakly by tides (20% of the total variability) 4-5 km offshore (Kovačević et al., 2004). Then, in the coastal areas between the inlets, some vortical structures have been seen, once more, from the HF Radar measurements. All these processes are the object of this PhD thesis and we will go deep in their description with the application of the modeling tool in the next chapters.

Chapter 2

Numerical Modeling in the Northern Adriatic Sea

2.1 Numerical models description

In oceanography the investigation of hydrodynamic processes is carried out by means of field campaigns, in situ measurements, moorings and satellite images as well as numerical modeling. In recent times modeling gained a major role in the study of the circulation in the Adriatic Sea, with several different implementations and approaches.

The Adriatic Sea has hydrodynamic, morphological and meteorological characteristics that render it a good lab for modeling studies both in terms of process studies and numerical tests.

In this chapter the different models recently applied in the Adriatic Sea or in some of its areas are presented. The aim is to stress the principal numerical characteristics, trying to explain some choices in the implementation and putting them in connection with the temporal and spatial scales of the simulated phenomena.

The modeling areas are presented in Fig. 2.1. In Tab. 2.1 the model characteristics are listed and they will be analyzed in the following paragraphs to draw a state of the art of numerical modeling in the Adriatic Sea.

To better understand the numerical characteristics of each model, more theoretical information is needed, therefore Appendix A is devoted to explain the different Arakawa Grids, usually applied in the ocean and atmospheric mo-

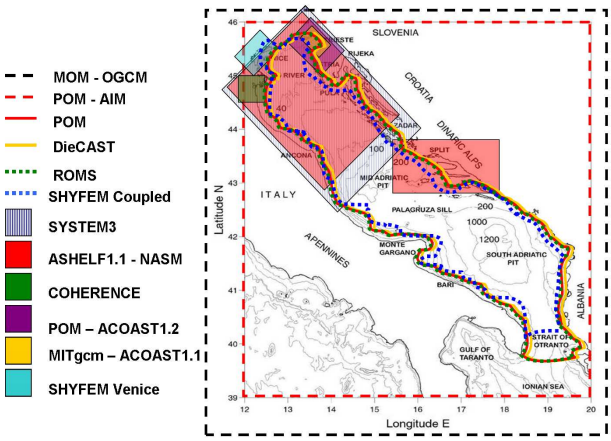

Figure 2.1: Areas of application for the considered numerical models

dels, and the basis of the turbulence closure schemes is treated in Appendix B.

2.1.1 POM

The Princeton Ocean Model (POM) (Blumberg and Mellor, 1987) is the basis for a number of models developed and applied in the Adriatic Sea. The differences in the numerics and the choices done in the discretization mainly identify two models, the one described in Bergamasco et al. (1999), and the one implemented by Zavatarelli and Pinardi (2003), Oddo et al. (2005) and Oddo and Pinardi (2008). The details of the model applied by Zavatarelli and Pinardi (2003) are described in Sannino et al. (2002).

POM is a 3D, finite difference, free surface model. It applies the hydrostatic and the Boussinesq approximations. Vertically, a σ coordinates system is imposed, following the morphological structure of bathymetry:

$$\sigma = \frac{(z - \eta)}{H + \eta} \tag{2.1}$$

with z absolute layer depth, η water level surface displacement, H total water depth. A higher density of levels can be imposed near the surface and the bottom, as done for the investigations in the Adriatic Sea (Zavatarelli et al., 2002; Bergamasco et al., 1999).

It uses a split mode time step, dividing it in external and internal modes.

MODEL	SCHEMES	GRID	LEVELS			TURBULENCE CLOSURE SCHEME
POM	finite differences	regular curvilinear orthogonal	σ level	hydrostatic	free surface	Mellor-Yamada
ROMS	finite differences	curvilinear orthogonal	coordinates stretched terrain following	hydrostatic	free surface	Mellor-Yamada K-profile
COHERENS	finite differences	regular	σ level	hydrostatic	free surface	algebraic expressions 1-2 equation turbulence energy models
NCOM	finite differences	regular	hybrid σ/z level	hydrostatic	free surface	Mellor-Yamada
DieCAST	finite differences	regular	z-level	hydrostatic	rigid lid	—
SYSTEM3	finite differences	regular	σ level	non-hydrostatic	free surface	—
MITgcm	finite volumes	regular	finite volumes	non-hydrostatic	free surface	kpp
SHYFEM	finite elements	unstructured	z-level	hydrostatic	free surface	K-ϵ

Table 2.1: Principal characteristics of the models applied in the Adriatic Sea.

The POM model solves the conservation of momentum equations, the continuity equation and the tracer equations (T and S) using finite differences schemes. No horizontal diffusion is applied to the temperature and salinity fields (Zavatarelli and Pinardi, 2003). The equation of state for the density is an adaptation of the UNESCO equation.

The model parameterizes the momentum mixing, the temperature and salinity small scale mixing with a horizontal diffusion that depends on the horizontal velocity shear and on the grid step by the Smagorinsky algorithm (Sannino et al., 2002). The turbulence closure is parameterized by the Mellor-Yamada 2.5 order turbulence closure model (Mellor and Yamada, 1982) (see Appendix B). The turbulent kinetic energy, the turbulent length scale and the vertical velocity shear permit to compute the vertical mixing coefficients (Bergamasco et al., 1999).

The models implemented by Zavatarelli and Pinardi (2003) (AIM-Adriatic Intermediate Model and NASM - North Adriatic Sea Model) and by Oddo et al. (2005) in the Adriatic Sea introduce different numerical schemes compared with the original POM applied by Bergamasco et al. (1999): the Smolarkiewicz (1984) scheme and the Clark's flux corrected upstream scheme (Smolarkiewicz and Clark, 1986) are used to compute the advection of tracers, instead of a centered differences scheme. The Clark's scheme is characterized by a small implicit diffusion (Zavatarelli and Pinardi, 2003). This choice is driven by the need to correctly compute the tracers in the Adriatic Sea where high horizontal and vertical density gradients occur due to the freshwater input.

2.1.2 ROMS

ROMS (Regional Ocean Model System) is a free surface primitive equation model, based on the finite differences approach. This model is a development of the S-coordinate Rutgers University Model (SCRUM). A part of the numerics has been rewritten to make it compatible with the last generation computer and to run it in a parallel mode. A more general description of the ROMS model can be found on the web[1].

Vertically it applies the stretched terrain following coordinates to increase the spatial resolution in the interest areas. The formulation is the following:

$$z = \zeta + (1 + \frac{\zeta}{h})[h_c\sigma + (h - h_c C(\sigma))] \qquad -1 \leq \sigma \leq 0 \qquad (2.2)$$

[1] http://marine.rutgers.edu/po/

where h is the total depth, h_c is either the minimum depth or the shallower depth above which more resolution is kept and

$$C(\sigma) = (1-b)\frac{\sinh(\Theta\sigma)}{\sinh\Theta} + \frac{\tanh[\Theta(\sigma+\frac{1}{2})] - \tanh(\frac{1}{2}\Theta)}{2\tanh(\frac{1}{2}\Theta)} \qquad (2.3)$$

where $0 < \Theta \leq 20$ and $0 \leq b \leq 1$ are surface and bottom parameters (Haidvogel et al., 2000).
Along the water column, centered second order finite differences are used on a staggered grid. Higher order schemes are not applied in the vertical to minimize the pressure gradient errors due to the higher sensitivity to topography. These errors are the result of the pressure gradient term splitting into an along sigma component and a hydrostatic correction.

Horizontally the model uses orthogonal curvilinear coordinates on an Arakawa C grid (See Appendix A). Also for the zonal-meridional plane a second order centered finite differences scheme is applied.

The hydrostatic approximation is introduced and the momentum equations are resolved with a split-explicit time-stepping numerical scheme. This method couples the two modes, the baroclinic and the barotropic ones, choosing a smaller time step for the former one.

The temporal discretization is based on a third order predictor (leap-frog) and a third order corrector (Adam-Molton), to stabilize the computation.

The model has several options to discretize the advection term: the second-fourth order centered differences or the third order upstream biased. These schemes are stable for the predictor-corrector approach[2].

There is the opportunity to choose different parameterizations: as an example, the horizontal mixing and the tracers can be expressed on the vertical layers, on the geopotential surfaces or on isopycnal ones; the mixing can be harmonic or bi-harmonic.

The applied turbulence closure scheme can be either local or not local: the former is based on the turbulent kinetic energy equations proposed by Mellor and Yamada (1982) (Appendix B); the latter is based on the K-profile formulation, also for the surface and bottom layers. Additionally a wave/current bed boundary layer scheme is used to identify the bottom stress and the sediment transport.

[2]http://marine.rutgers.edu/po/

2.1.3 COHERENS

COHERENS (COupled Hydrodynamical-Ecological Model for Regional and Shelf seas) is a 3D finite difference model that applies σ coordinates in vertical (Eq. 2.1). It is a multi function model applied mainly on coastal and shallow areas. It permits the coupling of different modules, dealing with the hydrodynamics, the ecological modeling and the water quality modeling.

It applies the Boussinesq approximation to the momentum equation defining the pressure terms as a combination of an equilibrium part (barotropic) and a deviation (baroclinic). Vertically the hydrostatic approximation is applied and the baroclinic pressure gradient term can be considered as an expression of the buoyancy term (Marinov et al., 2006).

The Joint Panel on Oceanographic Tables and Standards equation is used to determine the density (Fofonoff, 1985).

COHERENS applies a two equation turbulence closure scheme to compute the eddy viscosity coefficients and the momentum equations: the eddy viscosity is defined from the turbulent kinetic energy and the turbulent dissipation rate. The advection and diffusion terms, the temporal derivative, the horizontal diffusion and the source and sink terms are present in the momentum equations.

The mode splitting approach is used for the discretization (Blumberg and Mellor, 1987; Luyten et al., 1999). This technique consists of a decoupled solution of the barotropic part, for the vertical integrated momentum and for the continuity equation, and of the baroclinic part, for the momentum and the scalar transport: a smaller time step is chosen for the barotropic part to satisfy the stability criteria for the surface gravity waves. Longer timestep are chosen for the other terms.

2.1.4 NCOM

The Navy Coastal Ocean Model (NCOM) is POM based even if it introduces a number of variations in the numerical discretization compared with the original version. Differently from POM it uses a cartesian horizontal grid. It is free surface, with a implicit treatment of the surface, and it applies the hydrostatic and the Boussinesq approximations and the incompressibility.

It is a hybrid σ/z level model, that means that it uses σ coordinates for the upper layers and z coordinates for the lower ones and the model user can define the absolute depth where the σ to z switch occurs.

The horizontal pressure gradient term is treated on the σ layers as in the

POM model (Blumberg and Mellor, 1987), while the momentum and scalars computation is done with a quasi-third order upwind advection scheme (for scalars there is the opportunity to use the Flux-Corrected Transport advection scheme). The Coriolis term is computed with a fourth-order interpolation and the horizontal pressure gradient with a fourth-order evaluation (Barron et al., 2006).

The water density can be calculated either with the polynomial approximation of the equation of state proposed by Friedrich and Levitus (1972) or the UNESCO formula adapted by Mellor (1991).

It permits to compute the horizontal diffusion with the Smagorinsky algorithm or with a grid-cell Reynolds number scheme, defining for both the schemes a minimum value (Barron et al., 2006).

For the vertical eddy viscosity computation it introduces the Mellor Yamada turbulence closure scheme (Pullen et al., 2003).

The time discretization is leap-frog and all the terms are computed explicitly except for the free surface and the vertical diffusion which are treated implicitly (Barron et al., 2006).

2.1.5 DieCAST

DieCast is a 3D finite differences model that applies z levels on the water column. This model was developed as a variation of the Sandia Ocean Modeling System (SOMS) Model. It is based on primitive equations and applies the hydrostatic and the Boussinesq approximations. It is rigid lid, that simplifies the boundary condition treatment. This aspect is the main difference with all the other models applied in the Adriatic Sea (on the other hand also the MOM (Modular Ocean Model) is rigid lid but it is applied on a wider spatial area - the Mediterranean Sea).

This model is partially implicit and the main difference from SOMS is the application of an Arakawa A grid, instead of a C grid. The reason of this choice is the smaller computational weight for each timestep that permits to maintain the stability even with a longer temporal timestep[3]. It is not very dissipative because it applies a forth order numerical scheme in space and a leap-frog discretization in time, weakly filtered in the computation of the dominant terms as the pressure gradient or the Coriolis term (Cushman-Roisin et al., 2005).

The horizontal momentum, the potential temperature and the salinity are

[3]http://www.ssc.erc.msstate.edu/DieCAST/

computed with control volume averages. The vertical velocity is derived from the incompressibility equation (Cushman-Roisin et al., 2005). The viscosity and the horizontal diffusivity are kept constants 10 m^2s^{-1}; the vertical eddy viscosity is maintained at the order of 0.01 m^2s^{-1}.

2.1.6 SYSTEM3

SYSTEM3 is a 3D finite difference model based on the mass conservation and Reynolds equations (averaged Navier-Stokes).

It introduces the turbulence effects, the variable density and the salinity and temperature conservation equations adopting the UNESCO formula for the density computation.

It is a non-hydrostatic model, therefore it conserves the full vertical momentum equation applying the artificial compressibility method (Chorin, 1967; Rasmussen, 1993). To avoid spurious effects in the hydrodynamic process modeling due to the application of this method, the artificial speed of sound introduced into the continuity equation has to be kept higher than the celerity of surface and internal waves (Vested et al., 1998).

The model adopts a staggered grid computing the pressure, the temperature and the salinity at the nodes, while the velocity is computed in points equidistant to nodes. The continuity equation is discretized with spatial centered schemes. The momentum equations are resolved implicitly with the ADI (Alternating Direction Implicit) algorithm, while the advection and diffusion equations with QUICKEST (quadratic upstream interpolation for conservative kinematics with estimated streaming terms) scheme, a conservative control volume method.

The turbulent effects are simulated computing the vertical eddy viscosity either with the k model, a one equation closure model, or with the $k-\epsilon$ model, a two equation closure model (see Appendix B), or with the Smagorinsky sub grid model. In turbulence closure models the treatment of buoyancy effects must be considered: turbulence buoyancy effects must be considered because, if not, in the presence of density stratification, which damps out the diffusion, the entrainment and the mixing would be over-estimated. The Smagorinsky sub grid model introduces the buoyancy effects by means of the empirical formula of Munk and Anderson (Vested et al., 1998).

2.1.7 MITgcm

The MITgcm model has been created at MIT (Massachusetts Institute of Technology, Boston) and it is based on the Navier-Stokes primitive equation, with a finite volume spatial discretization that permits an easy reconstruction of complex bathymetries. The fluxes are computed in the normal directions with respect to the finite volume faces (Marshall et al., 1997).

It is a free surface model that applies the Boussinesq approximation. The particularity of this model is the opportunity to start the non-hydrostatic modality to identify small scale hydrodynamic structures, in relation with the depth of the basin (Crise et al., 2003). It permits the application of different schemes: centered differences for the horizontal diffusion and the advection; implicit backward for the vertical diffusion of the momentum and of the tracers. The quasi-second order Adams-Bashfort scheme is applied for the time discretization (Crise et al., 2003).

The horizontal turbulent effects are parameterized applying harmonic and bi-harmonic constant coefficients for the turbulent viscosity and diffusivity, while vertically, the mixing and diffusion processes can be parameterized either with harmonic constant coefficients or with the k-pp second order module. It permits to treat, separately on the water column, the surface limit layer and the internal layers.

Also for the density computation it is possible to adopt different choices: to consider it linear or to adopt the state equation of UNESCO.

This model is suitable to be used on parallelized platforms (clusters).

2.1.8 SHYFEM

The SHYFEM (Shallow water HYdrodynamical Finite Element Model) is the model chosen to develop the work presented in this PhD Thesis. For this reason a complete chapter is devoted to the treatment of the new aspects and of the structure of this model. In this section the basic information connected with previous works are enumerated to permit a comparison with the other models.

SHYFEM is a 3D model, primitive equation based, which combines the finite element treatment with finite difference schemes. The model applies z coordinates in the water column. Different numerical schemes are applied spatially and temporally. The water levels are described with a piecewise linear function and values are computed at nodes. On the other hand, transports are centered in each element and described with a constant form function on

the element. Williams (1981) proposed an algorithm similar to the one used for this model, introducing constant form functions for the velocity. The resulting grid is staggered. Transports for the zonal and meridional components are computed in the same point, the center of the element, adopting a type of Arakawa B grid on finite elements. The SHYFEM Model uses a semi-implicit time stepping algorithm to describe the time evolution of the variables. It permits to eliminate the stability constrains for the fast gravity and the Rossby waves.

2.2 Setup Comparison

On the basis of the given information, a preliminary comparison between the different models can be carried out, considering the different geographical areas of application in the Adriatic basin. The grids and the chosen forcings will be analyzed. Finally the results obtained by each model will be compared, defining the state of art of model development for the hydrodynamic investigation in this specific basin.

2.2.1 Numerical Grid

The models presented in the previous sections differ mainly in the typology of grid and in the area of application. Several models have been used to study the whole area of the Adriatic Sea. Four applications are POM based - the system AIM-NASM developed by (Zavatarelli et al., 2002), the study done by Oddo et al. (2005) and the implementation of Bergamasco et al. (1999) and NCOM (Pullen et al., 2003). The others are with DieCAST, described in Cushman-Roisin et al. (2005) and ROMS (Sherwood et al., 2004). Under the umbrella of the EU Mediterranean Forecasting System Pilot Project (MFSTep) (Pinardi et al., 2003), the AIM (Adriatic Intermediate Model) and the NASM (North Adriatic Shelf Model) have been implemented on different areas of the basin.

The former applies a regular grid with an horizontal resolution of 1/20 of a degree, around 5 km. It covers the basin from the northern end to 43.5 degrees North, applying 21 vertical layers in σ coordinates. The latter is nested in the former with a regular grid of 1/37 of a degree (1.5 km), rotated of about 67 degrees with respect to the AIM grid. It covers the Northern area of the basin (Fig. 2.2).

On the other hand, DieCAST simply applies a high resolution regular grid,

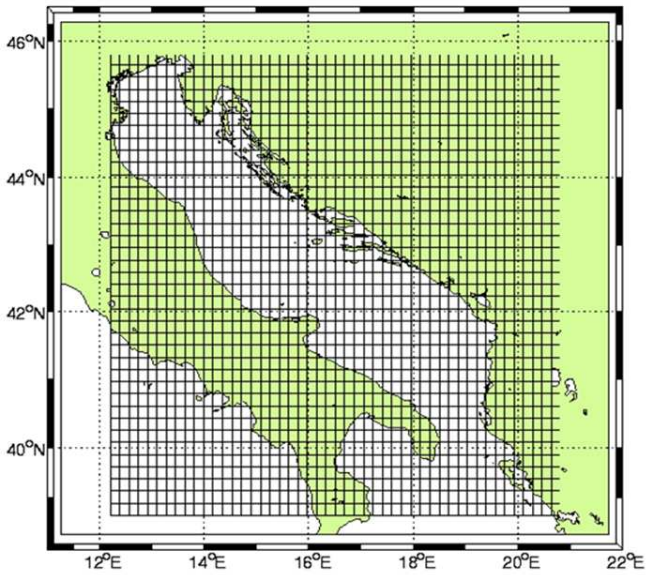

Figure 2.2: Example of a regular grid - AIM (Adriatic Intermediate Model) grid. Figure from (Oddo et al., 2005)

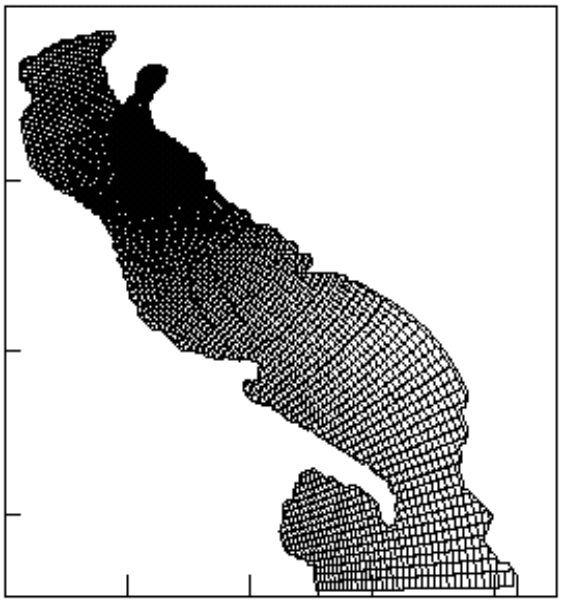

Figure 2.3: Example of a grid based on orthogonal curvilinear coordinates - AIM Model grid used in Zavatarelli et al. (2002).

1/50 of a degree, over the whole basin. This choice is against the computational economy of the model but it permits to identify processes over a larger spatial range. The same approach, with a 2 km regular grid on the whole basin, is seen in the NCOM implementation.

The ROMS Model approach is more interesting, applying a grid based on orthogonal curvilinear coordinates. It permits to increase the spatial resolution where there is the interest to resolve small scale structures. An analogous grid has been used for the AIM model in Zavatarelli et al. (2002) (Fig. 2.3). The opportunity to choose different resolutions in specific areas of the basin is also the advantage of using models like SHYFEM. It is based on an unstructured grid, which permits to reach resolution down to tens of meters if needed. The SHYFEM grid, in the applications discussed in this state of the art, has low resolution in the Southern part of the Adriatic Sea but it increases approaching the coast, in the proximity of the Venice Lagoon, where the hydrodynamic processes of interest for this work can be detected (Bellafiore et al., 2008). High resolution has been reached also in local ap-

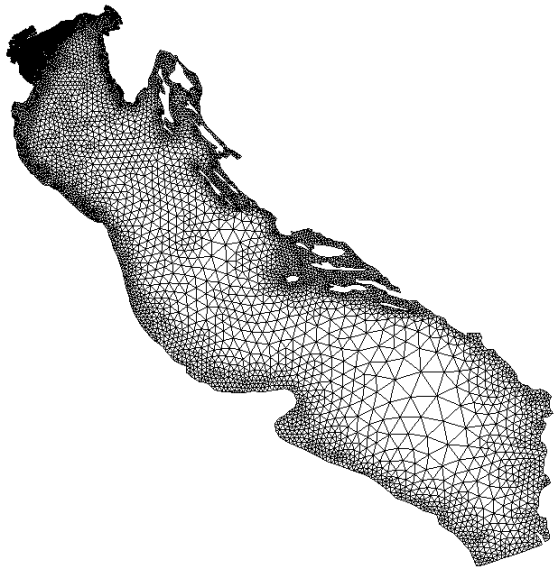

Figure 2.4: SHYFEM Finite Element Grid.

plications of other models, like the MITgcm in the Gulf of Trieste (regular grid with 250 m step - 88x128 cells) (Crise et al., 2003) or the COHERENS, applied in the "Sacca di Goro" (regular grid with 150 m step).

Finally, SYSTEM3, which covers the Northern-Central area of the basin, has

a lower resolution, 6 km, which is suitable to detect the general circulation pattern.

2.2.2 2D and 3D Model Implementations

All the models presented above are formulated in 3D. Notwithstanding this, some implementations done on the Adriatic Sea, particularly the ones on limited areas, are performed in 2D (i.e. SHYFEM Model, Venice Lagoon). This aspect shows how some elements lead to different choices, applying the modeling tool with a higher or lower degree of approximation on the basis of the typology of processes and of the investigated areas. Generally, very shallow bathymetries does not need a deep vertical investigation of the water column, because of the predominance of mixing and barotropic hydrodynamic structures, therefore a 2D implementation is preferred. There are many morphological differences between the Northern and the Southern part of the Adriatic Sea: the North Adriatic presents shallower bathymetries and the barotropic approximation is enough to reproduce the majority of circulation processes in limited zones like the Venice Lagoon where the depth is around 1 m (Cucco and Umgiesser, 2006). 2D runs are used for the reproduction of tidal currents (Malačić et al., 2000; Bellafiore et al., 2008) and also storm surge operational models can be cited as 2D implementations (Bajo et al., 2007).

On the other hand, where thermohaline processes and stratification conditions become the study focus, the 3D structure cannot be neglected (Bergamasco et al., 1999; Cushman-Roisin et al., 2005; Zavatarelli et al., 2002; Oddo et al., 2005).

This remark is important when keeping in mind the main goal of this work. The coast in front on the Venice Lagoon and, in particular, the three interconnection channels, show a variety of hydrodynamic processes of both barotropic and baroclinic nature. Following a procedure from low to high complexity, the model implementations there will be both 2D and 3D.

2.2.3 Boundary Conditions

The discussion about boundary conditions permits the discussion of several specific modeling approaches (finite differences - finite elements).
In models that adopt regular grids, the increase in spatial resolution is obtained by means of the nesting technique: it provides boundary and initial conditions to a high resolution model from an outer model, generally rougher

in resolution. This is what has been done in the implementation of AIM and NASM Models (Zavatarelli and Pinardi, 2003). AIM has also been nested in OGCM (Ocean General Circulation Model), development of the MOM Model, applied on the whole Mediterranean Sea. Nesting is based on the water and heat transport balance between the higher and lower resolution models fixing the boundary information on velocity, temperature and salinity fields (Zavatarelli and Pinardi, 2003).

A very recent work by Oddo and Pinardi (2008) deals specifically with different approaches at the lateral open boundaries with a test implementation in the Adriatic Sea. The first approach imposes the boundary conditions, coming from experimental data or models, as given values, like the Dirichlet condition. The limit of this approach is the possible inconsistency between the imposed values and the ones computed inside the domain. Keeping the nesting approach and trying to be consistent at the lateral boundaries, an additional technique, called nudging, can be useful. A spatial variable condition, near the boundary, links the imposed values and the ones computed by a relaxation time term, with a higher constraint near the border and a smaller one advancing further inside the domain. The boundary variable Θ is nudged with a reference value Θ_R. The formulation introduces an additional term to the equation for Θ that reads

$$\frac{\Theta - \Theta_R}{\tau} \tag{2.4}$$

where τ is the relaxation time that increases further into the domain.

Following the same philosophy, keeping a defined constraint at the boundary, another approach consists in the variation of viscosity and diffusivity in a border strip, called sponge layer (Oddo and Pinardi, 2008).

A completely different approach solves locally linearized primitive equations of motion at the border, simplifying the physics at the boundary (Oddo and Pinardi, 2008).

The radiation conditions, the advective conditions and the Flather conditions are some examples.

- **Radiation Condition**: it imposes the internal fields on the boundary by mean of a wave relation like

$$\frac{\partial \Theta}{\partial t} + c\frac{\partial \Theta}{\partial n} = 0 \tag{2.5}$$

  c is the wave phase speed and n the normal direction. c can be imposed

with different assumptions like the Orlanski one,

$$c = -\frac{\partial \Theta}{\partial t}(\frac{\partial \Theta}{\partial n})^{-1} \tag{2.6}$$

- **Flather Condition**: it is a kind of radiation condition that keeps the mass conservation at the boundary (Oddo and Pinardi, 2008). It was developed for the first time in tidal modeling and it puts in relation velocity and water elevation. Its formulation is

$$V^n_{BTf} = V^n_{BTc} - \frac{\sqrt{gH}}{H}(\eta_c - \eta_f), \tag{2.7}$$

  where V^n_{BTc} and η_c are the barotropic velocity and the surface elevation of the coarse model, and V^n_{BTf} and η_f of the fine resolution model.

- **Advective Condition**: It is a condition that advects the variable at the boundary with the normal velocity provided by the imposed boundary values. The relation is

$$\frac{\partial \Theta}{\partial t} + V_n \frac{\partial \Theta}{\partial n} = 0 \tag{2.8}$$

In the last implementations of the POM model the Flather condition (Oddo and Pinardi, 2008) is applied, in NCOM as well for the elevation (Pullen et al., 2003). In NCOM the Orlanski radiation condition is used for temperature, salinity and normal velocity, while a zero-gradient condition controls the tangential velocity (Rochford and Martin, 2001).

The water surface is also a boundary and the models that consider the mass and heat exchanges with the atmosphere need to impose further boundary conditions: this is the case of POM, ROMS and NCOM implementations.

In ROMS the treatment of the air-sea boundary is done applying the bulk parameterization proposed by Fairall et al. (1996), a kind of correction of the surface momentum flux, sensible heat and latent heat. This level is used for the one and two-direction nesting with the atmospheric models. ROMS has also an efficient data assimilation scheme.

NCOM receives information from the atmospheric model COAMPS and applies the bulk formulas of Kondo (1975). Evaporation obtained from the latent heat flux is used to compute the surface salt flux and the COAMPS solar radiation modifies the water temperature on the layers.

The POM implementation done by Zavatarelli et al. (2002) adopts the bulk formulas described in Castellari et al. (1998).

2.2.4 Initial Conditions

Initial conditions of temperature and salinity have been imposed for all the models applied to the whole Adriatic Sea basin (AIM, DieCAST, POM, SHYFEM, ROMS). Different datasets have been considered: the basic choice has fallen on ATOSMOM dataset (Artegiani et al., 1997a; Zavatarelli and Pinardi, 2003), which is the merge of two datasets, including data produced by MOM in the Ionian Sea to initialize AIM. Then the AIM T/S data permit to initialize NASM Model.

MOBD and ATOS2 databases have been used in DieCAST, to collect higher resolution information in the coastal area (Cushman-Roisin et al., 2005).

The implementation of POM by Bergamasco et al. (1999) is based on POEM1 and POEM3 data, imposing horizontally uniform temperature and salinity profiles (Artegiani et al., 1993).

The same choice, in terms of T/S profiles, has been applied for models on limited areas like MITgcm in the Gulf of Trieste (Crise et al., 2003).

Another MITcgm implementation (ACOST1.1), under the ADRICOSM Project, stresses a different initialization technique, similar to the one of Zavatarelli et al. (2002), introducing T/S fields produced by a larger scale model (ACOST1.2).

Simpler initial conditions have been used to simulate the Venice Lagoon circulation, in shallow water conditions. Unique typical values of temperature and salinity have been imposed on the whole basin.

2.2.5 Forcings

For the Adriatic Sea the more important forcings are wind, thermohaline fluxes coming from the rivers and from the air-sea interaction and the astronomical tides.

Trying to reconstruct realistic scenarios, wind fields are imposed from models: different dataset can be mentioned, like ECMWF (European Centre for Medium-Range Weather Forecasts), COAMPS (Coupled Ocean-Atmosphere Mesoscale Prediction System) and LAMI (Limited Area Model Italy) (Sciarra et al., 2006). In some applications, climatological forcings are chosen (Zavatarelli and Pinardi, 2003; Cushman-Roisin et al., 2005).

Two works have been written trying to define the variations in the circulation reproduction due to the different meteorological forcings chosen (Pullen et al., 2003; Signell et al., 2005). Pullen et al. (2003) applies the NCOM model coupled with the meteo model COAMPS. The coupling is tested with two different resolutions (36 km and 4 km). From this study a better capability of

the high resolution model in the medium scale wind phenomena reproduction (singular Bora events) is stressed (Pullen et al., 2003).

The second work compares different wind databases (ECMWF, LAMBO, LAMI e COAMPS) coupled with a wave model (SWAN) (Signell et al., 2005). The spatial resolution varies from 40 km (ECMWF) to 7 km (LAMI). Once more the best results are obtained with high resolution models. However a specification has to be made: LAMI is partially deterministic and partially stochastic and it is suitable for simulation over long time ranges although it is a local model and it is strongly affected by boundary conditions. The COAMPS Model shows the same problem therefore, for real time simulations, global models like ECMWF are preferable, even if lower in resolution (Signell et al., 2005). The meteorological models generally provide all the variables needed to impose or compute the surface heat fluxes.

The second forcing is river freshwater: it is introduced in Zavatarelli et al. (2002) and Oddo et al. (2005) as a climatological input, with a generalized information over the whole North-West littoral of the Adriatic Sea. In Zavatarelli et al. (2002) and Oddo et al. (2005) the only point source of freshwater is the Po river, because of its central role in the general circulation of the basin (Zavatarelli and Pinardi, 2003). On the other hand the ROMS Model considers different sources of freshwater along the basin (Po and some rivers in Central Italy - Pescara and Biferno). Data are imposed as mean daily averages.

The Otranto Strait is considered open boundary in many model implementations (POM, ROMS, SHYFEM, DieCAST). Zavatarelli and Pinardi (2003) imposes the OGCM nested fluxes instead of Sciarra et al. (2006) who apply the ROMS Model specifying tidal levels and fluxes produced by a model covering the whole basin.

The SHYFEM Model imposes water level time series as open boundary conditions to reproduce the tidal behaviour at the Strait.

In this state of art it is useful to mention also that many tidal models have been developed and applied in the Adriatic Sea (Malačić et al., 2000). The modelled water levels can then be used as tidal forcings in the circulation models.

Chapter 3

SHYFEM Model

SHYFEM is a finite element hydrodynamic model developed at ISMAR-CNR Istituto di Scienze Marine. The 3D SHYFEM model has been implemented to simulate the lagoon-sea interaction phenomena. The model, in the 2D version, has been applied in many studies to the Venice Lagoon (Umgiesser, 2000; Melaku Canu et al., 2001; Umgiesser et al., 2004; Cucco and Umgiesser, 2006). It is a primitive equation model, based on the solution of the momentum and continuity shallow water equations. In this work new aspects

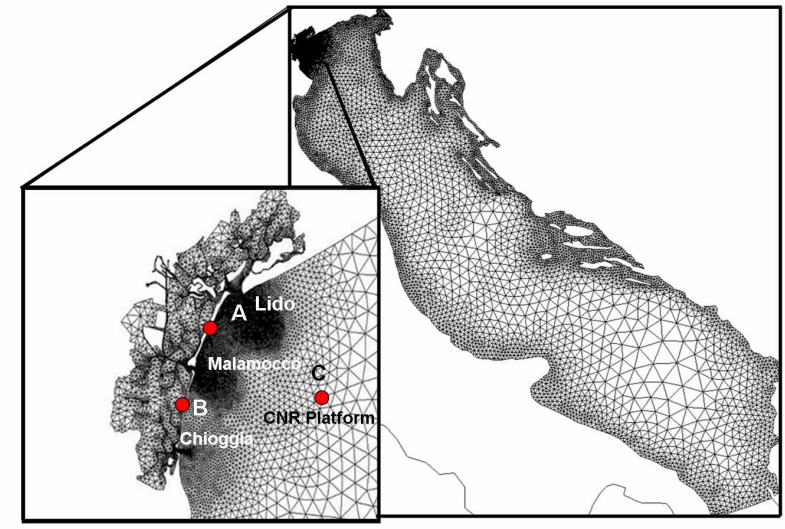

Figure 3.1: SHYFEM Finite element grid of the Adriatic Sea and the Venice Lagoon.

connected with the spatial discretization and with the introduction in the equations of important terms for the 3D implementation, such as the baroclinic pressure gradients, are presented. The other new aspect that has to be stressed is that the model is implemented in 3D on a coupled basin, Adriatic Sea-Venice Lagoon, for the first time. A finite element grid covering both the Adriatic Sea and the Venice Lagoon has been used with an increase in spatial resolution around the interconnection areas (Fig. 3.1) reaching resolution of 30 m. This grid consists of 15619 nodes and 28827 triangular elements.

3.1 The equations

The equations, integrated on each layer, read:

$$\frac{\partial U_l}{\partial t} + Adv_l^x - fV_l = -gh_l\frac{\partial \zeta}{\partial x} - \frac{gh_l}{\rho_0}\frac{\partial}{\partial x}\int_{-H_l}^{\zeta}\rho' dz + \tag{3.1}$$

$$-\frac{h_l}{\rho_0}\frac{\partial p_a}{\partial x} + \frac{1}{\rho_0}(\tau_x^{top(l)} - \tau_x^{bottom(l)}) + A_H(\frac{\partial^2 U_l}{\partial x^2} + \frac{\partial^2 U_l}{\partial y^2})$$

$$\frac{\partial V_l}{\partial t} + Adv_l^y + fU_l = -gh_l\frac{\partial \zeta}{\partial y} - \frac{gh_l}{\rho_0}\frac{\partial}{\partial y}\int_{-H_l}^{\zeta}\rho' dz + \tag{3.2}$$

$$-\frac{h_l}{\rho_0}\frac{\partial p_a}{\partial y} + \frac{1}{\rho_0}(\tau_y^{top(l)} - \tau_y^{bottom(l)}) + A_H(\frac{\partial^2 V_l}{\partial x^2} + \frac{\partial^2 V_l}{\partial y^2})$$

$$\frac{\partial \zeta}{\partial t} + \sum_l \frac{\partial U_l}{\partial x} + \sum_l \frac{\partial V_l}{\partial y} = 0 \tag{3.3}$$

where

$$Adv_l^x = u_l\frac{\partial U_l}{\partial x} + v_l\frac{\partial U_l}{\partial y} \qquad Adv_l^y = u_l\frac{\partial V_l}{\partial x} + v_l\frac{\partial V_l}{\partial y} \tag{3.4}$$

with l indicating the vertical layer, (U_l, V_l) the horizontal velocities integrated over the layer (transports), (u_l, v_l) the velocities in x,y directions, in p_a atmospheric pressure, g gravitational constant, f Coriolis parameter, ζ water level, ρ_0 the constant water density, $\rho = \rho_0 + \rho'$ water density, h_l layer thickness, H_l depth of the bottom of layer l, A_H horizontal eddy viscosity.

The stress terms are expresses as follows

$$\tau_x^{top(l)} = \rho_0 \nu \frac{(U_{l-1} - U_l)}{(h_{l-1} + h_l)/2} \qquad \tau_x^{bottom(l)} = \rho_0 \nu \frac{(U_l - U_{l+1})}{(h_l + h_{l+1})/2} \tag{3.5}$$

$$\tau_y^{top(l)} = \rho_0 \nu \frac{(V_{l-1} - V_l)}{(h_{l-1} + h_l)/2} \qquad \tau_y^{bottom(l)} = \rho_0 \nu \frac{(V_l - V_{l+1})}{(h_l + h_{l+1})/2} \tag{3.6}$$

with ν vertical viscosity.

3.2 Boundary and Initial Conditions

The boundary conditions for stress terms are

$$\tau_x^{sup} = c_D \rho_a w_x \sqrt{w_x^2 + w_y^2} \qquad \tau_y^{sup} = c_D \rho_a w_y \sqrt{w_x^2 + w_y^2} \tag{3.7}$$

$$\tau_x^{bottom} = c_B \rho_0 u_L \sqrt{u_L^2 + v_L^2} \qquad \tau_y^{bottom} = c_B \rho_0 v_L \sqrt{u_L^2 + v_L^2} \tag{3.8}$$

c_D is the wind drag coefficient, c_B is the bottom friction coefficient, ρ_a is the air density, (w_x, w_y) is the wind velocity and (u_L, v_L) is the bottom velocity.

The bottom drag coefficient c_B is usually assumed to be constant. However, in the case of the Venice Lagoon, it could be dependent on the depth through the Strickler formula

$$c_B = \frac{g}{C^2} \qquad C = k_s H^{1/6} \tag{3.9}$$

with C the Chezy coefficient and k_s the Strickler coefficient. Inside the lagoon different Strickler coefficient have been used to distinguish the behavior of channels, tidal flats and the rest and at the three inlets slightly different values of this coefficient are used in inflow and in outflow conditions to parameterize the unresolved physical processes such as the local head loss due to sudden expansion of the out-flowing water (Umgiesser et al., 2004).

The model gives the possibility to impose both water level timeseries as open boundary conditions or fluxes. The second approach is chosen to give the information about river discharge, while water levels are imposed at the Otranto Strait open boundary, as decribed in Bellafiore et al. (2008).

3D Velocity fields as initial condition are set to zero while two options are given to impose initial temperature and salinity fields: there are either set to a constant value over the whole basin or 3D matrices can be introduced. These two variables are given for each node and for each layer. They have to be also imposed at the boundary for each layer.

3.3 Discretization in time and space

As introduced in chapter 2, velocities are computed in the center of each element, whereas scalars are computed at each node. Vertically the model applies Z layers with variable thickness. Most variables are computed in the center of each layer, whereas stress terms and vertical velocities are solved at the interface between layers (Fig. 3.2).

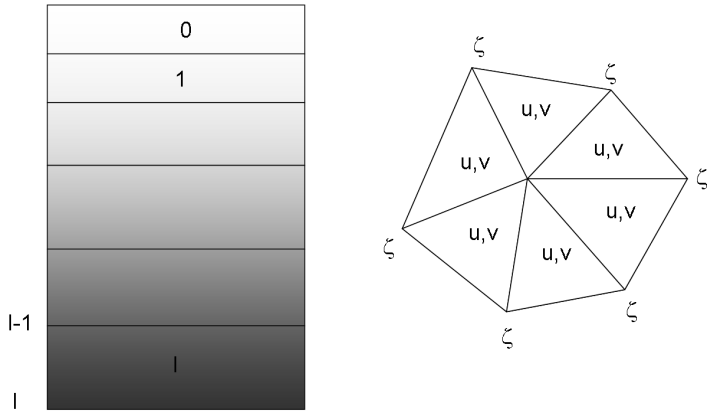

Figure 3.2: Left figure: vertical structure - all variables but stresses are computed in the middle of the layer. Right figure: finite element - scalars (as well as water levels) computed at nodes and vectors in the baricenters of each element.

What concerns the temporal discretization, the horizontal diffusion, the baroclinic pressure gradient and the advective terms in the momentum equation are treated fully explicitly. The Coriolis force and the barotropic pressure gradient terms in the momentum equation and the divergence term in the continuity equation are treated semi-implicitly. The adopted scheme is Crank-Nicholson. The semi-implicit treatment has to be considered a better choice compared with the explicit approach for long gravity waves with velocity $c = \sqrt{gH}$. In fact semi-implicit schemes are unconditionally stable with respect to the gravity wave and are energy conserving. The bottom friction is treated fully implicitly. This is done because no problems connected with the velocity inversion, in the cases of big bottom stresses, can be avoided.

Therefore the model is unconditionally stable what concerns the fast gravity waves, the vertical stress and the Coriolis acceleration because of the chosen time discretization (Umgiesser and Bergamasco, 1995).

Moving to the spatial domain, the specific approach that is applied in SHYFEM mixes finite element structure and finite differences schemes. Traditionally the Galerkin formulation (Williams, 1981) has been applied on unstructured grid: piecewise linear form functions are used to determine spatially the variables. A variable ζ can be defined as a sum of these functions over the nodes. The form functions ϕ_m are 1 at the node m and 0 on the other nodes for each element and linear inside each triangle.

$$\zeta = \zeta_m \phi_m \qquad m = 1...K \tag{3.10}$$

K is the number of nodes in the model domain.

Unluckily the Galerkin approach does not give satisfactory results if the model treatment is semi-implicit, as it is in the SHYFEM Model. For this reason the Galerkin approach is still applied for the water levels computation but not for horizontal transports. To discretize horizontal transports, not continuous, constant functions ψ_m, defined over the whole domain are chosen. Their value is 1 at the element m and 0 on the rest of the basin. There is a discontinuity at the border of the element. So transports can be defines as

$$U = U_n \psi_n \qquad n = 1...J \tag{3.11}$$

with J total number of elements. Transports are defined in the center of the element, whereas scalars are computed at nodes. The advantage in the adoption of this kind of formulation is connected with better properties of wave propagation, geostrophic adjustment and total mass and energy conservation (Umgiesser and Bergamasco, 1995).

The theoretical basis of this approach can be described defining a linear differential equation where L is the differential operator

$$L(\tilde{u}) = 0. \tag{3.12}$$

Because it is impossible to compute the exact solution $\tilde{u}$, the approximation u is needed. It produces a residual term $R = L(u)$ that has to be minimized

$$\int_\Omega \Psi_n R d\Omega = \int_\Omega \Psi_n L(u) d\Omega = 0 \tag{3.13}$$

where Ψ_n are the weight functions and Ω is the domain where the equation has to be solved.

All the unknown and the spatially variable coefficients are developed in a series of indipendent linear functions Φ_m, that are the form functions.

$$u = \Phi_m u_m \qquad m = 1...K \tag{3.14}$$

K total number of nodes. Anyway the Galerkin approach is used to choose the weight functions Ψ_n, which are defined equal to the form functions Φ_m. What is obtained is

$$\int_\Omega \Phi_n R d\Omega = 0 \tag{3.15}$$

The integral is considered a scalar product and R is posed orthogonal to the sub-space defined by the functions Φ_n. Introducing the linear development of u in the initial integral and remembering the linearity of the operator L, what results is $a_{nm}u_m = 0$, n=1,K and m=1,K, with $a_{nm} = \int_\Omega \Phi_n L(\Phi_m) d\Omega$ matrix element of $A = (a_{nm})$.

At the end of the procedure the problem of solving this partial differential equation can be simplify to the solution of a linear equations system, with the correct boundary conditions (Umgiesser and Bergamasco, 1995).

The application of the semi-implicit algorithm leads to the formal solution of the momentum equations for the transports and these are substituted in the continuity equation. The obtained linear system has only water levels as unknowns in the nodes of the spatial domain. After the solution of this linear system, transports can be computed directly from the momentum equations.

For the computation of the vertical diffusivities and viscosities a turbulence closure scheme is used. This scheme is an adaptation of the k-ϵ module of GOTM (General Ocean Turbulence Model) described in Burchard and Petersen (1999). Some theoretical info in Appendix B.

Because of the objective of this PhD work, the simulation of coastal and interaction processes, two terms in the equations, the baroclinic pressure gradient term and the turbulent diffusion term, result very important. The modules in which these terms are computed have been checked, changed and developed, in order to be confortable of their performances in realistical runs. In the next chapter and in Appendix B a description of numerical choices in the discretization and computation of these terms and test cases are presented.

Chapter 4

Test Cases - Process Study in ideal basins

4.1 Baroclinic Module

The study of coastal hydrodynamics requires the resolution of processes connected with river outflow and other sources of freshwater. The occurrence of temperature and salinity gradients due to the rivers action produces horizontal and vertical variations in the density field, as well as the evaporation and precipitation at the air-sea interface. These kind of processes are simulated by means of the baroclinic pressure gradient term in the momentum equations.

In the past the real case of Po river outflow has been simulated applying a previous version of the 3D SHYFEM Model (Umgiesser and Bergamasco, 1998). Starting from that version, the baroclinic pressure gradient terms have been developed and adapted to the version here tested.

4.1.1 Estuarine Outflow Test Cases

In order to test the model with the introduction of baroclinic terms, three computational test cases, proposed by Chao and Boicourt (1986), were run. The estuarine dynamics is here simulated describing the dynamics of a freshwater flow injected by means of a channel into a regular basin. Even if in the work of Chao and Boicourt (1986) many cases are treated, the three test

cases here presented are considered enough to define the correctness of the baroclinic pressure gradient term discretization.

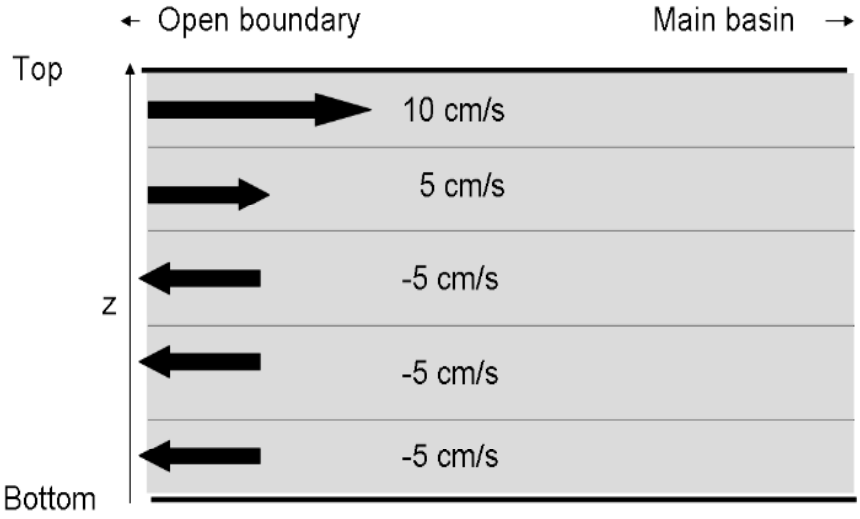

Figure 4.1: Vertical Section of the channel connected with the ideal basin. Input Velocity imposed at the open boundary.

Before the explanation of each case one aspect has to be stressed: the Chao hydrodynamic model is a rigid lid model and this means that only cases where the net water flux into the basin is 0 with no vertical water level displacement can be treated to permit a comparison with SHYFEM, which is free surface. The three test cases are run in an ideal rectangular basin, which is 60 km wide and 140 km long. A channel, 15 km large and 52.5 km long, is connected to the basin along one of its borders. The whole basin is 15 m deep (Chao and Boicourt, 1986). Five vertical layers, which are 3 m thick each, are imposed (Fig. 4.1).

A 0.1 ms^{-1} freshwater inflow velocity is set at the open boundary upper layers of the channel connected to the ideal basin. Outflow is set at the lower layers to obtain no barotropic flux at the open boundary (Fig. 4.1). The three test cases differ in the choice of vertical eddy viscosity and bottom friction values.

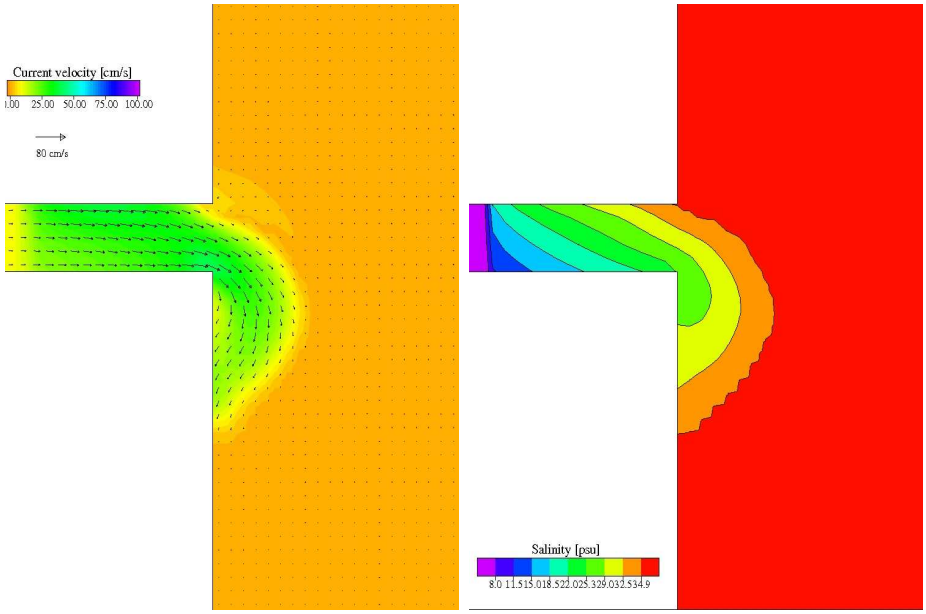

Figure 4.2: Chao Experiment 1 - Velocity and salinity plots after five days, first layer

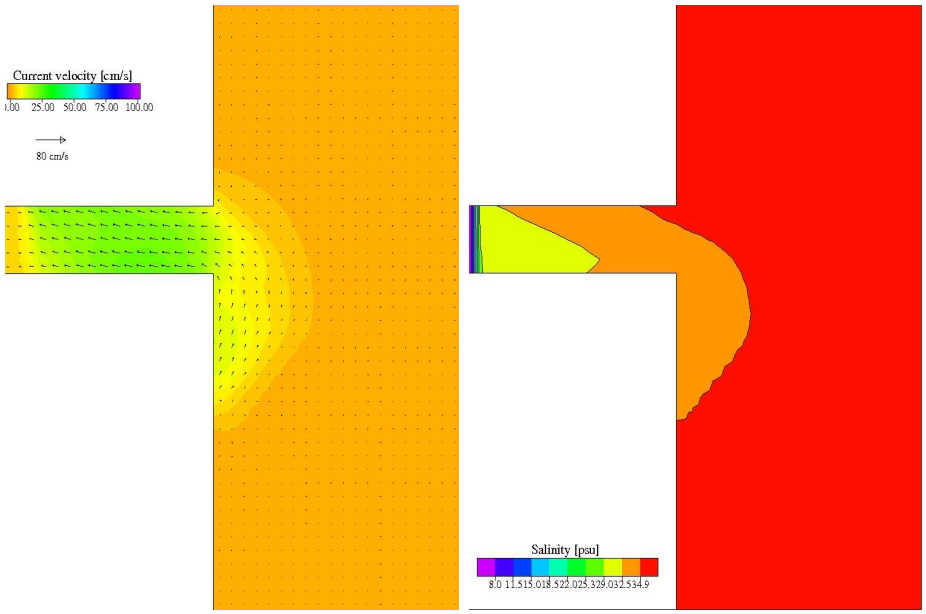

Figure 4.3: Chao Experiment 1 - Velocity and salinity plots after five days, fourth layer

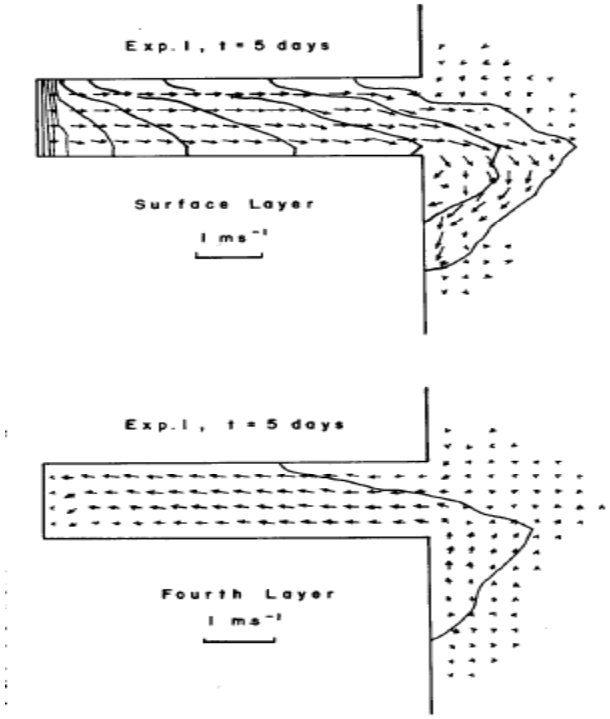

Figure 4.4: Chao Experiment 1 - Velocity and salinity plots after five days produced by Chao and Boicourt (1986), first and fourth layer

The first run setup considers bottom friction 0.01, vertical eddy viscosity 10E-4 m^2s^{-1}, horizontal diffusion 10 m^2s^{-1} and beta plane Coriolis approximation for latitude 30 degrees North. After 5 days the velocity and the salinity fields are as presented in Fig. 4.2 and Fig. 4.3. These patterns are in agreement with the results presented by Chao and Boicourt (1986). To permit a visual comparison the figure obtained in Chao and Boicourt (1986) is here shown in Fig. 4.4. The velocity and salinity values are of the order of the Chao results and this is a encouraging result. After five days the salinity gradients can be seen close to the channel mouth, weakening from surface to bottom. As expected, a general deflection of currents to the South is seen.

Observing the velocity and salinity fields after 10 days, the results are still comparable with the Chao test even if the patterns are smoother than the original ones (Figs. 4.5, 4.6, 4.7). In the Chao and Boicourt (1986) test the freshwater is spreading more offshore and, perhaps, some effects at the boundary opposite to the channel can affect the SHYFEM results.

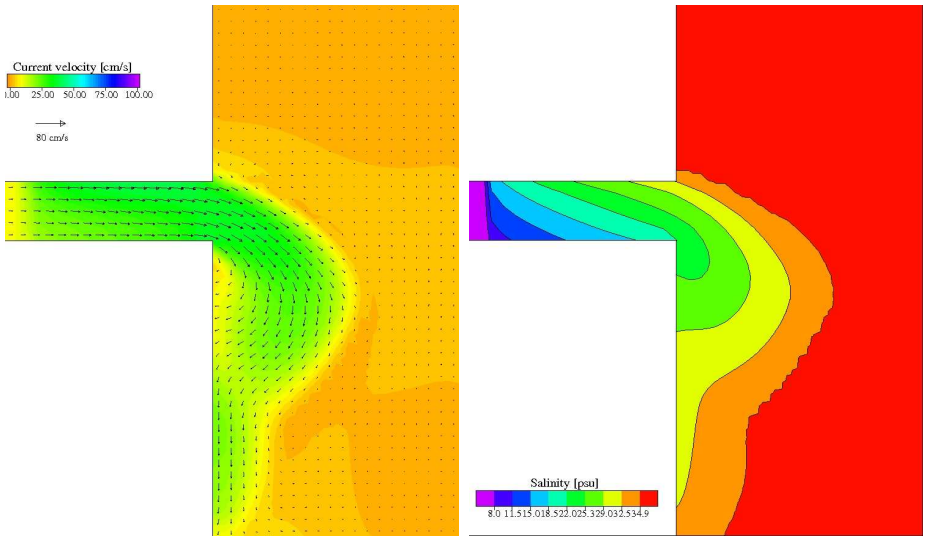

Figure 4.5: Chao Experiment 1 - Velocity and salinity plots after ten days, first layer

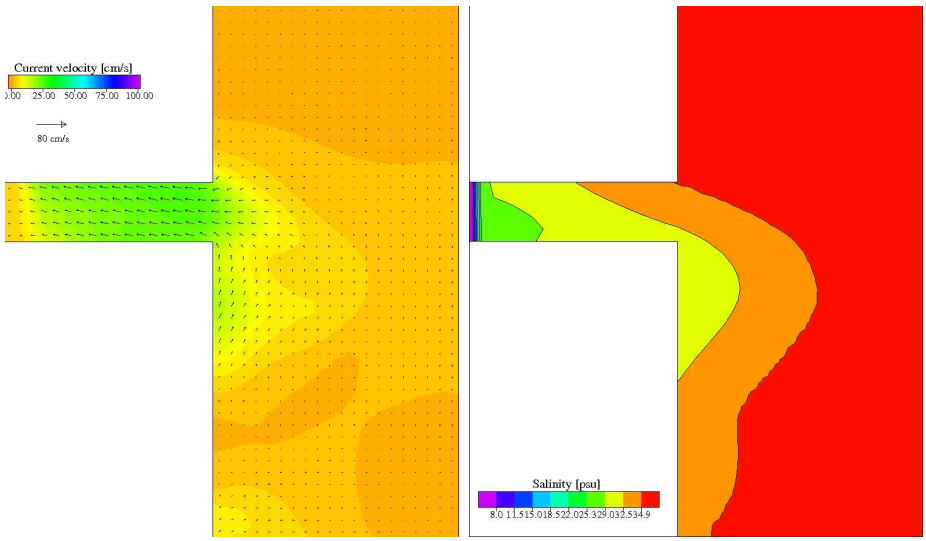

Figure 4.6: Chao Experiment 1 - Velocity and salinity plots after ten days, fourth layer

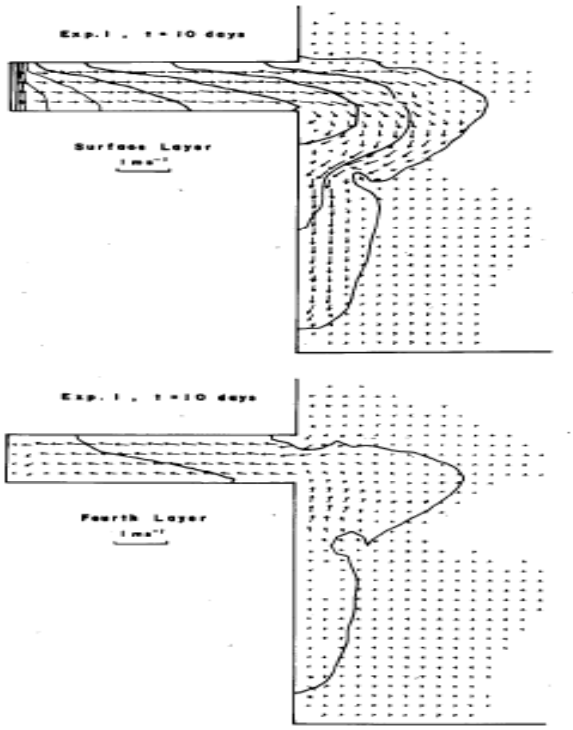

Figure 4.7: Chao Experiment 1 - Velocity and salinity plots after ten days produced by Chao and Boicourt (1986), first and fourth layer

The same problem can be detected also in the other test cases but the structure of the plume is comparable with the reference one. The second experiment keeps the setup of the previous test but uses a higher vertical viscosity of 5 cm^2s^{-1} and the same bottom friction (0.01). What is expected is an increase in the mixing effects and, in fact, the same horizontal salinity gradients in the channel can be seen both in the surface and in the fourth layer after twenty days of simulation (Figs. 4.8, 4.9, 4.10).

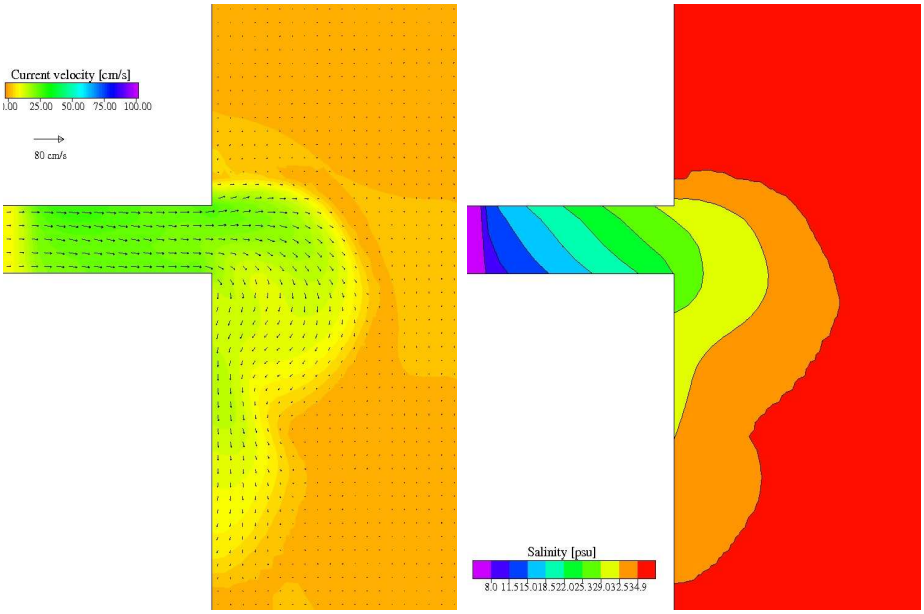

Figure 4.8: Chao Experiment 2 - Velocity and salinity plots after twenty days, first layer

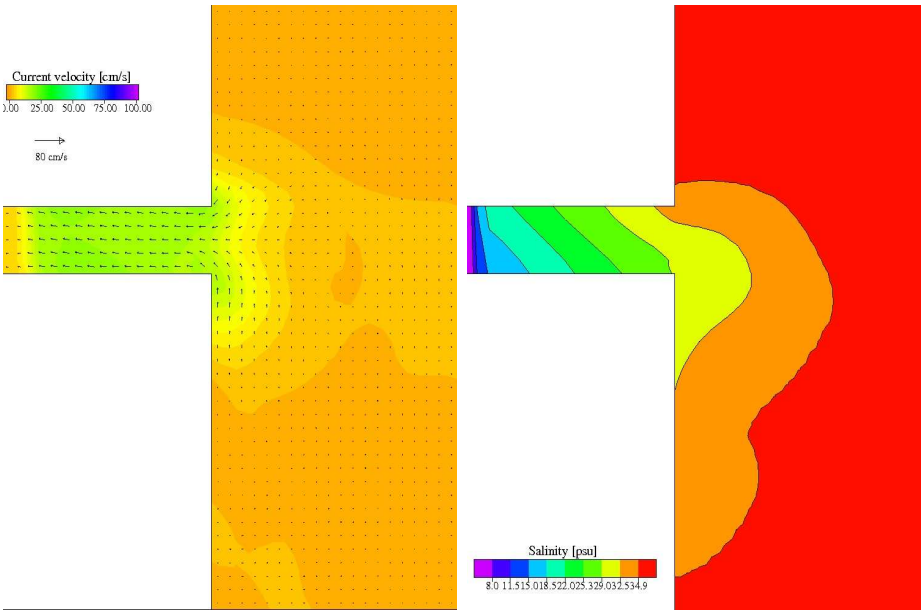

Figure 4.9: Chao Experiment 2 - Velocity and salinity plots after twenty days, fourth layer

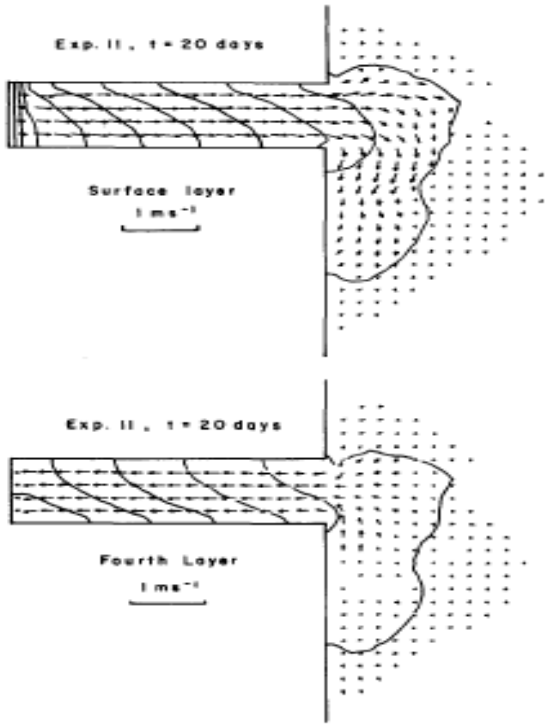

Figure 4.10: Chao Experiment 2 - Velocity and salinity plots after twenty days produced by Chao and Boicourt (1986), first and fourth layer

The third and last experiment keeps the vertical eddy viscosity at 1 cm^2s^{-1} but sets the bottom friction to zero. As a consequence of the absence of friction in the bottom layer some freshwater fingers can be detected in the fourth layer. The same reference bottom layer patterns from Chao and Boicourt (1986) simulation (Fig. 4.13) are modelled by SHYFEM Model (Fig. 4.12), after 10 days. The surface layer shows a recirculation cell not really seen in the Chao results (Fig. 4.11). Once more it could be considered as the influence of the eastern border of the ideal basin boundary.

Considering the obtained results it can be said that the behaviour of SHYFEM in computing the baroclinic pressure gradient term is correct and not affected by numerical spurious effects.

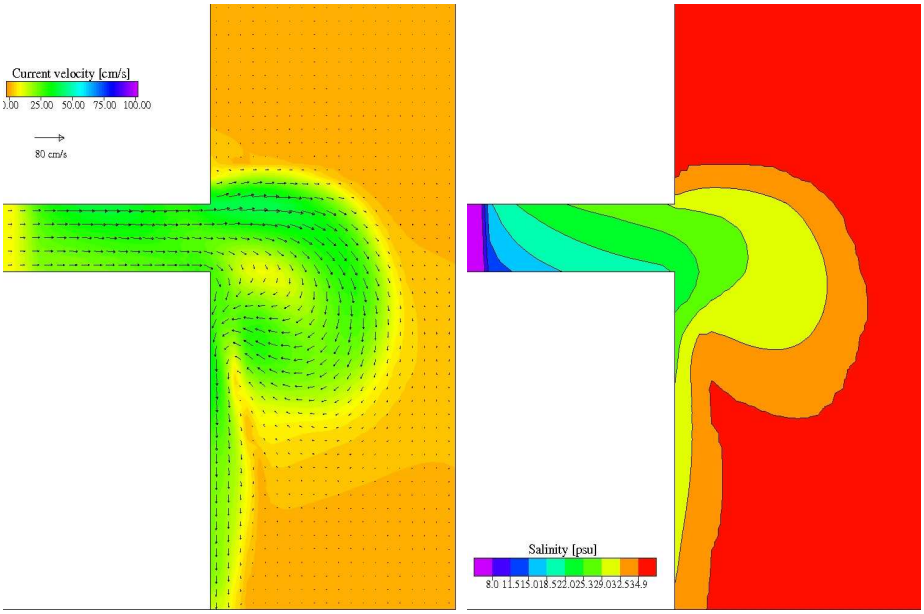

Figure 4.11: Chao Experiment 3 - Velocity and salinity plots after ten days, first layer

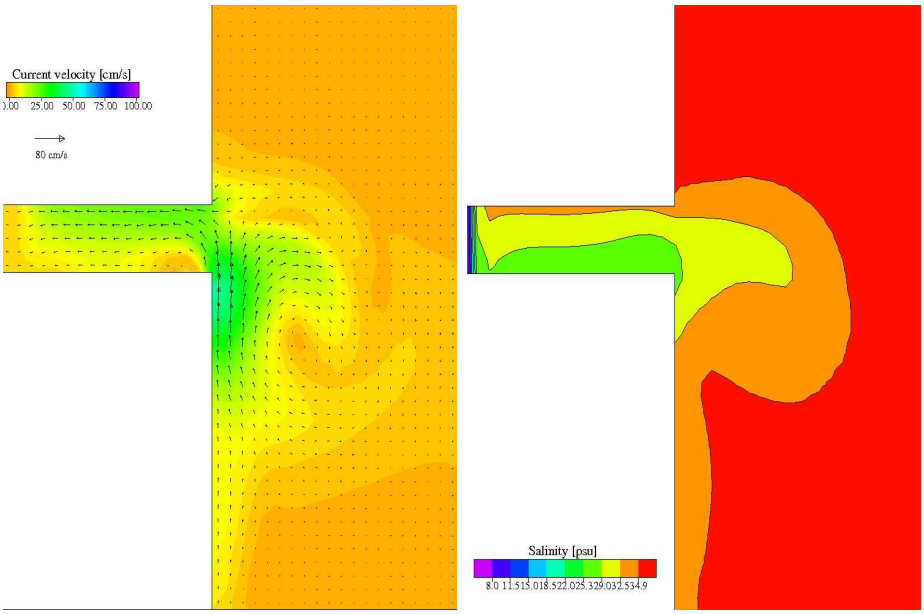

Figure 4.12: Chao Experiment 3 - Velocity and salinity plots after ten days, fourth layer

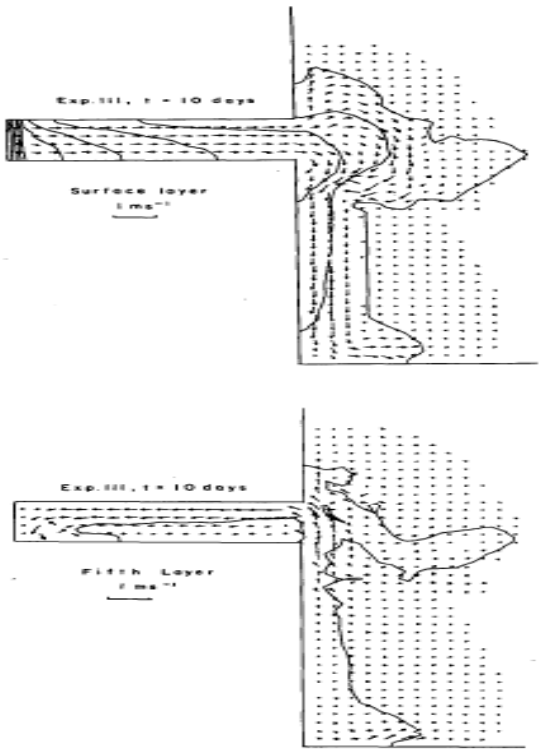

Figure 4.13: Chao Experiment 3 - Velocity and salinity plots after ten days produced by Chao and Boicourt (1986), first and fourth layer

4.2 Turbulence Module

The vertical temperature and salinity profiles, particularly near estuaries and sources of freshwater, are mainly controlled by the turbulence distribution in the water column and by the vertical mixing (Burchard and Petersen, 1999). Turbulent effects cannot be neglected in narrow channels and in the connection areas as the inlets of the Venice Lagoon, where water can either have stratified or mixed vertical structure. Therefore the turbulence effects modeling is not an easy task that requires the introduction of parameterizations, approximation and closure models, as better explained in Appendix B.

To test the correct computation of the turbulence effects in SHYFEM with the implementation of the GOTM Turbulence Closure Module, two test cases have been studied.

4.2.1 Kato-Phillips Test Case

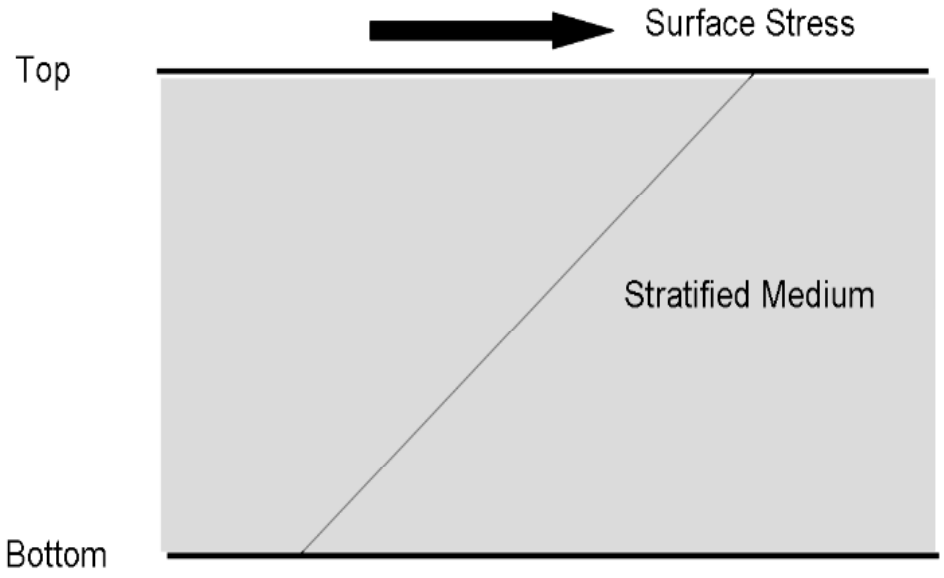

Figure 4.14: Setup of the Kato-Phillips Experiment. Surface stress imposed on a vertically stratified medium

The first test case reproduces the mixed layer deepening induced by a constant surface stress. This kind of effect is due to the wind action on the surface (Fig. 4.14). The wind mixing generally is created by the turbulent kinetic energy production and the energy transfer connected with the wave breaking (Burchard and Petersen, 1999). Therefore the surface stress action is investigated along the whole water column initially stably stratified. The model is run in 1D, along the vertical coordinate. The visual comparison, in this test case, is done between model outputs and the laboratory results obtained by Kato and Phillips (1969).

This particular experiment has the property, in absence of Coriolis force, to present self-similar solutions for the equation of motion and density when the stratification profile is given by a power law of z, as in this case (Luyten et al., 1996). Given a linear stratification, the analytical formula of the depth of the turbulent layer is

$$h(t) = (2R_i)^{1/4} u_* (t/N_0)^{1/2} \tag{4.1}$$

with the Richardson Number $R_i = N_0^2 h^2 / \hat{U}^2$, $\hat{U}$ mean value of current over the turbulent layer.

The initial conditions imposed at the water column are a constant Brunt-Väisälä frequency N_0 $10^{-2}\mathrm{s}^{-1}$ and a surface friction velocity u_* $10^{-2}\mathrm{ms}^{-1}$ (Luyten et al., 1996). The applied Richardson number, homogeneous for self similarity with the initial values of surface friction and buoyancy, is R_i 0.53.

The chosen time step is 50 s and the vertical discretization is 0.5 m. The total depth of the water column is 100 m to avoid the bottom effects.

In Fig. 4.15 the mixed layer evolution in time is shown. The abscissa is in the adimensional unit tN_0. As it can be seen, the trend is reconstructed by the SHYFEM Model, comparing it with the results obtained by Luyten et al. (1996) (Fig. 4.15 central panel) and by Burchard and Petersen (1999) (Fig. 4.15 bottom panel). Burchard and Petersen (1999) tested both the k-ϵ turbulence closure scheme, which is also adopted in SHYFEM, and the Mellor-Yamada scheme. More information about these two schemes in Appendix B.

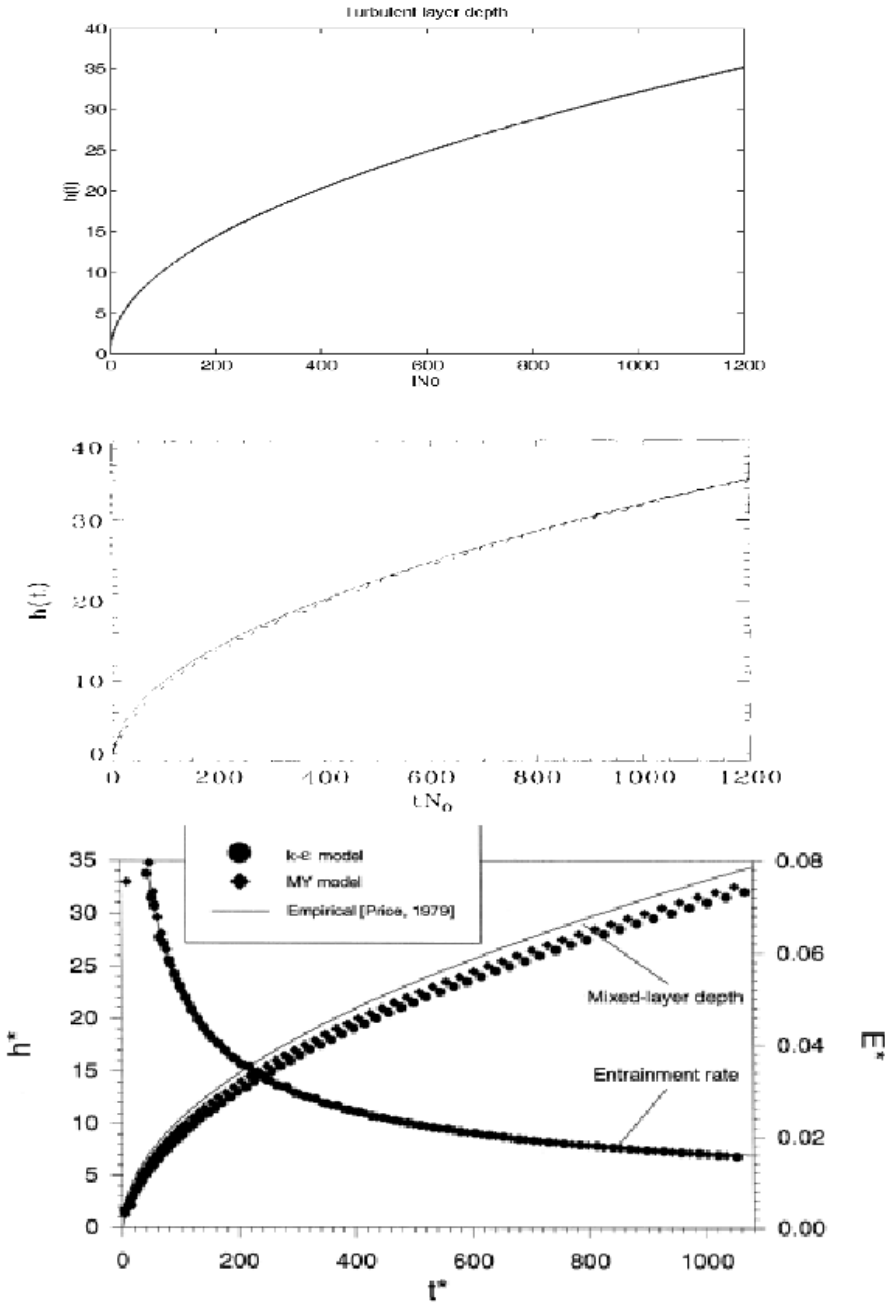

Figure 4.15: Kato-Phillips Experiment -The upper panel shows the evolution in time of the turbulent layer from SHYFEM results, the central is taken from Luyten et al. (1996) and the bottom panel is from Burchard and Petersen (1999). Burchard and Petersen (1999) shows both the results applying the k-ϵ and the MY (Mellor-Yamada) turbulence schemes.

4.2.2 Deardorff Test Case

The second test case is the so called Deardorff experiment, which studies the mixed layer deepening by free convection. In this case the investigated effect over a stably stratified water column is the one produced by a bottom injection of heat. The initial surface temperature is set to 22 degrees Celsius, with a decrease of 1 degree in 10 m. A 100 Wm^{-2} is injected from the bottom (Fig. 4.16). It has been impossible to compare the absolute values

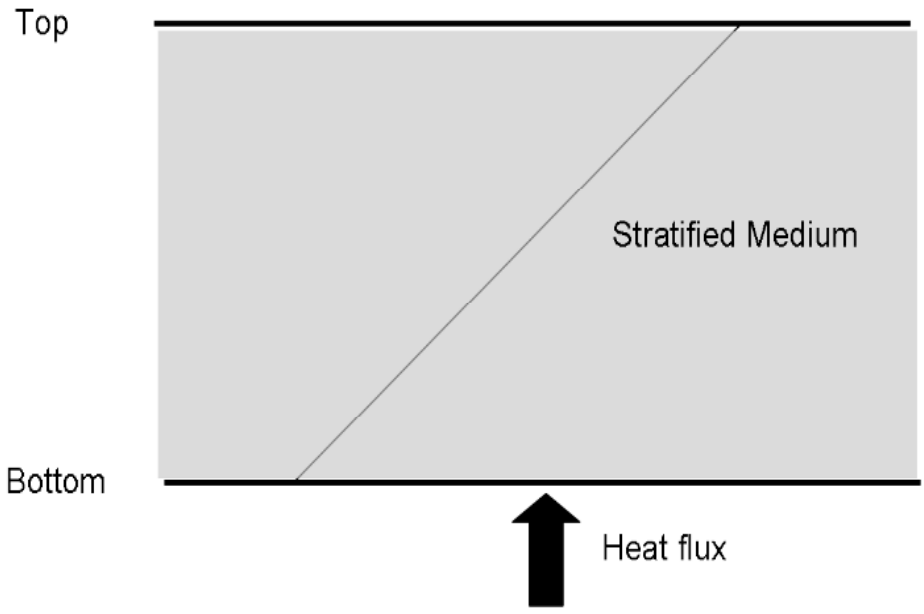

Figure 4.16: Setup of the Deardorff Experiment. Constant heat flux from the bottom on a vertically stratified medium.

of the evolution of the temperature profile in time because the axis scaling applied in Burchard and Petersen (1999) are referred to the original paper from Deardorff, not accessible. Therefore the visual comparison in trends with the Burchard and Petersen (1999) results is shown in Fig. 4.17. Even if on a different scale the temperature profiles obtained with SHYFEM are really similar to the ones from Burchard and Petersen (1999), where both the values computed making use of the k-ϵ scheme and of the Mellor-Yamada scheme are shown. In any case the two schemes give identical results in this test.

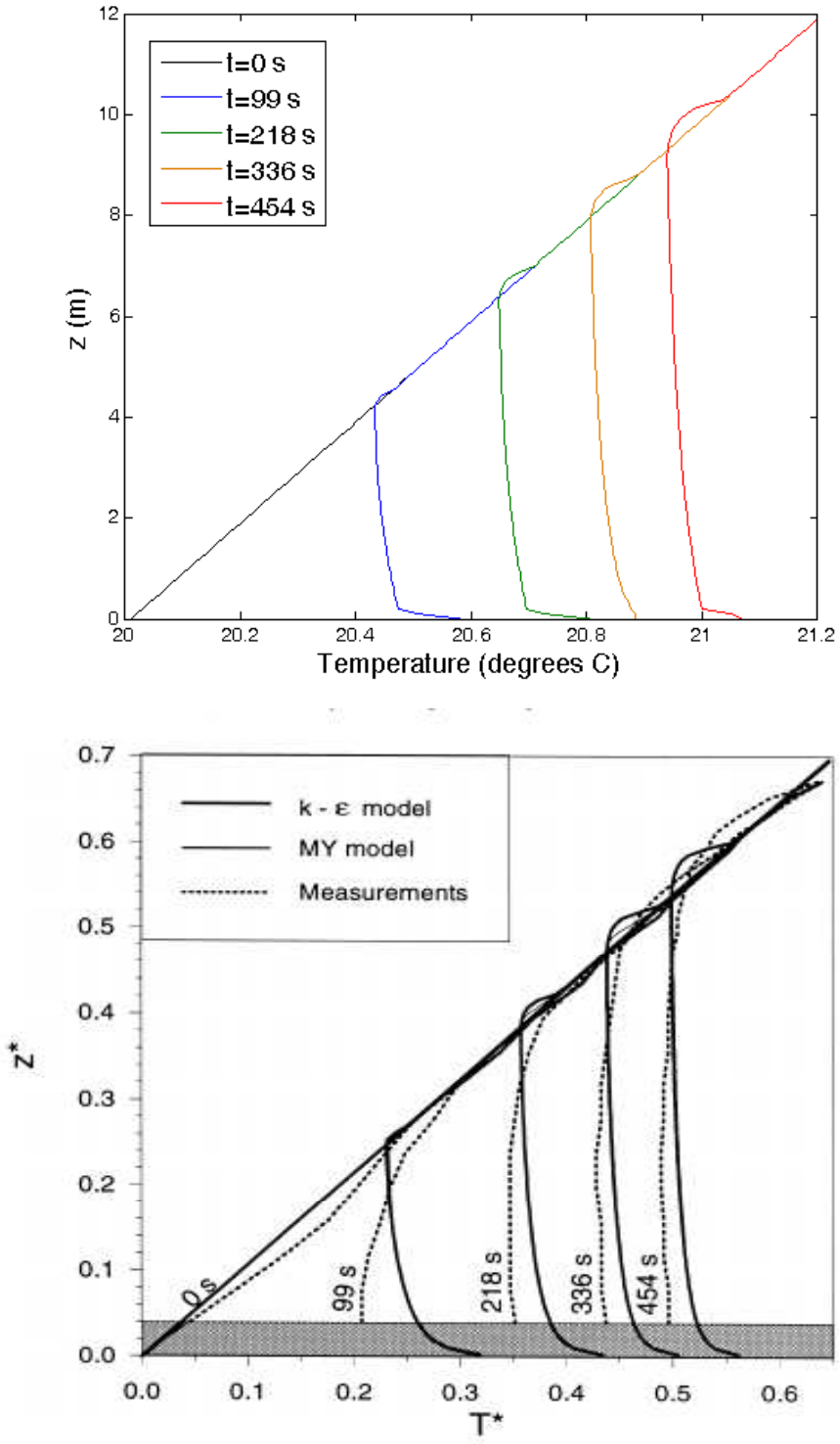

Figure 4.17: Deardorff Experiment - The upper panel shows the temperature profiles at different times obtained from the SHYFEM Model, the bottom panel shows the results of k-ϵ and MY Schemes from Burchard and Petersen (1999). The second graph uses scaled axis.

Chapter 5

Data Treatment and Model Input Preparation

The implementation of a model to study the hydrodynamic processes of a specific area is not only a mere application of a numerical tool but is also deeply connected with the availability of data both for the definition of forcings, initial, boundary conditions and for its validation. Knowing the behaviour of the principal physical variables in the study area permits to define how to choose input datasets to realistically reproduce the phenomena. As explained in chapter 1, the forcings that mainly influence the hydrodynamics in the Northern Adriatic littoral in front of the Venice Lagoon are winds, tides and temperature and salinity gradients. In the following sections the characteristics of these variables are described and information is given on the available model or measurements datasets. All these aspects are at the basis of modeling choices in terms of model grid setup and input preparation.

5.1 Wind

The meteorological contribution can affect strongly the dynamics of the water exchanges at the lagoon inlets (Gačić et al., 2002). The residual water level in the Adriatic Sea and the related residual flow through the lagoon inlets are generated by the intense meteorological phenomena that occur in this area. The first step done is an analysis on historical data to define the spatial variability of winds in the Venice Lagoon. Afterwards the chosen model input is described.

5.1.1 Historical wind dataset analysis

Several meteorological stations have been installed inside the lagoon and in its proximity for a long time. Therefore an analysis of these stations can provide a spatial pattern covering more than one century in time. The stations considered here are Istituto Bioclimatologico and ITAV San Nicoló Airport located on the Lido Island, ITAV Tessera Airport inland and the CNR Oceanographic Platform 15 km offshore. These stations permit to describe the variable from offshore to inshore, perpendicularly to the main Venice Lagoon axis (Fig. 5.1).

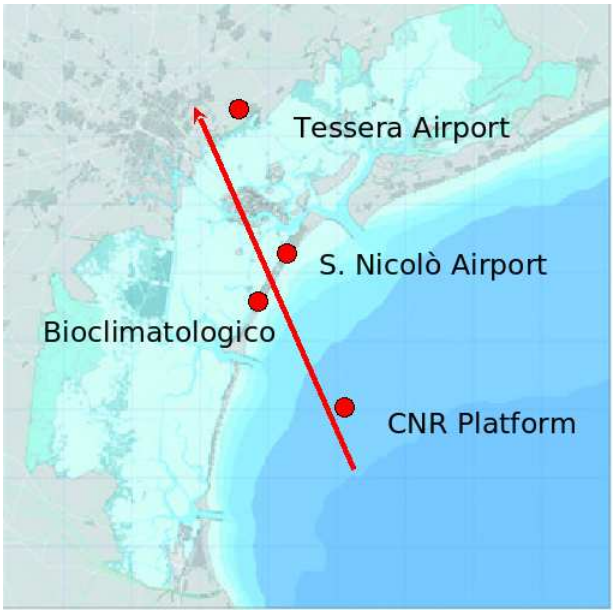

Figure 5.1: Location of the analyzed meteorological stations: CNR Platform 15 km offshore, Istituto Bioclimatologico and ITAV San Nicoló Airport on the Lido Island, ITAV Tessera Airport inland.

The majority of historical data is in the Venice Lagoon environmental database and can be downloaded from the Istituto Veneto website[1].

As a first step, basic statistics have been computed (variance, skewness and kurtosis) in order to understand if the data sets are homogeneous enough to be merged into a unique data set. This procedure is necessary because the three locations, CNR Platform, Lido and Tessera, have different types

[1]http://www.istitutoveneto.it/venezia/

of anemometers. The ITAV San Nicoló Airport and the Istituto Bioclimatologico databases are merged because sequential in time and because the two stations (Fig. 5.1) are not so far from each other. The same procedure has been adopted for the CNR Platform where both ISMAR and the Venice Municipality collected data in different periods. The analyzed period reaches from 12th of March 1972 to 31th of December 1987 giving a wide temporal coverage with few data gaps.

In Fig. 5.2 the graph in the top shows a high variance for the first years of the period, probably connected with the large presence of strong wind events. In the year 1983 there is a decrease in variance, in correspondence with the change of the instrument. The Venice Municipality anemometer, that measures from 1983, is located in a higher position than the one from ISMAR. Moreover Cavaleri et al. (1984) state that the previous measurements were influenced by the Platform structure. Therefore the two datasets can hardly be considered part of the same population and this aspect has to be taken into account in the following analysis.

The second graph of Fig. 5.2 evaluates the merging of the S. Nicoló Airport and the Istituto Bioclimatologico datasets. Excluding the years 1977-1978, because of a lack of data, and two situations (1979 and 1986) where the high kurtosis value is due to extreme wind events, the rest of the timeseries is homogeneous. The two datasets are considered part of the same population.

The last graph of Fig. 5.2 shows the database of Tessera collected by the Military Air Force: once more the occurrence of extreme events in 1986 justifies the high kurtosis seen for that year.

For each location the principal wind speeds and directions are identified comparing them with the ones obtained by Pirazzoli and Tomasin (2002). In Fig. 5.3 Tessera and Lido data are expressed in fractions of a degree whereas the other data are with a unit degree variation. Wind direction, as usual in meteorology, is given as the direction of provenance. The two main wind regimes can be seen from these histograms: Bora wind from North-East and Sirocco wind from South-East. The same pattern occurs in the Tessera and CNR Platform stations, while Lido shows a high directional variability. Putting in relation the results shown in Fig. 5.4 and in Fig. 5.3, the high number of measured calm wind suggests that a filter over the low speed events can help in better defining the principal wind directions. From Fig. 5.4 another aspect has to be noted: the high frequency of strong wind events recorded at the CNR Platform is due to the ISMAR anemometer that systematically overestimates the real wind speed (Cavaleri et al., 1984). On the other hand, the other two stations show a progressively attenuated wind signal approaching the land: the mean speed for the CNR Platform is 8.16

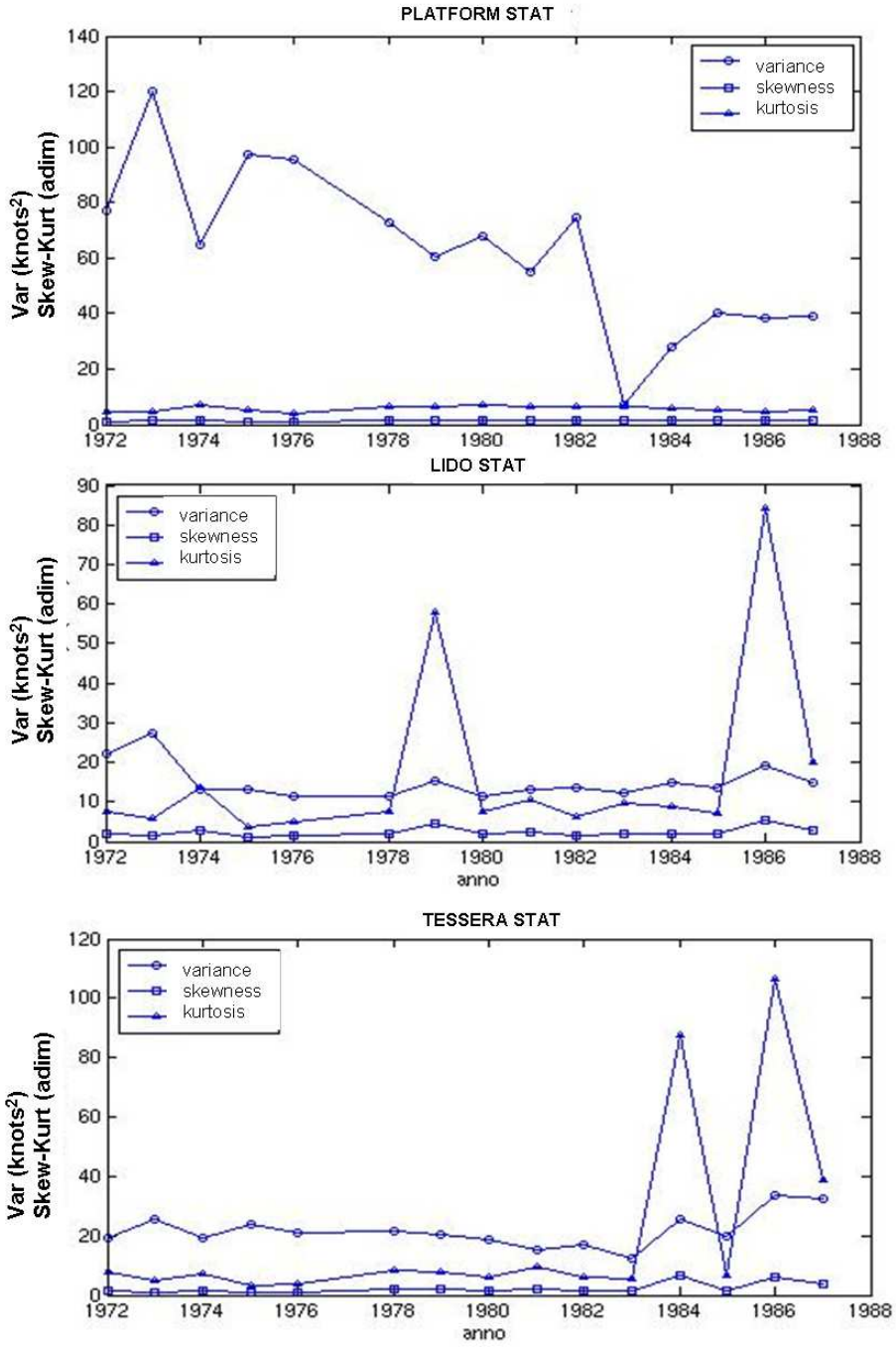

Figure 5.2: Variance, skewness and kurtosis graphs for the three locations CNR Platform, Lido and Tessera.

knots, for Lido it is 5.76 knots and for Tessera it is 4.01 knots. In Fig. 5.5 also, the maximum, the 95% percentile and the mean values for the two subsamples corresponding to Bora (provenance direction in the range 0-90 degrees) and to Sirocco (provenance direction in the range 90-180 degrees) are shown.

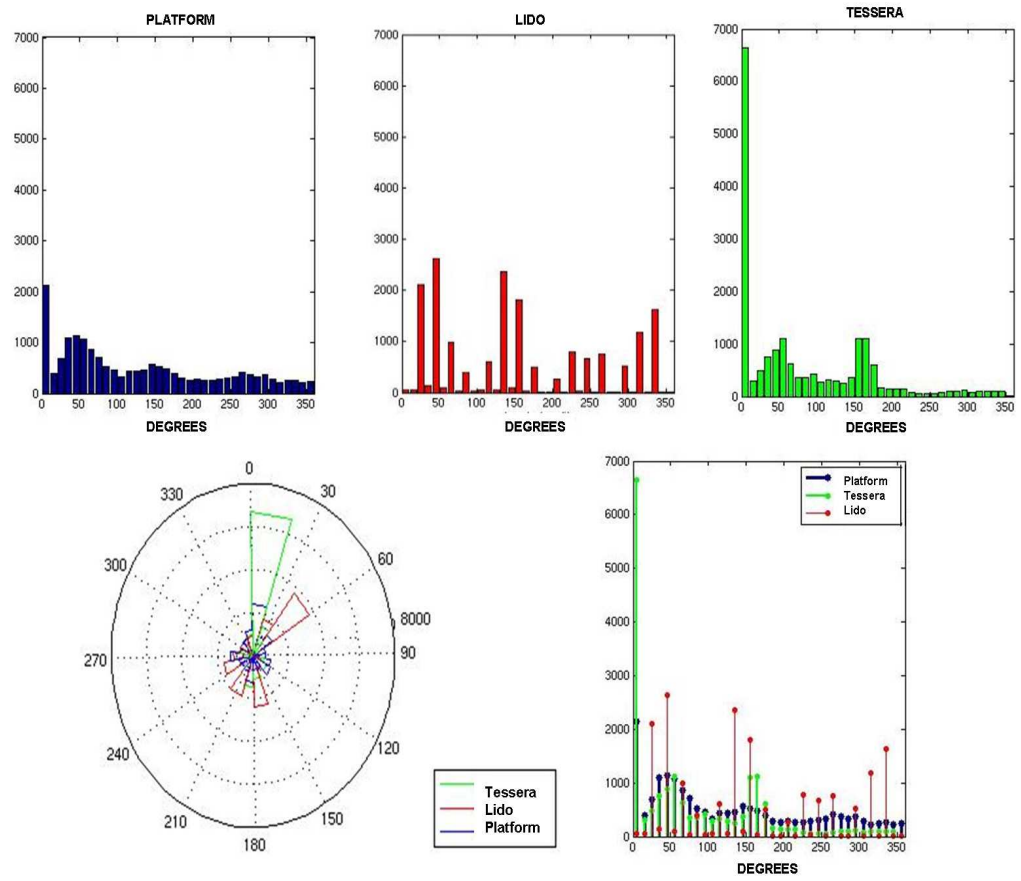

Figure 5.3: Wind Direction Histograms for the three locations: CNR Platform, Lido and Tessera.

The speed and direction correlation analysis between the stations can add information about the possible small scale spatial variability of the wind. To perform this analysis only values every three hours have been considered because the three timeseries have different sampling intervals (hourly vs 3 hours). The correlation has been computed first for the whole dataset but the obtained values are not really significant (Tab. 5.1). The correlation

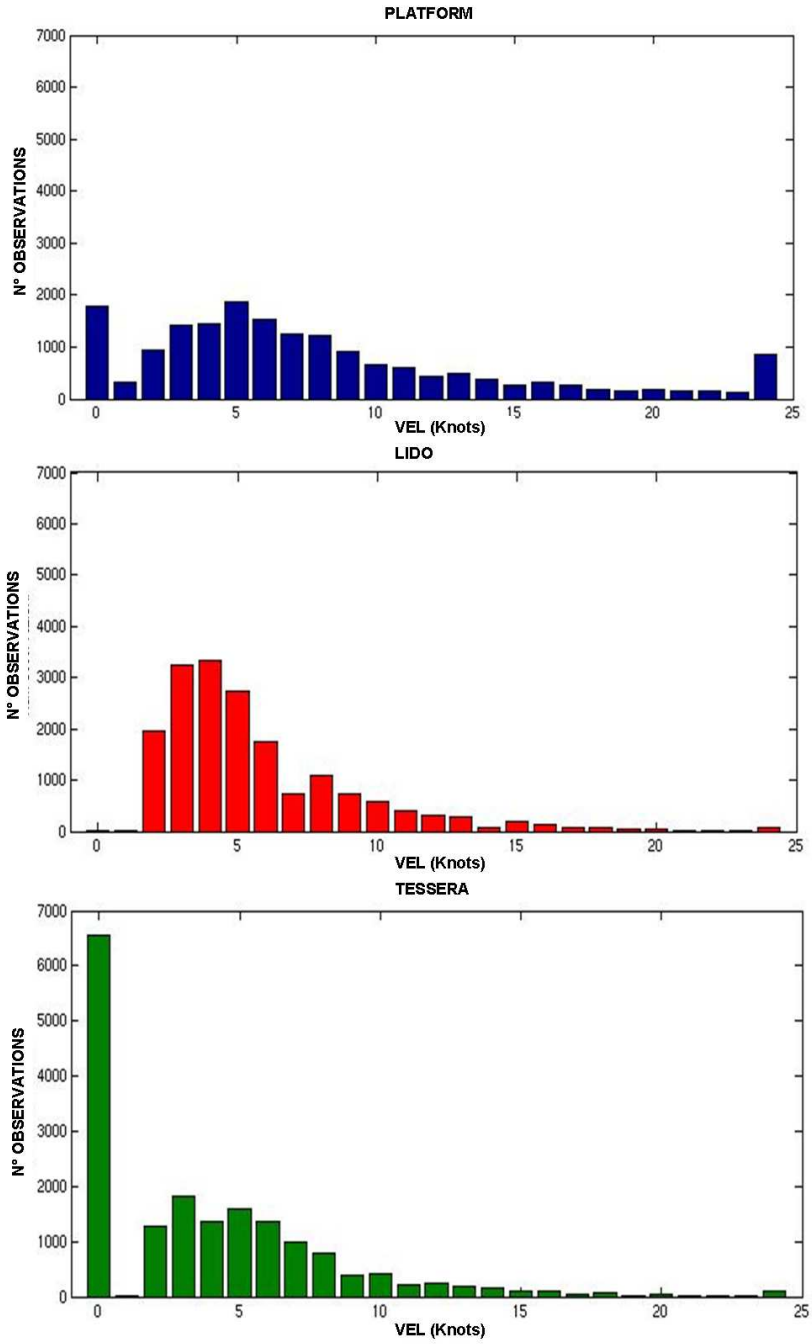

Figure 5.4: Wind Speed Histograms for the three locations CNR Platform, Lido and Tessera.

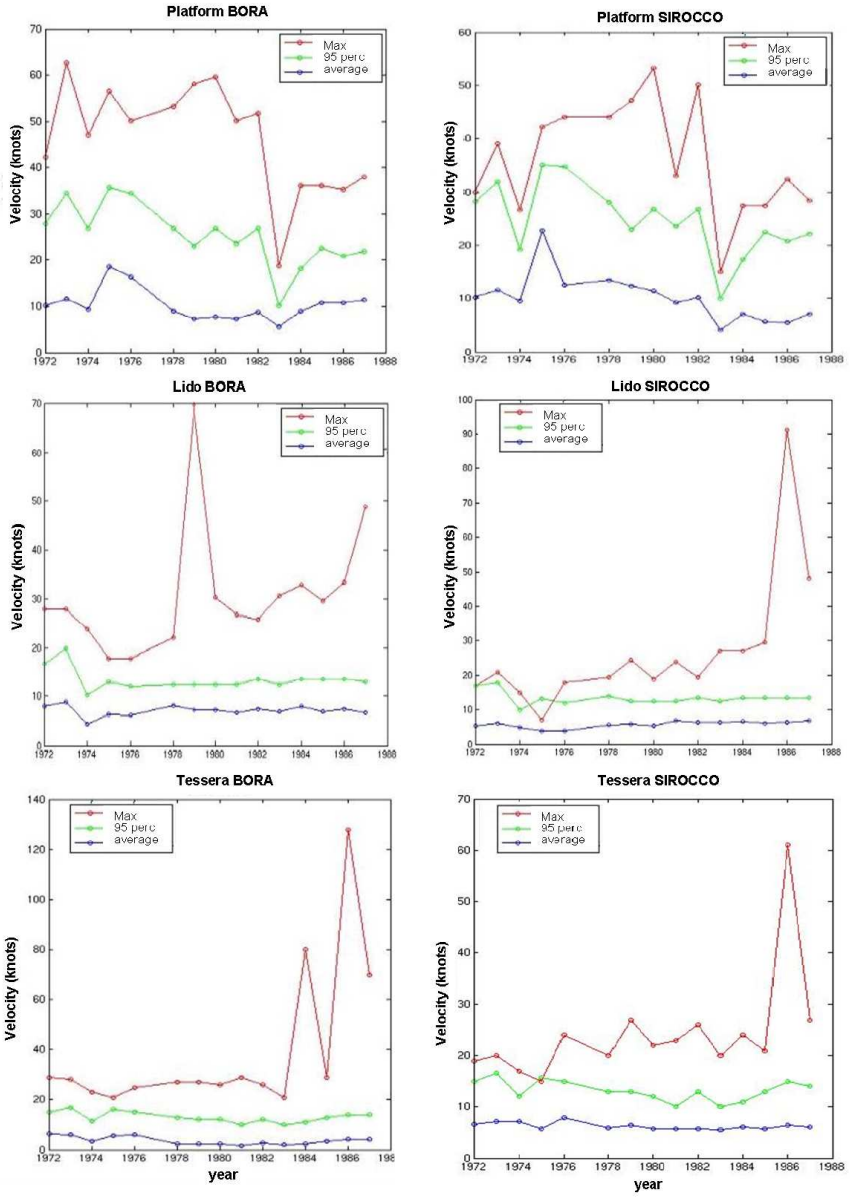

Figure 5.5: Maximum, 95% percentile and mean values for the two subsamples corresponding to Bora Events (left column) and Sirocco Events (right column)

coefficients increase if it is computed only over the Bora subsample (Tab. 5.1). Correlation coefficients obtained considering the whole dataset or filtering the data with speed lower than 5 knots are not substantially different stressing how correlation is better in semi calm regimes than during extreme events. During extreme wind events high errors in the detection of the real direction can arise because of the high directional variability so that the definition of the Bora and Sirocco subsamples can be a difficult task. This aspect can explain the small correlation coefficients computed for the wind events subsamples. Both for the whole dataset and for the two subsamples, the CNR Platform and the Lido stations are the best correlated, because spatially closest.

Table 5.1: Table of the correlation coefficients for the whole set of data and for the Bora and Sirocco subsamples. Also the correlation coefficients for the datasets where speeds below 5 knots are filtered is shown.

	Corr Coef			Corr Coef v<5knots		
Stations	ALL	BORA	SIROCCO	ALL	BORA	SIROCCO
Ptf-Lido	0.6071	0.6971	0.6599	0.5264	0.6599	0.6501
Lido-Tes	0.6874	0.6601	0.5479	0.4365	0.5479	0.5057
Tes-Ptf	0.5491	0.5937	0.5904	0.4256	0.5904	0.5458

Moreover, the monthly average speed values have been computed for the period March 1961 - December 1987 to study possible trends. Fig. 5.6 shows the monthly averaged values for March, August and November. It stresses an attenuation of the signal in the recent years, particularly for November in the CNR Platform station. A more uniform behaviour is seen for the other two stations. No further trend analysis has been done because the period is not long enough and with gaps in the timeseries.

The average of the monthly averaged speeds have been computed following the approach of Pirazzoli and Tomasin (2002) to better define the spatial characteristics of the wind field. In Fig. 5.7, once more, the progressive attenuation of the signal going inshore is seen and the Lido and Tessera stations present the same trend. A different picture is seen for the CNR Platform station during the winter months, which can be explained by the extreme events occurring especially in the open sea not reaching the coast.

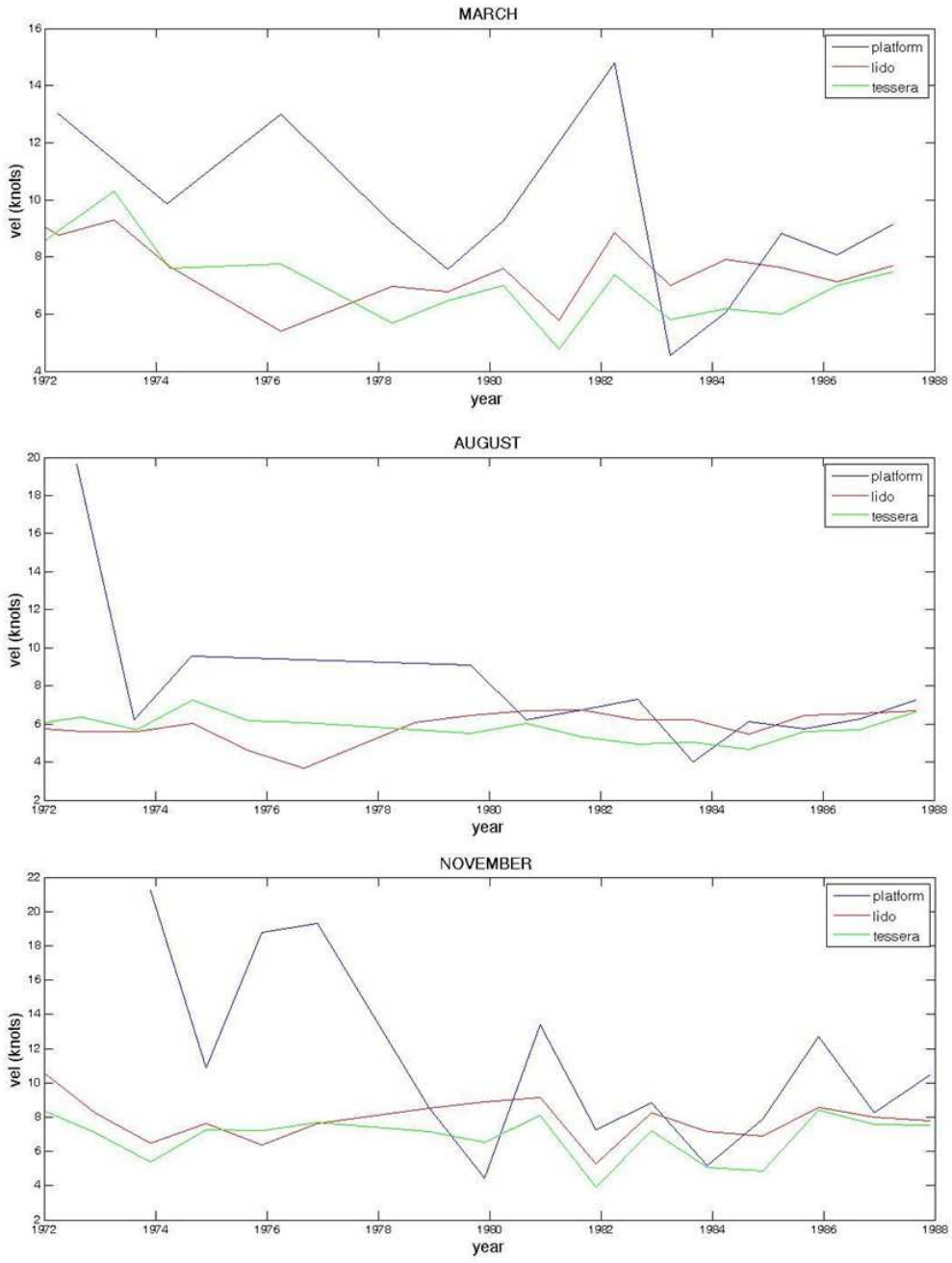

Figure 5.6: Monthly averaged value for each year for the three locations CNR Platform, Lido and Tessera. The month of March (upper panel), August (middle panel) and November (lower panel) are shown.

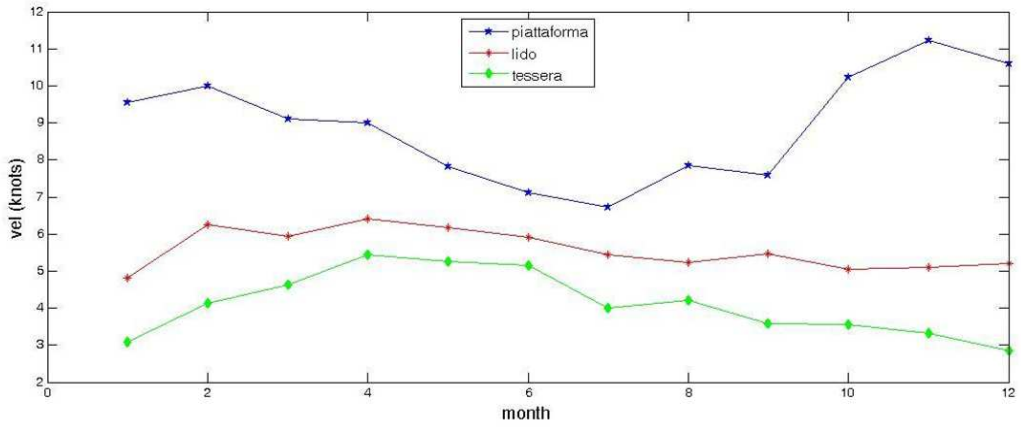

Figure 5.7: Average of the monthly averaged values over the period 1972-1987 for the three locations CNR Platform, Lido and Tessera.

5.1.2 Wind database used as model input

The previous analysis about the local variability of the wind field gives an important information for the model input treatment. Wind and pressure fields over the whole Adriatic Sea are the needed surface boundary forcings. The available wind fields are the 0.5x0.5 degrees T511 ECMWF (European Centre for Medium Weather Forecast) 6 hours data.

As previous studies pointed out (Cavaleri and Bertotti, 1996), these data underestimate the real meteorological status, especially in the Venice Gulf, where the meteorological phenomena are more intense at the synoptic scale. In the last years various correction factors have been proposed for ECMWF wind fields over the Mediterranean sea, both in direction and speed. In this work a spatially variable correction factor provided by Cavaleri and Bertotti (1996) has been applied on the wind dataset used to force the model. In Cavaleri and Bertotti (1996) the corrected wind fields have been compared with measured data in the CNR Oceanographic Platform, 15 km offshore in front of the Venice Lagoon (Fig. 5.1).

The same correction mask has been adopted to set up an operational storm surge finite element model at the Venice Municipality (Bajo et al., 2007) with the aim of forecasting the water level elevation generated by the meteorological action (the residual water level). During this application it has been seen that it was not necessary to apply the correction mask to the pressure because it is correctly reproduced by the ECMWF model over the whole

basin (Zampato et al., 2005). The results obtained are in good agreement with other forecast models of the area.

The introduction of the correction mask gives a certain confidence on the correct reproduction of the open sea wind field in front of the Venice Lagoon. Anyway, the previous analysis done on the wind variability going inshore gives the awareness that there is a difference close to the coast between the real winds and the input values introduced in the model. This aspect will be taken into account trying to interpret the modeling results.

5.2 Tides and Currents

Because one of the goals of this work is the simulation of interaction processes between the Venetian Lagoon and the open sea, a fundamental role is played by the tidal forcing. ADCP measurements at the Lido inlet stress the major role of tides in the inflow-outflow cycle (Gačić et al., 2002).

In this work two different sets of measured data are used to calibrate and validate model results. The first dataset consists of the harmonic constants (amplitude and phase) of the main tides that characterize the sea surface elevation (SSE) of the Adriatic Sea. For the lagoon inlets and for the Otranto Station the harmonic constants are computed from available time series, ISMAR data for Lido and APAT (Environment Protection Agency) data for Otranto. The second dataset contains the discharge data through two of the three lagoon inlets measured by ADCP probes.

5.2.1 Tidal data

The Adriatic sea is a basin characterized by moderate tides. The highest amplitudes are found in the Northern sub-basin, extending from the line connecting Pesaro to Kamenjak to the Northern coast (Fig. 3.1), where the amplitude of the M2 frequency reaches 0.266 m. Because of the impact of this phenomenon in the area, tidal observations in the Northern sub-basin have been collected from the middle of the 18th century. Three relevant stations are present in the Northern part of the basin, Trieste, Venezia-Lido, Rovinj (Fig. 3.1), where the monitoring of tidal behavior covers more than a century.

Modeling the tidal currents in the Adriatic Sea means to be able to reproduce the behavior of the seven main tidal constituent in the basin, the four semidiurnal ones M2, S2, N2, K2, and the three diurnal ones, K1, O1 and

P1 (Polli, 1960). The knowledge about tides in the Adriatic Sea derives from previous works (Polli, 1960, 1961; Mosetti, 1987) where the main harmonic constituents were derived analyzing the tide gauge measurements in a number of stations along both the western and the eastern coast (Fig. 3.1).

For what concerns the tides in the Venice Lagoon, measured data of amplification and delay of the main diurnal and semi-diurnal constituents with respect to the Diga Sud Lido tide gauge are reported for many stations inside the lagoon by Goldmann et al. (1975). This dataset has been considered for the calibration of the model to reproduce the tidal propagation in the Venice Lagoon (Umgiesser et al., 2004).

Recently, new harmonic constants, calculated from tide gauges time series, have been provided for the Venice Lagoon by the Environment Protection Agency APAT (Ferla et al., 2007). In the same paper even an accurate analysis on long term variations in the tidal regime in the Venice Lagoon has been presented. From this data set the harmonic constants for the Lido station has been derived.

From a comparison between the cited papers, the two sets of harmonic constants computed for the lagoon are significantly different and the main hypothesis is the influence of the deep morphological changes occurred in the last century (Ferla et al., 2007).

5.2.2 The flow rate ADCP data

Recent campaigns in the area of interest provide ADCP data for years 2001-2002. The aim of these measurements is to study the time-dependent variability of the inlet currents as well as of water exchange rates. The current data have been collected using bottom-mounted ADCPs installed in each inlet. Current speed and direction along the water column are recorded every 10 minutes with a vertical resolution of 1 meter in selected locations inside the inlets.

During a preliminary phase, measurement campaigns have been carried out to estimate the relationship between the vertically averaged water velocity collected by the fixed ADCP and the inlet flow rate. About 100 ship-borne ADCP surveys were conducted to estimate the water inflow and outflow through each inlet both during spring and neap tide.

Comparing the discharge results with the vertically averaged velocity collected by the bottom mounted ADCP for the same period, the parameters of a linear correlation function have been calculated (Gačić et al., 2004). Therefore, the flow rate is available every 10 minutes applying the calculated

linear regression formula to the vertically integrated measured current values (Gačić et al., 2002).

5.3 HF Radar

The HF Radar dataset of surface currents is used for the comparisons with simulations. The dataset is the result of records taken by three antennas, two of them located along the coast near the Venice Lagoon in Lido and in Pellestrina and one at the CNR Oceanographic Platform, located 15 km offshore (Fig. 5.8). The specific description of the collection of data and their analysis can be found in Kovačević et al. (2004). In this work the used data are hourly values, low-pass filtered, to eliminate the influence of inertial frequencies, and detided, to permit the analysis of residual currents (Kovačević et al., 2004). The HF Radars installed in the littoral area in front of the Venice Lagoon have an efficiency angle where the radial measurement is not affected by high errors, in the range of 30-150 degrees. Along the ideal line that connects the antennas there is a so called blind area where measurements cannot be considered correct, because of signal refraction effects and propagation loss (Kovačević et al., 2004). After post processing (that includes the elimination of spikes) the HF Radar data are interpolated onto a regular grid with grid size of 750 m.

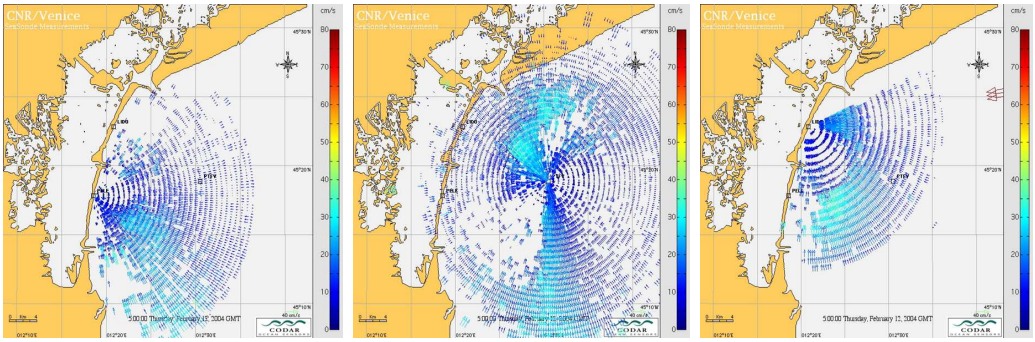

Figure 5.8: Maps of the HF Radar coverage in the proximity of the Venice Lagoon. Two of them are located on the Pellestrina and Lido Islands, the third is at the CNR Platform. Codar HF Radar images.

5.4 Temperature and Salinity

Water temperature and salinity are fundamental values if the aim is to reproduce the coastal currents due to thermohaline gradients.

During the search of the best database that fits the coastal modeling needs, two problems had to be solved: no measurements from cruises or transect could be used because they did not cover the whole basin. On the other hand, many models provide temperature and salinity data over the whole Mediterranean Sea but with low resolution.

The temperature and salinity 3D matrices adopted as initial condition are from MFStep (Mediterranean Forecasting System Toward Environmental Predictions) daily dataset. They are computed by the OPA Model and their horizontal resolution is 1/16 of a degree[2].

This database is considered a good compromise between spatial and temporal coverage and high resolution. On the other hand the models applied in MFStep introduce approximations and they are forced with climatological forcings that not permiting to resolve a number of processes. Additionally there is the awareness that, using these fields as initial and boundary conditions, an error is introduced along the coast also because the model resolution cannot cover up to the real coastline but only up to some kilometers offshore. Therefore a linear extrapolation is the proposed solution, adding, along the coast, the thermohaline information coming from rivers.

In the 3D simulation also the river discharge has to be imposed in the North Adriatic Littoral. The annual mean values provided by the Basin Authority of Friuli Venezia Giulia have been imposed as river open boundaries forcings. Daily discharge values are provided for the Po river, because this time step permits to describe in a realistic way the high variable changes that occur seasonally and that strongly influence the dynamics of the Northern Adriatic Sea.

[2] $www.bo.ingv.it/mfstep/WP8/model_des_opa.htm$

Chapter 6

Modeling Barotropic Processes

The given description of the context in which the processes study is done and the definition of the main forcings needed to simulate them permit to do a step further, the numerical reproduction. In this chapter and in the next, the system complexity is faced starting from a 2D investigation connected with all the coastal and interaction barotropic processes to reach, then, a more general physical view, even exploring the water column and the baroclinicity.

In this chapter the tidal currents reproduction is the focus and the water mass balance between the Venice Lagoon and the open sea is investigated, both in terms of tidal and residual signals.

6.1 The 2D Simulation Setup

All simulations presented in this part are for the year 2002 and have been carried out using a time step of 300 seconds. This time step could be achieved due to the unconditionally stable time integration scheme of the finite element model. The bathymetric data interpolated on the Adriatic Sea finite element grid (Fig. 6.1) are taken from the NOAA 1 minute resolution dataset. All simulations have been run with the same wind forcing of the year 2002 and the lateral boundary conditions at the Otranto strait for the water levels derived from the harmonic constants and the storm surge model. The open boundary has been chosen as a straight line across the Strait of Otranto (Fig. 6.2). This parameterization was suggested by the results obtained in a previous work by Cushman-Roisin and Naimie (2002) who applied with success a finite element tidal model of the Adriatic Sea. This seems a logical choice for the

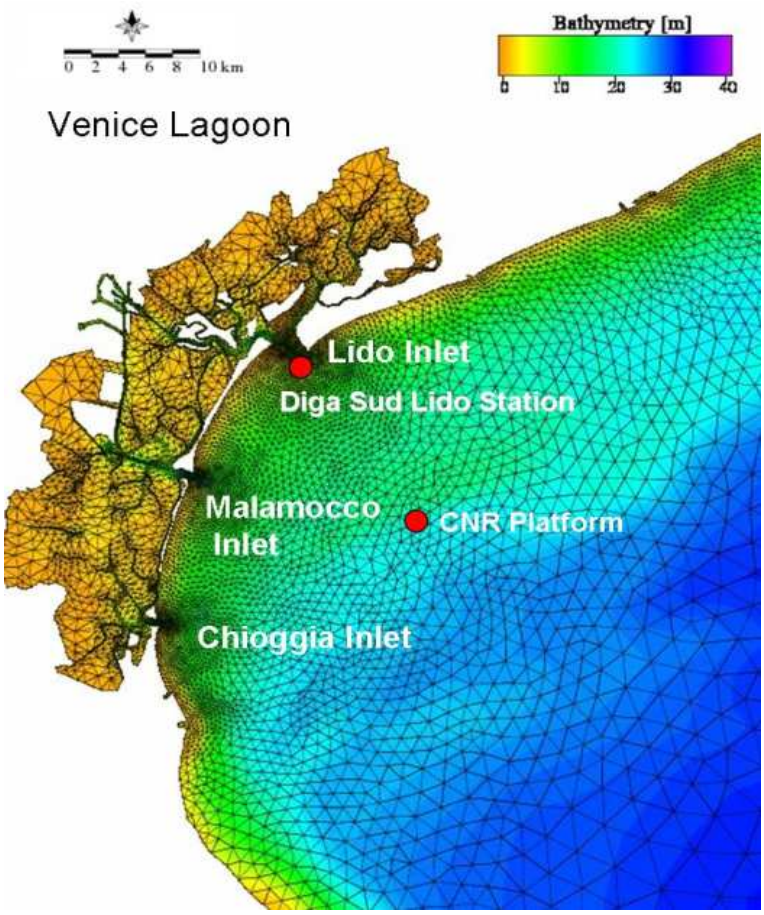

Figure 6.1: Bathymetry and finite element grid of the Venice Lagoon and the Gulf of Venice, a subset of the numerical domain of the model.

Adriatic Sea being the Strait of Otranto the narrowest part of the whole basin. Furthermore, being the Otranto line far away from the study area (Venice Lagoon and northern Adriatic coast), disturbances to the numerical solution for the region of interest, induced by the artificial imposition of boundary conditions, can be avoided. At each node of the Otranto open boundary, water level time series are imposed. They are obtained by adding a surge signal coming from an operational storm surge model (Bajo et al., 2007) to the astronomical tide computed from harmonic constants. The contribution of the fresh water input released inside the basin by the main Italian rivers is not taken into account. Flow discharge measurements at the Malamocco inlet register a flow rate of 10000 m^3s^{-1} and all three inlets together may show

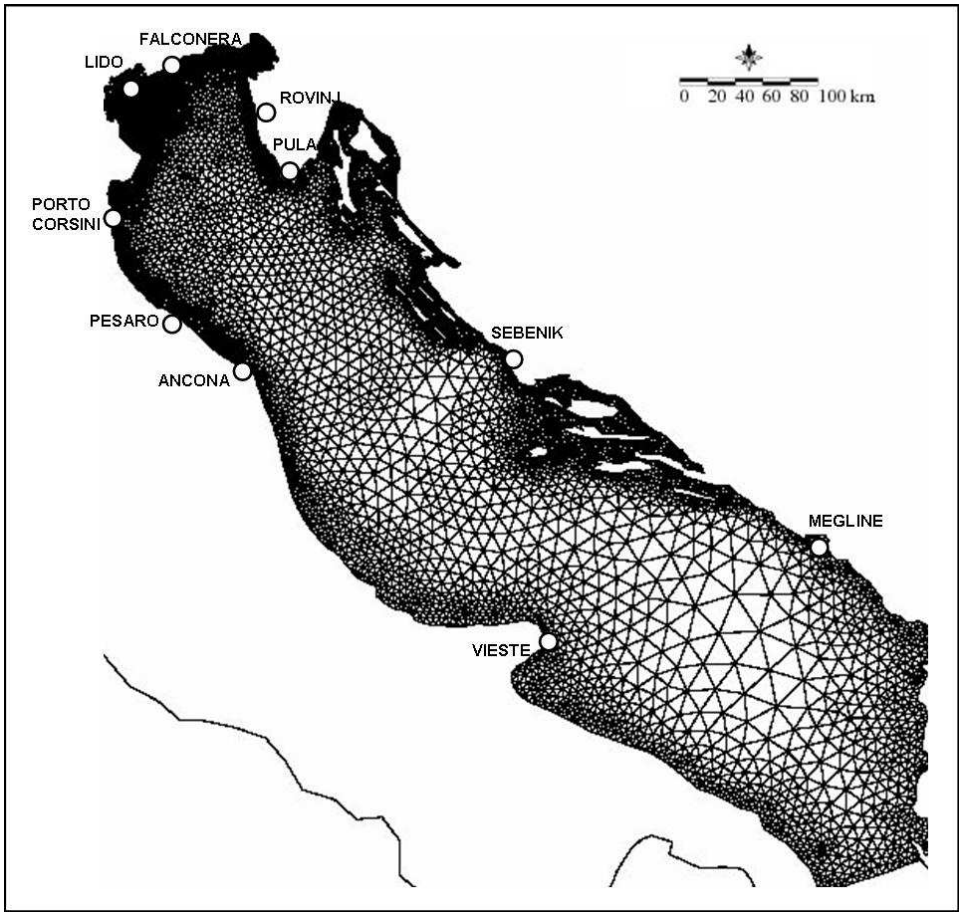

Figure 6.2: The numerical domain of the Adriatic Sea and the location of the tide gauges considered during the calibration process.

flow rates as high as 24000 m^3s^{-1}. This numbers can be compared with the main river in the Adriatic Sea, the Po river, that shows an average discharge rate of 1500 m^3s^{-1} (Gačić et al., 2002). Even if the river run-off strongly influences the baroclinc circulation in the Adriatic Sea, it is far from giving appreciable contributions to the barotropic water circulation in the coastal area in front of the Venice Lagoon. In particular, considering the Po river runoff, the advective fluxes and the water level gradient induced by the river discharge induce a momentum flux over the water column which influences the water circulation only locally. Simulations in Umgiesser and Bergamasco (1998) show how the jet created by the Po first deviates to North East but then deflects southward due to the conservation of potential vorticity. Maps

show how it does not influence the study area near the inlets of the Venice Lagoon. Therefore the influence of the barotropic contribution of the Po river runoff on the sea-lagoon water exchanges and local water circulation can be neglected.

The bottom boundary condition enforces quadratic friction based on barotropic (depth-averaged) velocity according to the classical quadratic drag law. In this application two formulations for the bottom friction coefficient c_B have been considered. For the deeper areas of the domain (Adriatic Sea) the coefficient is imposed to be constant with a value of $2.5{\cdot}10^{-3}$. However, in the shallow parts (Venice Lagoon) the Strickler formula has been used where the friction parameter depends on the water depth. This approach was suggested by the application of the model to the Venice Lagoon alone (Umgiesser et al., 2004). Inside the lagoon, different Strickler coefficient have been used to distinguish the behavior of channels, tidal flats and the rest and at the three inlets slightly different values of this coefficient are used in inflow and in outflow conditions to parameterize the unresolved physical processes such as the local head loss due to sudden expansion of the out-flowing water (Umgiesser et al., 2004).

What concerns the wind drag coefficient c_D, a constant value of $2.5{\cdot}10^{-3}$ has been adopted. The lateral diffusion parameter A_H has been set to 0. The initial conditions for the water levels and the velocities are zero in the whole basin and a spin-up time of 30 days for all the simulations has been imposed (Cucco and Umgiesser, 2005). This time was enough to damp out all the noise that was introduced through the initial conditions.

6.2 Barotropic Simulation Results

In this section the model results are presented. First the model calibration through harmonic constants is described and then the water levels are validated. In the third section, the fluxes through the lagoon inlets are computed and compared with the ADCP data. The fourth part analyzes the reproduction of the total levels and fluxes, considering both the astronomical and the meteorological signals. Finally the focus is the reproduction of strong wind events, considering the two major winds blowing in the Northern Adriatic. The first one, is the cold Bora wind from NE, that characterizes extreme events generally occurring during winter time (Orlić et al., 1992). The second one is the wet, warm Sirocco wind, coming from SE largely present in autumn and mostly responsible for the flooding events of the city of Venice (Orlić et al., 1992).

6.2.1 Calibration of harmonic constants

The model has been calibrated to reproduce the harmonic constants of the tidal constituents M2, S2, K1, N2, K2, O1 and P1 in the Adriatic Sea and, more specifically, in the Gulf of Venice. These tidal constituents are known for Otranto from a 9 years long hourly water level time series recorded by APAT at the Otranto station. They are representative for the tides of the western Italian border of the strait. In addition to the astronomical signal, surge values, produced by a numerical model applied to the whole Mediterranean Sea, are imposed at the Otranto open boundary (Bajo et al., 2007). This surge model is adopted by the Venice Municipality, running operationally to predict the flooding in the city.

To determine the tidal constituents for the eastern Albanian border, an iterative procedure has been applied which can be schematically explained as follows. First the harmonic constants of Albania are set to the same values as the ones for Otranto. A one year long time series is produced from these constituents and the surge signal is added to these water levels. For every node on the border a linear interpolation is carried out between the water levels at Otranto and Albania.

With these water levels for the open boundary, a one year long (8760 hours) simulation is carried out. This period is needed because it is the necessary and sufficient time to separate the K2 and S2 frequencies in the harmonic analysis of results (Foreman, 1996).

At the end of each calibration run the harmonic constants are extracted from the model for the station closest to the study area, Diga Sud Lido (Fig. 6.2), and compared with the empirical ones. The differences between modelled and observed harmonic constants are then used in changing the harmonic constants imposed for the Albanian side of the open boundary. In particular, the proportion of observed and modelled amplitudes and the time lag for the phases is used to compute new tidal constituents for Albania. With these new values, a new set of boundary conditions is computed for each node on the open boundary as explained above and a new run is performed.

The calibration is ended when the difference between the amplitude of the three main measured and modeled harmonic constants (M2, S2, K1) falls below 3 % and the phase shift is less than 2 degrees at Diga Sud Lido. To reach this result, around 20 iteration were needed. At this point a comparison for the other 10 stations in the Adriatic Sea is performed to assure a realistic tidal behavior in the whole Adriatic Sea and not only an ad hoc solution for the Venice Lagoon.

6.2.2 Water level validation

First a comparison between modeled and measured harmonic constants at Diga Sud Lido station has been carried out. In Tab. 6.1 the set of harmonic constants obtained at Diga Sud Lido from the model calibration and from measurements taken by ISMAR-CNR in the year 2002, is shown. In Tab. 6.2

Table 6.1: Comparison between model results (m) and observations (o) of the amplitude H and phase g of the whole set of tidal data at Diga Sud Lido station.

Constituent	H_m [cm]	H_o [cm]	g_m [deg]	g_o [deg]
M2	23.00	23.38	292.5	291.4
S2	14.67	14.71	298.2	296.7
N2	4.13	4.16	290.4	290.1
K2	5.67	5.83	312.8	311.3
K1	20.53	20.00	88.6	87.9
O1	6.32	6.55	59.0	53.4
P1	5.56	5.39	70.9	72.0

the final set of harmonic constants of the open boundary (Otranto and Albania) is listed. In Tab. 6.3 and Tab. 6.4 the amplitudes and the phase lags of the main semi-diurnal and diurnal tides (M2, S2 and K1) are compared with the observations along the coasts of the Adriatic sea (see Fig. 6.2 for reference).

The phase in the table is expressed with respect to the meridian of Central Europe, as conventionally applied in Polli (1960). As explained in Tomasin (2005) the harmonic constants are subject to the periodical changes in the orbits of the sun and moon and for this reason they slightly change in time. The algorithm described in Tomasin (2005) gives the opportunity to update the date shown in Polli (1960), annualizing them for the year 2002.

As I could expect, the calibrated model reproduces the SSE at Diga Sud Lido station with high accuracy. I do not show the comparison graph for Lido Station because the results are quite obvious even on the basis of the harmonic constants shown in Tab. 6.1: small differences with observed data for the harmonic constants in this station are registered, with differences

Table 6.2: Open boundary condition. Amplitude H and phase g of the main tidal constituents for the western (Otranto, O) and eastern station (Albania, A) of the SSE imposed as forcing along the open boundary of Otranto.

Constituent	H_O [cm]	g_O [deg]	H_A [cm]	g_A [deg]
M2	6.8	133.1	8.58	59.33
S2	4.0	141.0	4.65	71.89
N2	1.2	131.2	1.61	1.84
K2	1.1	136.9	1.52	221.33
K1	2.3	91.1	4.04	19.33
O1	0.9	75.7	1.71	33.77
P1	0.8	85.1	1.37	29.04

of millimeters in amplitude and some degrees for the phases; the highest difference at Diga Sud Lido is less than five degrees for the O1 component which is one of the less important components of the ones taken into account. The area of interest for this application is the Northern Adriatic Sea, which is limited in the Southern part by the line connecting Pesaro to Pula (Fig. 6.2). The stations located in this area are Falconera, Porto Corsini, Trieste, Rovinj, Pesaro and Pula (Tab. 6.3). In the northern half of the basin the two semi-diurnal components are well reproduced with an absolute difference in amplitude never higher that 2 cm (Tab. 6.3). Following the North-East coast of the basin, amplitude differences are oscillating slightly around zero. These two harmonic components are quite in phase with measurements, with differences never higher than -6.7 degrees. This value is reached in Falconera station. There is a 20 minutes delay in the modelled data for these components. In the same stations the major diurnal component is well reproduced, with -1.93 cm (-7 %) as the highest difference in Trieste. When considering what is the main aim of this work, the modeling of the interaction between the Venice Lagoon and the open sea, these results can be considered satisfactory. For the other stations in the Adriatic Sea, the result for Ancona station is striking. Near Ancona the M2 amphidromic point is located. This means that tidal variation are small and water level measurements can be affected by higher errors because of the low signal to noise level. This could explain the high difference in phase (around -12 degrees). Going South, a general

Table 6.3: Comparison between model results (m) and observations (o) of the amplitude H and phase g of the most energetic tidal constituents (M2, S2 and K1) at the tidal stations in the northern part of the Adriatic Sea.

Site		H_m [cm]	H_o [cm]	H_m - H_o [cm]	$(H_m - H_o)/H_o$ [%]	g_m [deg]	g_o [deg]	g_m-g_o [deg]
Lido	M2	23.30	23.38	-0.08	-0.3	286.2	285.1	0.6
	S2	14.67	14.71	-0.04	-0.3	298.1	296.7	1.4
	K1	20.53	20.00	0.53	2.6	78.5	77.8	0.7
Porto	M2	16.54	15.50	1.04	6.7	301.2	305.10	-3.9
Corsini	S2	10.31	9.2	1.11	12.1	306.9	310.0	-3.1
	K1	18.89	16.5	2.39	14.5	92.5	89.3	3.2
Falconera	M2	23.01	23.8	-0.79	-3.3	285.0	291.1	-6.1
	S2	14.80	14.10	0.70	5.0	290.3	297	-6.7
	K1	20.49	19.0	1.49	7.84	85.4	87.3	-1.9
Trieste	M2	24.47	26.4	-1.93	-7.31	280.9	278.1	2.8
	S2	15.84	16.00	-0.16	-1.0	286.1	284.0	2.1
	K1	20.81	19.3	1.51	7.82	83.4	78.3	5.1
Rovinj	M2	17.94	19.10	-1.16	-6.1	272.7	272.1	0.6
	S2	11.38	11.2	0.18	1.6	277.2	277.0	0.2
	K1	19.13	16.7	2.43	14.55	80.2	79.3	0.9
Pula	M2	14.82	15.0	-0.18	-1.2	266.1	267.1	-1.0
	S2	9.28	8.7	0.58	6.7	269.9	273.0	-3.1
	K1	18.19	16.1	2.09	12.98	78.4	77.3	1.1

Table 6.4: Comparison between model results (m) and observations (o) of the amplitude H and phase g of the most energetic tidal constituents (M2, S2 and K1) at the tidal stations in the southern part of the Adriatic Sea.

Site		H_m [cm]	H_o [cm]	H_m - H_o [cm]	(H_m - H_o)/H_o [%]	g_m [deg]	g_o [deg]	g_m-g_o [deg]
Pesaro	M2	11.23	12.7	-1.47	-11.57	310.5	313.1	-2.6
	S2	6.77	6.8	-0.03	-0.4	316.9	313.0	3.9
	K1	17.34	16.0	1.34	8.38	95.3	92.3	3.0
Ancona	M2	6.15	6.5	-0.35	-5.38	324.0	334.1	-10.1
	S2	3.46	3.5	-0.04	-1.1	333.9	347.0	-13.1
	K1	15.59	13.7	1.89	13.80	96.3	96.3	0.0
Sebenik	M2	6.16	6.2	-0.04	-0.65	138.9	137.1	1.8
	S2	4.46	4.4	0.06	1.4	138.7	132.0	6.7
	K1	11.48	9.7	1.78	18.35	70.9	65.3	5.6
Vieste	M2	8.71	9.3	-0.59	-6.34	103.8	107.1	-3.3
	S2	5.81	6.0	-0.19	-3.2	110.0	115.0	-5.0
	K1	6.92	5.3	1.62	30.57	102.8	99.3	3.5
Megline	M2	9.440	9.0	0.44	4.88	108.3	101.1	7.2
	S2	6.16	5.9	0.26	4.4	112	103.0	9.0
	K1	6.85	5.2	1.65	31.73	73.8	60.3	13.5

overestimation of the diurnal component K1 can be observed but it has to be mentioned that the difference never exceeds 1.5 cm, even if this translates into a high error in terms of percentage (Fig. 6.3, middle panel, Tab. 6.4). The relatively high amplitude errors for K1 in the stations of the Dalmatian coast should be stressed. This might be due to the grid resolution along the coast. Because of the interest in simulating the North Adriatic coastal dynamics, the applied finite element grid has high resolution in proximity of the Venice Lagoon. The Dalmatian coast is less resolved than the Northern part of the Adriatic Sea, because of the attempt to limit the number of elements of the grid and to lower the time of computation.

For the other two components, M2 and S2, no general trends in amplitude difference can be observed. Phase differences do oscillate around zero for all the stations along the Adriatic Sea, increasing in module approaching the southern open boundary at the Otranto Strait (Fig. 6.3, lower panel). A smooth anticipation of the real signal along the low resolved eastern coast of the southern Adriatic and a specular delay along the western littoral, near Vieste station (Fig. 6.2), is observed for these harmonic constituents. The presence of the open boundary, where water levels are imposed, is certainly influencing the results for the stations located close to it.

In conclusion, the choice of moving the open boundary to the Otranto strait was correct. In the southern part of the basin, errors are higher, mostly due to the influence of the open boundary. On the other hand results in the Northern part of the basin do not evidence an influence of these modeling choices. What concerns the model results of the propagation of the tide inside the Venice Lagoon I always refer to Umgiesser et al. (2004) for a more accurate description.

6.2.3 Flux data validation

Once the model had been calibrated and validated with the water levels, it has been used to estimate the water exchange through the three inlets. The presence of both tidal and meteorological data forcings has to be stressed because the simulation of barotropic currents in the Adriatic Sea needs to consider the whole set of significant forcings. From the evidence of measurements at the inlets it can be deduced that the flow acceleration is generated by the pressure gradient due to the sea-level slope. Velocities are of the order of 1 m/s and the bottom friction term is balanced by the local acceleration and the horizontal pressure gradient (Gačić et al., 2004). The wind action is mainly barotropic at the inlets (Gačić et al., 2002). The conjunction of tidal

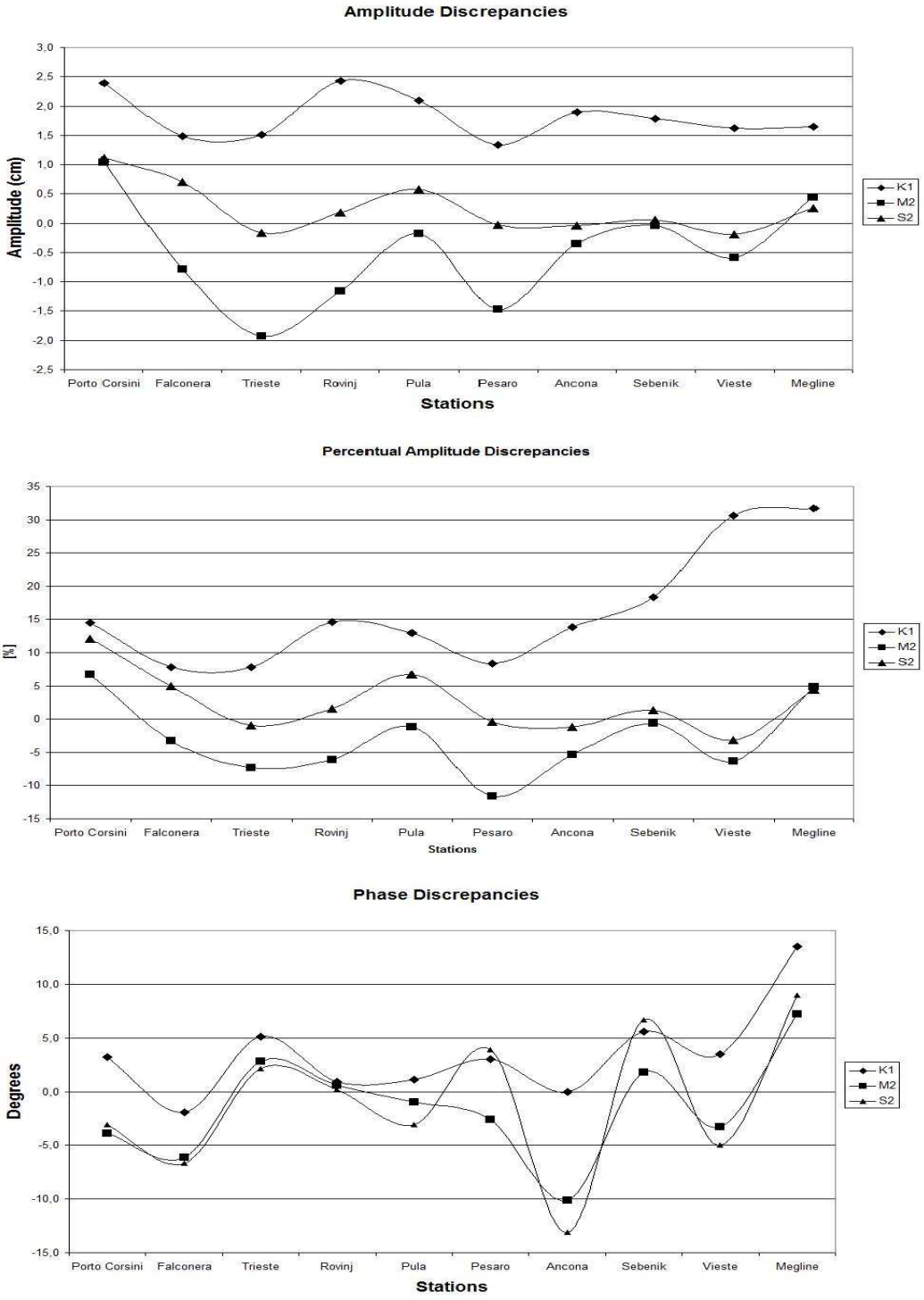

Figure 6.3: Graph of amplitude, relative amplitude and phase differences of the three main modeled and measured harmonic constants (M2, S2, K1) for the ten stations in the Adriatic Sea.

cycles and atmospheric pressure and wind produces extreme events propagating into the lagoon from the inlets, in particular when SE wind (Sirocco) is blowing in a low pressure configuration (generally in winter time) (Gačić et al., 2004).

To validate the model results, only the tidal signal of the measured discharge data has been considered. Harmonic analysis is therefore applied to the ADCP data collected at Lido and Malamocco inlets for the year 2002, as has been done before for the water levels. The contribution of the three major diurnal and semi-diurnal tidal components to the total flow rate - M2, S2 and K1 - is obtained and the parameters related to these constituents are presented in Tab. 6.5. As it can be seen from graphs in Fig. 6.4 the two signals match nicely. To quantify the error a comparison between the computed flux amplitudes and phases has been done in Tab. 6.5.

Table 6.5: Water discharge of the Lido and Malamocco inlet. Comparison between empirical data (o) (derived from ADCP measurements) and model results (m) of the amplitude A and phase g of the most energetic diurnal and semi-diurnal frequencies (M2, S2 and K1).

Inlet		A_m [m^3/s]	A_o [m^3/s]	$A_m - A_o$ [m^3/s]	$(A_m - A_o)/A_o$ [%]	g_m [deg]	g_o [deg]	$g_m - g_o$ [deg]
Lido	M2	4400.1	4366.8	33.28	0.76	254.9	244.8	10.1
	S2	2596.3	2504.8	91.5	3.65	267.2	255.4	11.8
	K1	1895.8	1790.4	105.4	5.9	21.3	14.4	6.8
Malamocco	M2	4725.2	4682.0	43.2	0.92	245.5	232.1	13.4
	S2	2825.0	2790.7	34.3	1.23	258.4	243.1	15.3
	K1	1892.1	1717.4	174.7	10.2	13.2	4.0	9.2

Analyzing the tidal reproduction of water fluxes, different considerations can be done for diurnal and semi-diurnal components. Satisfactory results are obtained in simulating the M2 and S2 components: the amplitude error is always less than 3.65 % for both inlets (Fig. 6.4, Tab. 6.5). The M2 and S2 modelled fluxes anticipate the measured ones by around 20 minutes at Lido Inlet and 30 minutes at Malamocco Inlet. The worst reproduction, as in the case of water levels, is again for the K1 constituent. Following the results of the harmonic analysis, from ADCP data it can be stated that M2,

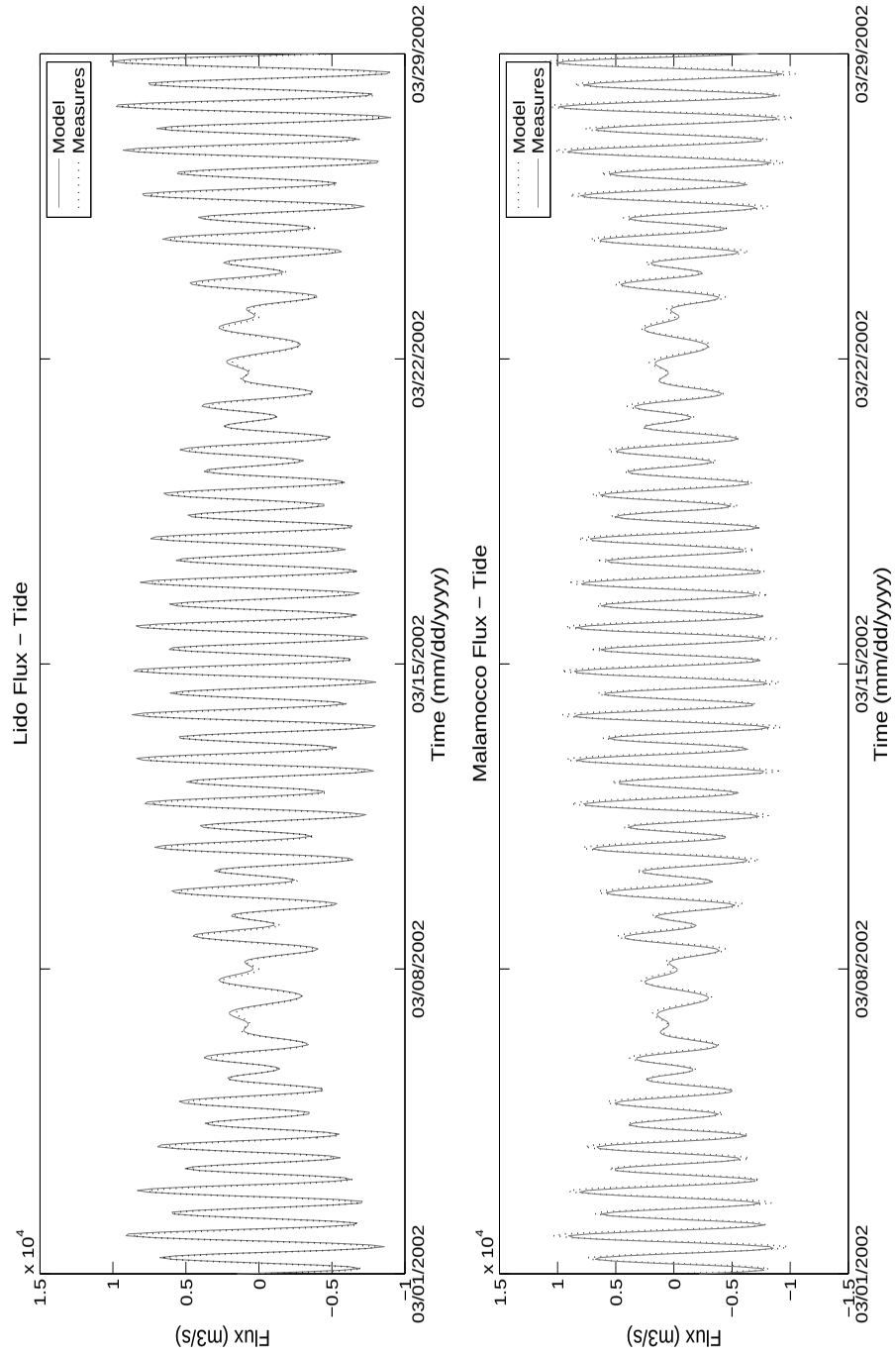

Figure 6.4: Tidal discharge time series comparison between modeled and measured data in Lido and Malamocco inlet.

S2 and K1 components represent about 50 %, 30 % and 20 % of tidal signal (Tab. 6.6). Weighting each component with these values the comprehensive tidal difference in amplitude is 2.7 % for Lido inlet and 2.9 % for Malamocco inlet. The phase anticipation of modelled tidal fluxes is 23 minutes for Lido and 30 minutes for Malamocco. Moving from harmonic constituents to the modelled and observed tidal time series, the computed correlation coefficient is 0.99 both for Lido and Malamocco inlets. Moreover, the model reproduces

Table 6.6: Weighted differences of discharges in amplitude (A) and phase (g)(in terms of minutes) for Lido and Malamocco inlets.

Inlet		Perc of modelled Tidal Fluxes [%]	A[%]	g[min]
Lido	M2	49.5		
	S2	29.2	2.7	23
	K1	21.3		
Malamocco	M2	50		
	S2	30	2.9	30
	K1	20		

an additional aspect, already seen in measurements (Gačić et al., 2002). The observed semi-diurnal signal at the Malamocco inlet anticipates the Lido one by about half an hour (Gačić et al., 2002). The simulated phase lag is of about 20 minutes, nicely matched, even if slightly underestimated.

The flux modeling is strictly connected with two factors: the capability in reproducing the dynamics in the lagoon and the parameterization of the bottom stress inside the three connection channels. The bottom friction coefficients chosen during the calibration phase are specific for each inlet with different values applied to simulate the inflow and outflow dynamics. The final values chosen are the ones that more uniformly distribute the error on all three inlets and reproduce the interaction processes.

To explain the differences with the empirical data I can distinguish two different groups of errors: one related to the measured data and one related to the numerical model. The empirical discharge data, as explained in section 2.3, have been obtained from the vertically averaged water velocity value measured by ADCP probe for one fixed location inside each inlet. From Gačić et al. (2002) I know (table 1) that the ADCP velocity data are affected by

an error of around 5 % for the M2 and 10 % for the K1. Since the discharge data is computed from the velocity data by applying a regression formula, the errors given above are certainly a lower bound for the errors of the flux data.

A further source of error for the empirical data is related to the harmonic analysis. In fact, due to the high residual signal generated by intense meteorological events, the amplitude and the phase values obtained for each main tidal constituents from the harmonic analysis are subject to high relative errors.

What concerns the model, a source of error can be related to the reproduction of the SSE outside and inside the inlets. The discharge rate through the inlet is dependent on the SSE gradient along the inlet channel and therefore the accuracy of the SSE inside and outside the lagoon strongly affects the model results. The increase in resolution for what concerns the lagoon, describing in a more realistic way shallow areas and channels, in terms of internal dynamics and bottom friction, can improve the internal reproduction of SSE. Finally, as mentioned in Ferla et al. (2007), the harmonic constants measured in the lagoon have changed significantly during the last decades because of the morphological changes. It is realistic to suppose that the use of new bathymetric data to reproduce the morphology could reduce the error of the model for the SSE and consequently also the discharge rate through the inlets.

6.2.4 Residual Levels and Fluxes

An analysis on the reproduced fluxes with respect to the meteorological impact on hydrodynamics has also been carried out. In Fig. 6.5 the Fast Fourier Transform (FFT) graph for the residual signal, calculated subtracting the tides from water level at the Lido inlet, is presented. For this final part the Foreman harmonic constant analysis has been applied to produce the residual water level time series (Foreman, 1978). An interesting aspect is the presence of two peaks, related to the 11 hours and 22 hours periodical signals. These are the two main seiches of the Adriatic Sea (Tomasin and Pirazzoli, 1999) and the model is able to reproduce them, better the 22 hours seiche than the 11 hours one. Comparing model and real data signals, it can be noted that the model, even if it is able to reproduce the 11 hours seiche, presents a displacement in frequency, with a shift to higher frequency values (Fig. 6.5).

Applying the same kind of analysis to the residual fluxes for Lido and Malam-

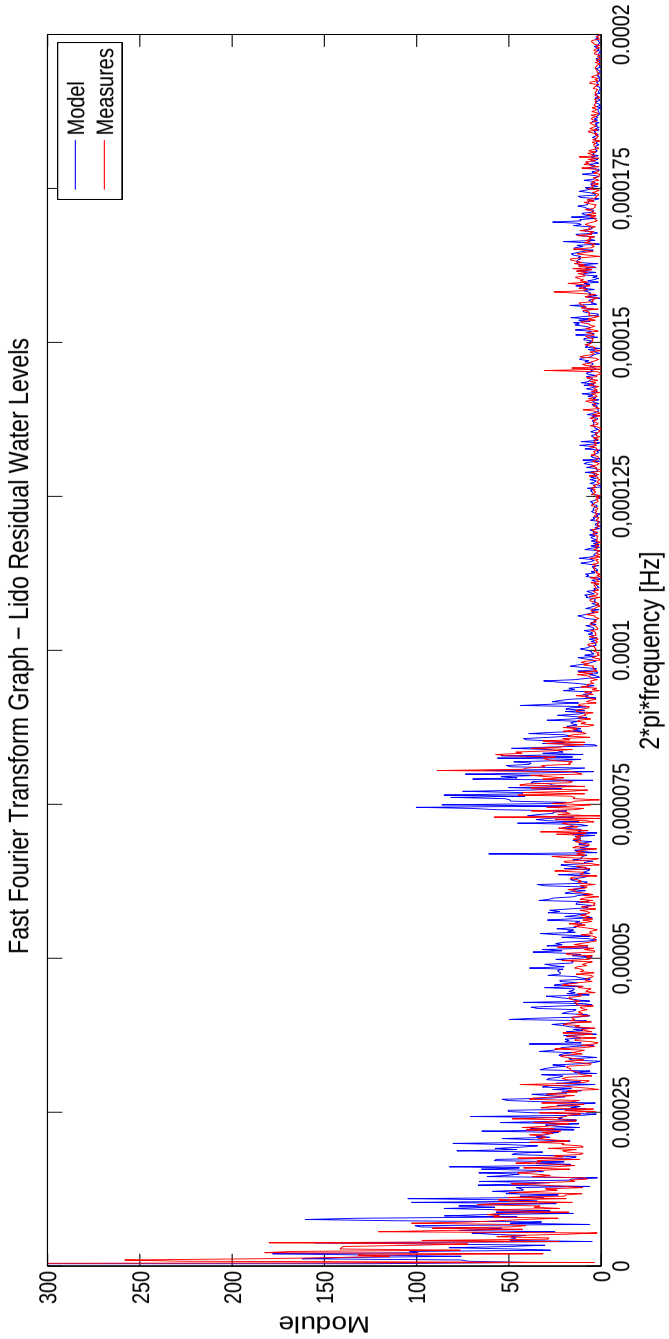

Figure 6.5: Fast Fourier Transform of residual components of levels in the Lido inlet.

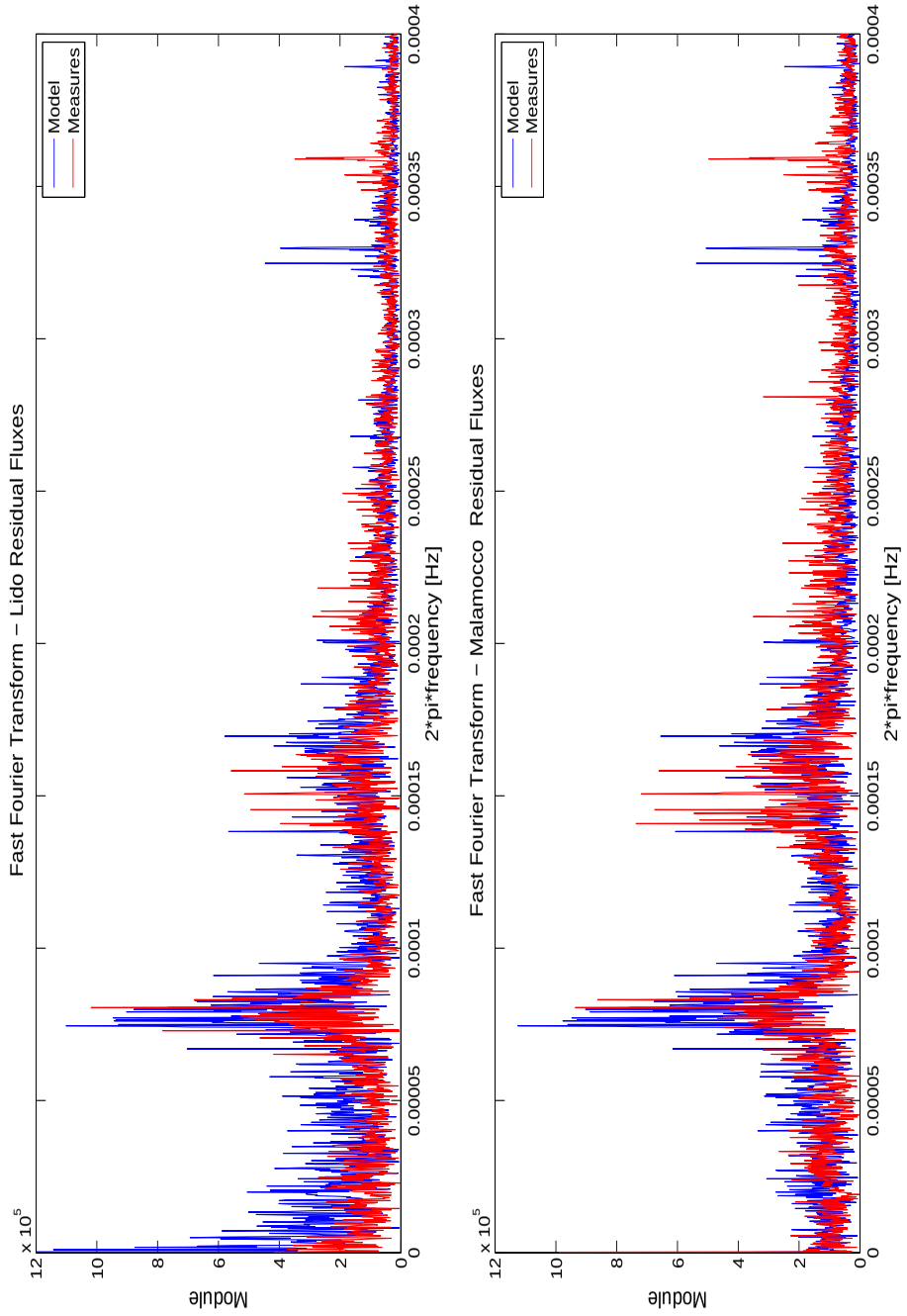

Figure 6.6: Fast Fourier Transform of residual component of fluxes in the Lido and Malamocco inlets.

occo once more the two seiches are registered by the model (Fig. 6.6) which are even more evident. It seems that some semi-diurnal components still remain in the residual signals, perhaps the overtide portion of sea breeze. The model does not reproduce them but this can be explained by the meteorological forcing that was applied coming from ECMWF model data. These data have a frequency of 6 hours and it is certainly not possible, with this coarse temporal and spatial resolution of 0.5 degrees, to produce a signal of limited space and time extension like the sea breeze. Additionally it has to be said that the meteorological data time step, 6 hours, could introduce some artificial frequencies in the model results and that could explain the peak around 3.2E-4 Hz in the model data. These results could be interfaced with other studies done on residual currents at the Venice Lagoon inlets from ADCP data (Gačić et al., 2004). In Gačić et al. (2004) the seiches signals can be isolated and the obtained information is comparable with the one from our study, even if the analysis has been done on axial velocities and not on fluxes as done here.

Considering the whole modeled fluxes for Lido and Malamocco inlet it can be noted that the tidal signal contained is 95 % of the total variance for Lido inlet and 97 % for Malamocco inlet, values comparable with the ones obtained by measurements (Gačić et al., 2004). From Fig. 6.6 it can be seen that the residual variability is due to the meteorological forcings.

6.2.5 Extreme wind events

The whole simulated period has been analyzed and a particular portion, from the 20th of November to the end of December, has been considered. This period shows the two main extreme events of the year, with a strong Sirocco wind blowing around the 24th of November and a long Bora event lasting several days before the 8th of December. In Fig. 6.7 the wind data measured by the Oceanographic Platform CNR for the chosen period are shown, both speed and direction.

The Pearson correlation coefficient has been computed, first on the complete chosen time window, and then on the two singular extreme wind events. The interval of confidence chosen is 5 %. High correlation is registered for fluxes, 0.89 for the total temporal range, 0.96 for the Bora event and 0.89 for the Sirocco event. In the three cases the p-value is nearly 0.

On the other hand the correlation of water levels is higher for the two single wind events, 0.9 for Sirocco and 0.94 for Bora, compared with the correlation of the whole time series, 0.82. This could be ascribed to the choice of imposing

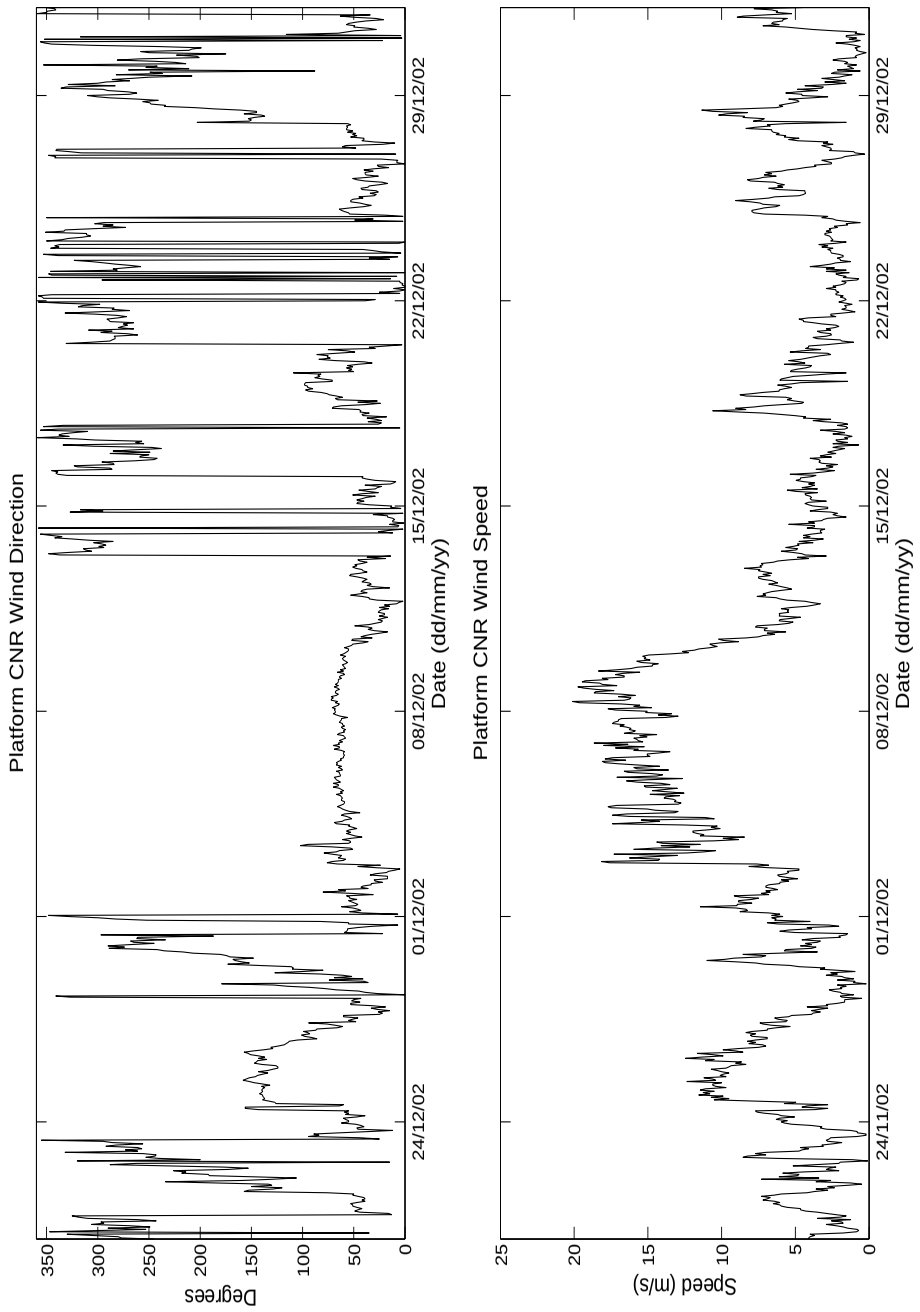

Figure 6.7: Wind data (direction and speed) for a significant extreme event period of December 2002.

modeled storm surge forcings at the open boundary instead of measured ones. In fact it has to be mentioned that storm surge modeling is a difficult task because of the strong dependence on the choice of meteorological forcings. Anyway, it can be stressed that the correlation computed here is comparable with the one in Bajo et al. (2007).

Because the sub-sample for the Sirocco wind event consists only of around 30 values, it has been decided to compute also the Kendall's Tau, better suited for small samples. The Kendall's Tau gives a value of 0.74 for the water levels (p-value 2.2E-9), and 0.84 for the fluxes (p-value 1.266E-14). These values prove a good correlation even on this short wind event.

It is interesting to note that total fluxes seem to be reproduced better than total water levels (Fig. 6.8). This can be explained because fluxes at the inlets are mainly tidally driven (Gačić et al., 2004) and, as shown, the tidal signal is better reproduced than the residual one. As an example Fig. 6.8 shows the comparison between the measured and the modeled total water levels and fluxes time series, stressing clearly the good match.

Some differences in extreme event reproduction can be also connected with the rough resolution of ECMWF data, 1/2 of a degree, which does not reproduce adequately the wind variability in the study area. A previous work compared results from the SHYFEM model, in its operational version, forced with different wind fields, the ECMWF ones described above and the Limited Area Model (LAMI) wind fields (Zampato et al., 2007). The latter one produced more intense wind fields and was capable of resolving the mesoscale features of the wind in the study area with a higher correlation with measured data (Zampato et al., 2007). Unfortunately, LAMI wind fields were not available for the considered period.

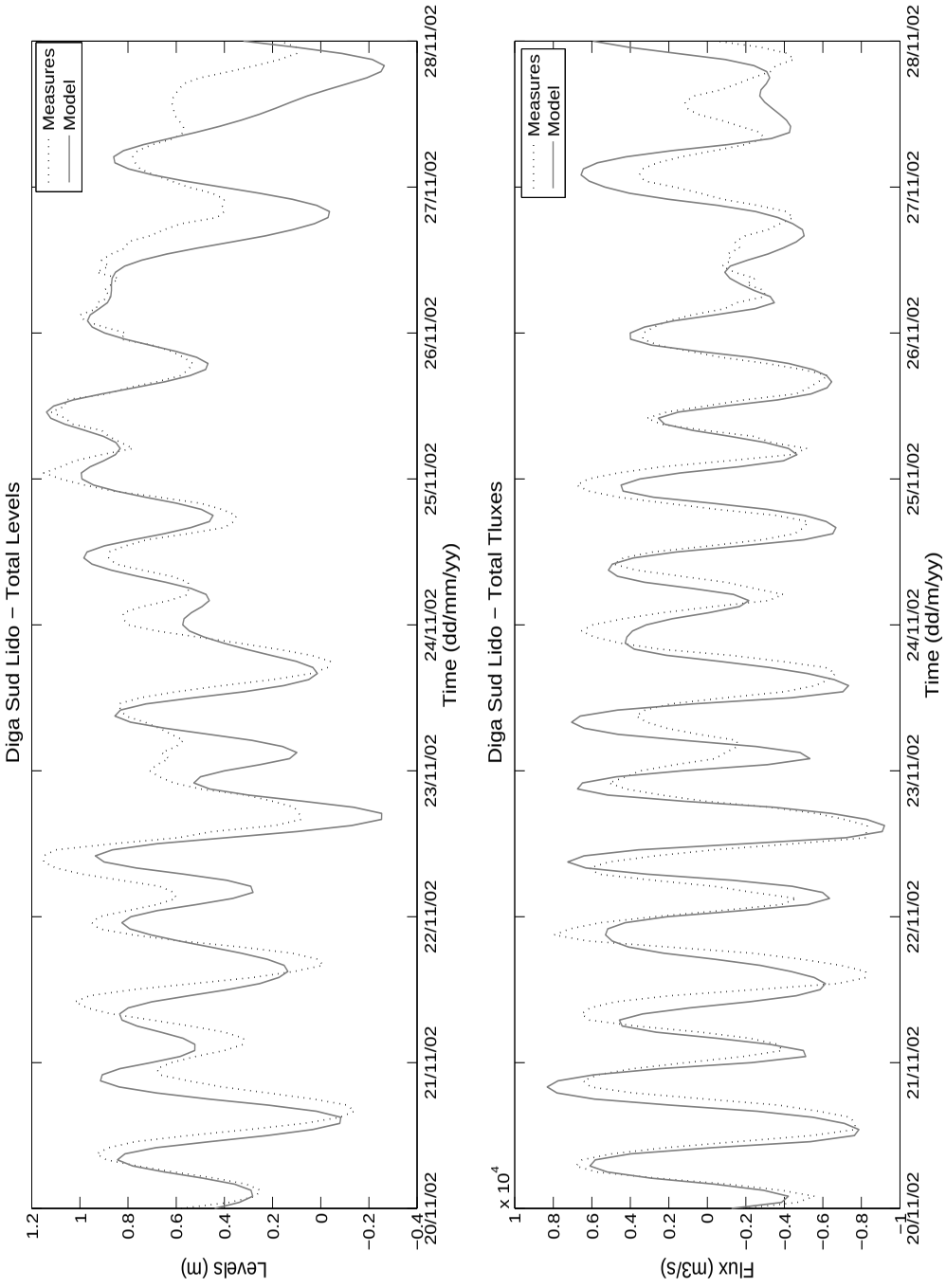

Figure 6.8: Comparison between residual levels and fluxes modeled and measured in Lido inlet.

Chapter 7

Modeling Baroclinic Processes

7.1 The 3D Simulation Setup

Two different sets of simulations have been carried out to study the 3D hydrodynamic processes in the area. The first is connected with the application of idealized forcings over the realistic basin and the study of its response, the second deals with realistic forcings where the baroclinic pressure gradient terms and the advection terms are considered or neglected.

7.1.1 Idealized Forcing Simulations

Three simulations have been performed over the Adriatic Sea-Venice Lagoon basin. The first simulation introduces an idealized tidal signal at the open boundary at the Otranto strait: a sinuisoidal 12 hours period, amplitude 40 cm, tidal timeseries is chosen. This choice is driven by the fact that this could be a realistic approximation of the M2 tide in the Adriatic Sea, which is one of the most energetic tidal signals in the northern part of the basin (Polli, 1960; Bellafiore et al., 2008). Constant values of temperature (14 degrees) and salinity (35 psu) are imposed over the whole basin as initial conditions. Idealized river discharges are given, with freshwater flowing into the sea at the same temperature of the basin. The amount of discharge is taken from average annual means. The simulation period is 16 days, because 15 days are considered a suitable period for the spin up. The 16th day is analized.

The second two simulations introduce idealized wind fields: a persistent Bora event, direction from NE and wind speed 14 ms^{-1}, which is a realistic value

considering measures; and a persistent Sirocco event, direction from SE, wind 12 ms^{-1}. No tidal forcing is introduced and river discharges are set as in the previous simulation. As initial conditions, temperature, salinity, velocity and water level fields from a 15 day simulation of real conditions of January 2004 have been used. These initial conditions are representative of a typical winter situation in the North Adriatic with the presence of the coastal current. After this, three days of wind events are simulated and the last day is averaged and analyzed.

7.1.2 Sensitivity Simulations

The second set of simulations deals with realistic forcings during year 2004. The choice is connected with the availability of HF Radar measurements for the same year, that will be compared with model results in the next section. The wind fields are taken from T511 ECMWF (European Centre for Medium Weather Forecast) 0.5x0.5 degrees, 6 hour data. The temperature and salinity 3D matrices adopted as initial condition are from MFStep (Mediterranean Forecasting System Toward Environmental Predictions) daily dataset. Their horizontal resolution is 1/16 of a degree. A realistic water level tidal signal is imposed at the open boundary at the Otranto Strait applying the procedure described in Bellafiore et al. (2008) and obtained by real harmonic constants for the Otranto Strait in the year 2004. The seven major harmonic constants in the Adriatic Sea are imposed and the surge signal, produced by a surge model running over the whole Mediterranean Sea (Bajo et al., 2007), is added to the tidal water level timeseries at the open boundary. The month of May is simulated and the monthly average is analized. This average filters out the main influence of tides, being the most energetic tidal signals in this area the components M2, S2, K1. Three simulations have been performed: the first uses the complete terms of the primitive equations (run A), the second neglects the baroclinic pressure gradient terms (run B) and the third neglects also the advection terms (run C).

7.1.3 Realistic Simulation of the year 2004

A complete simulation for the year 2004 has been performed. All the forcings described in the previous section have been imposed. The results of this simulation are used to provide information about the different vorticity patterns in three different periods of the year (February, May, November) to stress the response to forcings that could produce specific horizontal and ver-

tical structures (vortices, vertical stratification). Monthly averaged surface currents maps are provided, comparing model results with HF Radar Data. The second kind of analysis is done to define the persistent surface structures connected with the action of different winds (Bora Events, Sirocco Events, other wind events, calm Events). Detided velocity fields are considered to eliminate the tidal effects. Even in this case a comparison with HF Radar data is provided.

7.2 Baroclinic Simulation Results

One of the variables that can easily give an overview of the dynamic of the study area is vorticity and in the following sections, averaged vorticity maps will be investigated to add information about persistent small scale processes. The investigation is carried out in the surface layer and in the second layer, between 2 m and 4 m.

7.2.1 Idealized forcing impact

The simulations using idealized forcings are here discussed. The first simulation (Fig. 7.1) is shown as 12 hours average over the 16th day of simulation under the only forcing of a 12 hours tidal signal. The choice to consider the average value is connected with the fact that the interest is not focused on tidal currents, already investigated in the previous chapter, but on tidal induced currents (secondary effects). In fact, what is seen is the presence of positive (to the North) and negative (to the South) vorticity poles, in correspondance with each layer. This is not connected with the main tidal signal but with a residual persistent signal. The same pattern is mantained even on the second layer, confirming a barotropic behaviour of tidal currents near the inlets. A first result that emerges from this evidence is that the action of tides, even if modelled in 3D, are barotropic in this coastal interaction area, in their primary and secondary signals. It has to be mentioned that the vorticity values presented in these maps are contained in a small range [-2E-5,+2E-5] due to the focus on the secondary circulation caused by tides. From Fig. 7.2 it can be seen how different winds change abruptly the surface pattern of vorticity: Bora Wind defines a large strip of coastal negative vorticity. This result has to be interpreted considering the fact that the initial condition of the simulation is realistic, that means that the wind acts on a current pattern in which the general geostrophic current can be seen

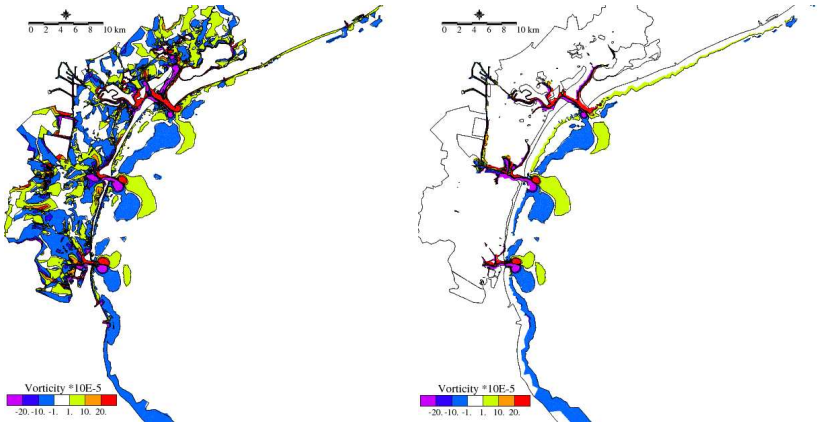

Figure 7.1: Vorticity maps of the surface and second layer for the idealized semidiurnal tide simulations. A 12 hours average is applied to eliminate the tidal impact.

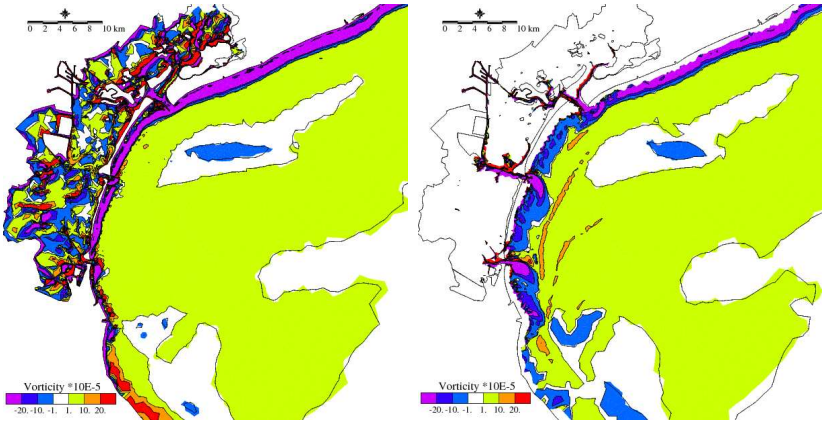

Figure 7.2: Vorticity maps of the surface and second layer for the idealized Bora wind simulations, averaged over the 3rd day of simulation.

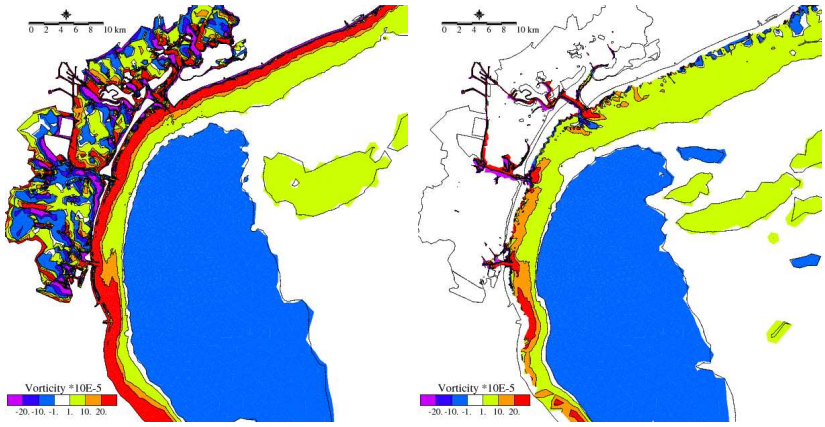

Figure 7.3: Vorticity maps of the surface and second layer for the idealized Scirocco wind simulations, averaged over the 3rd day of simulation.

along the littoral. The water, as an average, continues to flow from North to South. A map of negative coastal vorticity should be interpreted as the evidence of a decrease in currents from offshore to the littoral. The coastal currents tend to flow parallel to the coast following the isobaths, decreasing in intensity along the 2 km littoral strip during wind events and seem not to be effected by the action of the inlets dynamics on the surface.

The second layer (Fig. 7.2) shows a more dynamic pattern, which is interpreted as a weaker action of the wind and an increased persistence of typical interaction processes at the inlets. A tongue of more negative vorticity is seen at the Malamocco and Chioggia Inlets (the central and the southern ones) that should be due to the outflow coming from the Lagoon. In Cucco and Umgiesser (2006) it is shown how the Bora winds set up a circulation in the Venice Lagoon where water enters in the Lido inlet and outflows from the central and the southern ones, exactly what can be seen in this simulation. It has to be mentioned once again that, in this idealized simulation, no tidal influence is considered during the three days run.

Fig. 7.3 shows the impact of Sirocco wind, which changes strongly the surface pattern. Considering also the surface current patterns (not shown here) the positive vorticity can be interpreted as a change in current direction and as a displacement of the more energetic coastal currents. Sirocco wind detaches the mean geostrophic coastal current offshore, keeping stronger currents a couple of km from the littoral. As Bora, it acts mostly at the surface. The interesting aspect is the lack of symmetry between the action of the two winds on the second layer: the positive vorticity, between Chioggia and Malamocco

inlets, is stronger than the one between Malamocco and Lido inlets. This means that the Sirocco wind acts predominantly in the Southern end of the Venetian littoral. On the other hand the two areas between the inlets have quite a similar behaviour during Bora events, with a more homogeneous action of this wind on the whole area.

The last consideration is on the area of non-zero vorticity in the three simulations. The action of winds involves the whole basin, while the action of tides can be detected just in the near coastal area and in the proximity of the three inlets. This result is in agreement with what has been seen by Kovačević et al. (2004), from HF Radar measurements. Data showed that the tidal influences is below 20% 4 km offshore, while is predominant in the inlets (Gačić et al., 2004).

7.2.2 Sensitivity Analysis

From HF Radar measurements and analysis (Mancero Mosquera et al., 2007) vortical sub-mesoscale structure are seen, when the wind is blowing weakly, in front of the littoral areas between the Venice Lagoon inlets. Additionally, really close to the littoral, where the HF Radar cannot collect measures, other small scale vortical recirculation structures are seen. In order to study the processes that lead to the formation of these additional small velocity patterns, three simulations are performed for the month of May 2004, applying the realistic set of winds, tides and river runoff. As described in section 7.1.2, we call the first simulation, which uses the complete terms of the primitive equations, run A, the second one, which neglects the baroclinic pressure gradient terms, run B and the third one, which neglects even the advective terms, run C.

In Fig. 7.4 the surface and the second layer monthly averaged vorticity fields are shown, specifically for the area between Malamocco and Chioggia inlet. The monthly average eliminates the tidal signal, which is mainly defined by diurnal and semi-diurnal signals, permitting the analysis of residual currents. The maps of run A, show a core of positive vorticity along the littoral, that persists even in the second layer. Run B, which does not compute baroclinic pressure gradients, still maintains the positive core but the values are weaker. This means that a small impact of temperature and salinity gradients influence the dynamics of this area. However they cannot be considered the driving processes keeping this vortical persistent structure. Run C, in which even the advection terms are not computed, gives a clear information: no vortical structure are detected in the area and even the two inverse vorticity

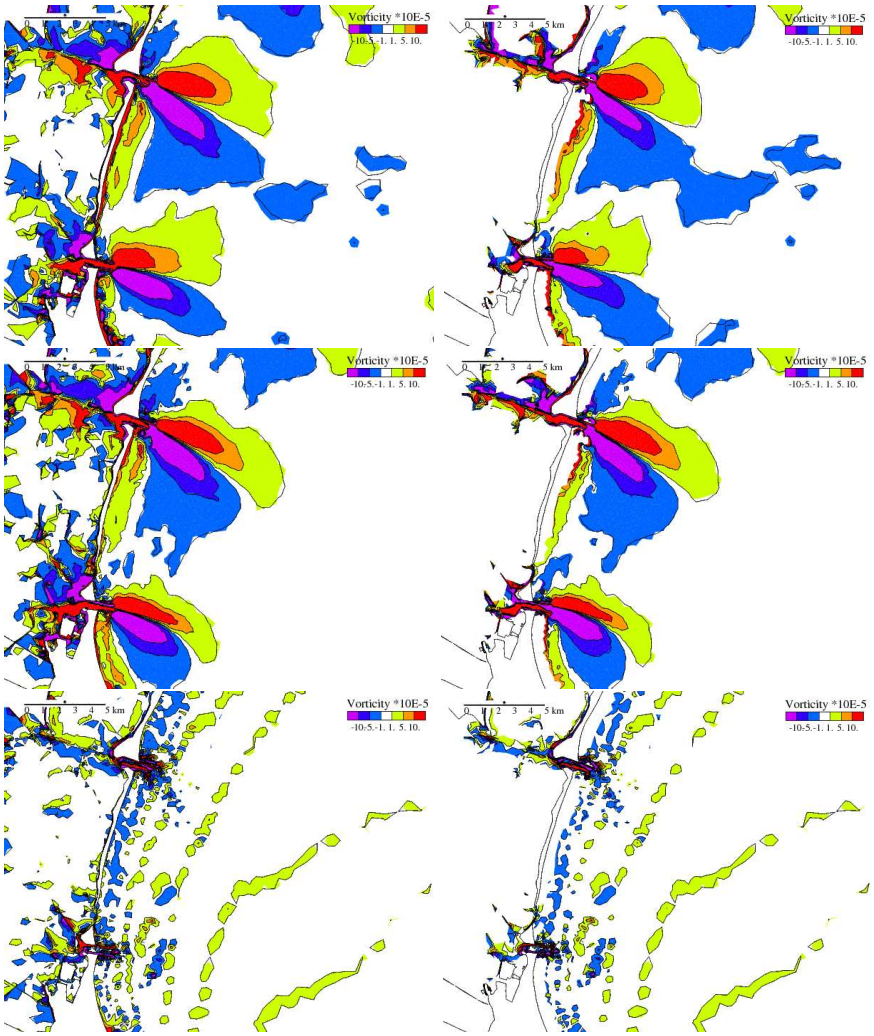

Figure 7.4: Vorticity maps of the surface and second layer for the three sensitivity runs: with all the terms computed (A), neglecting the baroclinic pressure gradient only (B), neglecting the baroclinic pressure gradient and the advection terms (C).

poles at the inlets disappear. It can be concluded that the physics connected with these vortical phenomena are due to advection mainly. The positive vorticity characterizing these patterns, identify them as a kind of interaction process, strictly connected with the inlet dynamics.

7.2.3 Run of the year 2004

All the following maps (the monthly averaged vorticity and total surface current maps and the detided surface currents maps) are referred to the year 2004. Processes connected with seasonal patterns are investigated, following the approach proposed in Mancero Mosquera et al. (2007). For the analysis of wind action the data have been divided in subsamples. The wind measurements in the CNR Platform (Fig. 3.1) are used to divide the wind events into four categories: calm events (wind speed under 3 m/s), Bora winds (directions in the range 202.5-247.5 degrees Azimuth, from North-East) and Sirocco winds (directions in the range 297.5-342.5 degrees Azimuth, from South-East) (Mancero Mosquera et al., 2007). Other wind events are the ones not included into these three categories. Some processes have already been detected by HF Radar and these measurements are used here to validate the model results.

Monthly Averaged Surface Current Patterns

In Fig. 7.5 the surface and second layer vorticity pattern for February 2004 is shown. To interpret this field the surface current field presented in Fig. 7.6 is necessary. A mean current flowing to the South is detected and the coupled pole of positive and negative vorticity near the inlets can be interpreted as the enhancement of its meandering shape, approaching the coast North of the central inlet and then deviating offshore in the proximity of it. The mean current is reproduced by the model even if the effect of the inlets mean outflow is stronger than measures. In fact the higher direction errors are mostly close to the inlets and to the borders of the comparison area, where the HF Radar measures direction with an increased error due to the existence of the blind area, already explained. Comparing the first and the second layer of February vorticity maps, the same patterns are seen, comfirming that a well mixed, barotropic vertical structure persists for this month, in agreement with the general information about the Northern Adriatic (Franco et al., 1982).

May 2004 has a completely different current pattern, showing a current reversal. The interesting thing is that surface vorticity maps are quite similar

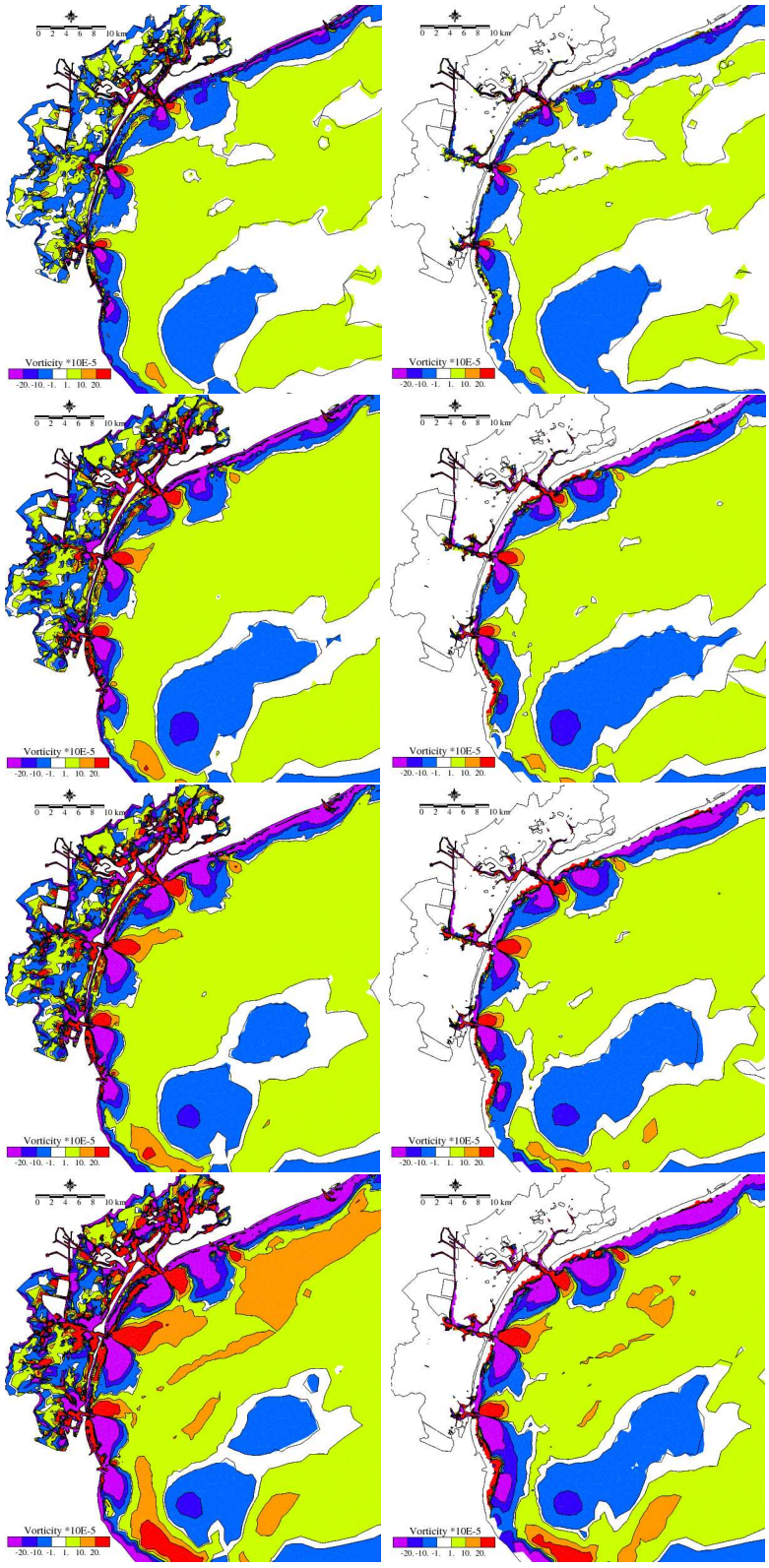

Figure 7.5: Monthly averaged vorticity maps of the surface and the second layer for months February (A), May (B), July (C) and November (D), referring to the year 2 004.

to the ones of February (Fig. 7.5) but the mean current shows a meandering flow from South to North. The reason can be found in the presence of many Sirocco Events in this month. Also in this case the mean flow is reproduced by the model, even if the HF Radar data show higher variabilities in the meanders. As for February the higher directional errors are registered in the southern end of the area (Fig. 7.6). Generally, in the area in front of the central inlet there is a small underestimation of measured surface current speed (-0.05 m/s).

The month of July 2004 presents more persistent vortical structures, which are well reproduced by the model (Fig. 7.7). This patterns could be seen because of weaker wind events in that month (speed less than 6 m/s). As in the previous cases the higher direction errors are registered at the border. The surface and second layer vorticity patterns for this month differs more than the previous cases and this evidences the evolution of a vertical structure that is weakened by depth (Fig. 7.5).

November 2004, which is characterized by strong Bora events, shows an aligned surface current pattern from North to South, well matched by the model. This is the month best reproduced in direction by the model. It seems that the model is better reproducing periods of small variability in wind direction. In fact, the wind forcing is from ECMWF dataset, with a horizontal resolution of 0.5 degrees, not enough to describe all the small scale wind variations.

For the four months an additional aspect is seen, connected with the river dynamics. Along the coast a strip of negative vorticity is seen, which is enhanced in July and November. In correspondence with the main rivers, poles of positive vorticity are present: it seems that there is a deviation to the North near the river mouth and then a deviation to the South going offshore, as an effect of potential vorticity conservation.

Response to wind events - Comparison with HF Radar Data

The complete dataset of year 2004 (from February to December) has been analyzed producing, both for model and for measurements, four sub-samples corresponding to detided surface currents during Bora, Sirocco, calm and other winds events. In Fig. 7.8 the Bora pattern can be analyzed: there is a good match between model and measurements and the main effect of the wind is the enhancing of the coastal currents in the southern direction. The strength of the wind tends to eliminate the effects of the three inlets aligning the current to the littoral. The Bora wind effect in direction is reproduced with errors not higher than 20 degrees in most of the area. Higher errors

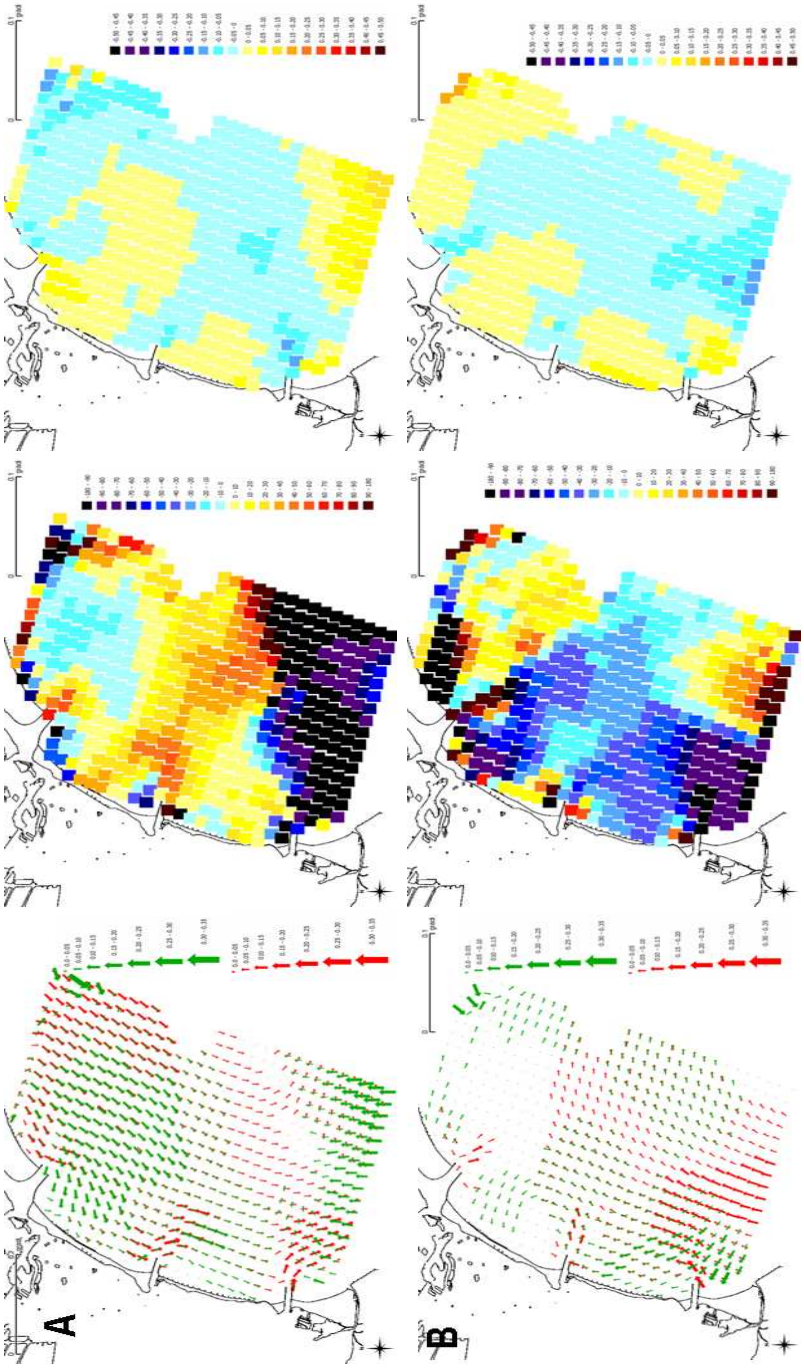

Figure 7.6: Monthly averaged maps of HF Radar (green) and Model (red) surface currents (left panel) for months February (A) and May (B) 2004. Direction errors [degrees] and speed errors [m/s] maps are shown in the central and right panels.

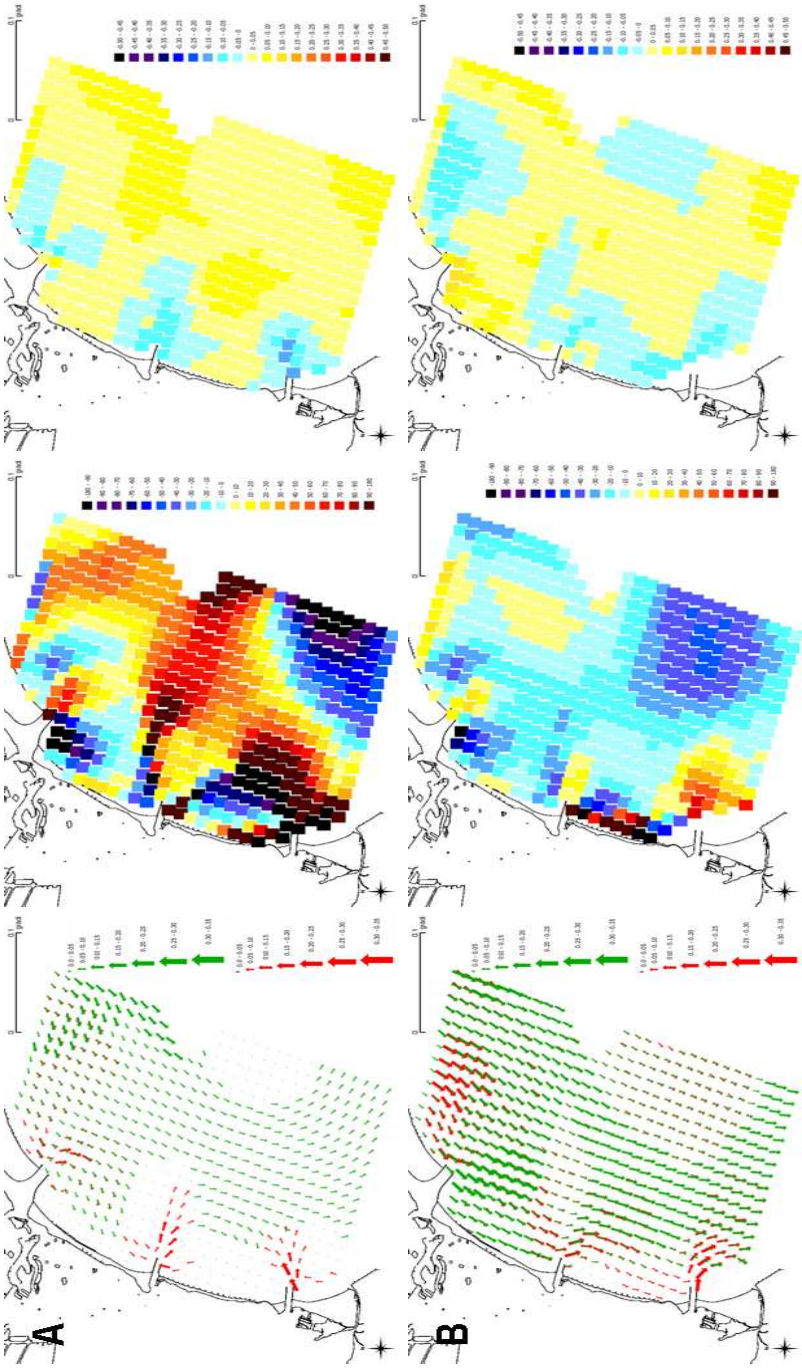

Figure 7.7: Monthly averaged maps of HF Radar (green) and Model (red) surface currents (left panel) for months July (A) and November (B). Direction errors [degrees] and speed errors [m/s] maps are shown in the central and right panels.

are seen, once more, at the southern border. The Sirocco wind produces a countercurrent from South to North interacting with the secondary inlet dynamics. The dynamic is the same as in the idealized simulations, confirming the predominant action of the wind even when all the other forcings are introduced. Fig. 7.9 shows two vortical structures South of the Lido and the Malamocco inlets both for calm and other wind events. During calm wind events the sub-mesoscale structures are maintained by the tide and the influence of the inlets is predominant. This emerges also from the sensitivity analysis done in section 7.2.2, that connects this kind of processes to the advective action of inlet tidal cycles.

The error in direction are quite high for Sirocco, calm and other wind events, while Bora is well reproduced. Once more the reason can be connected with the difficulty of the model to simulate local variable wind events with the low resolution wind forcing dataset chosen.

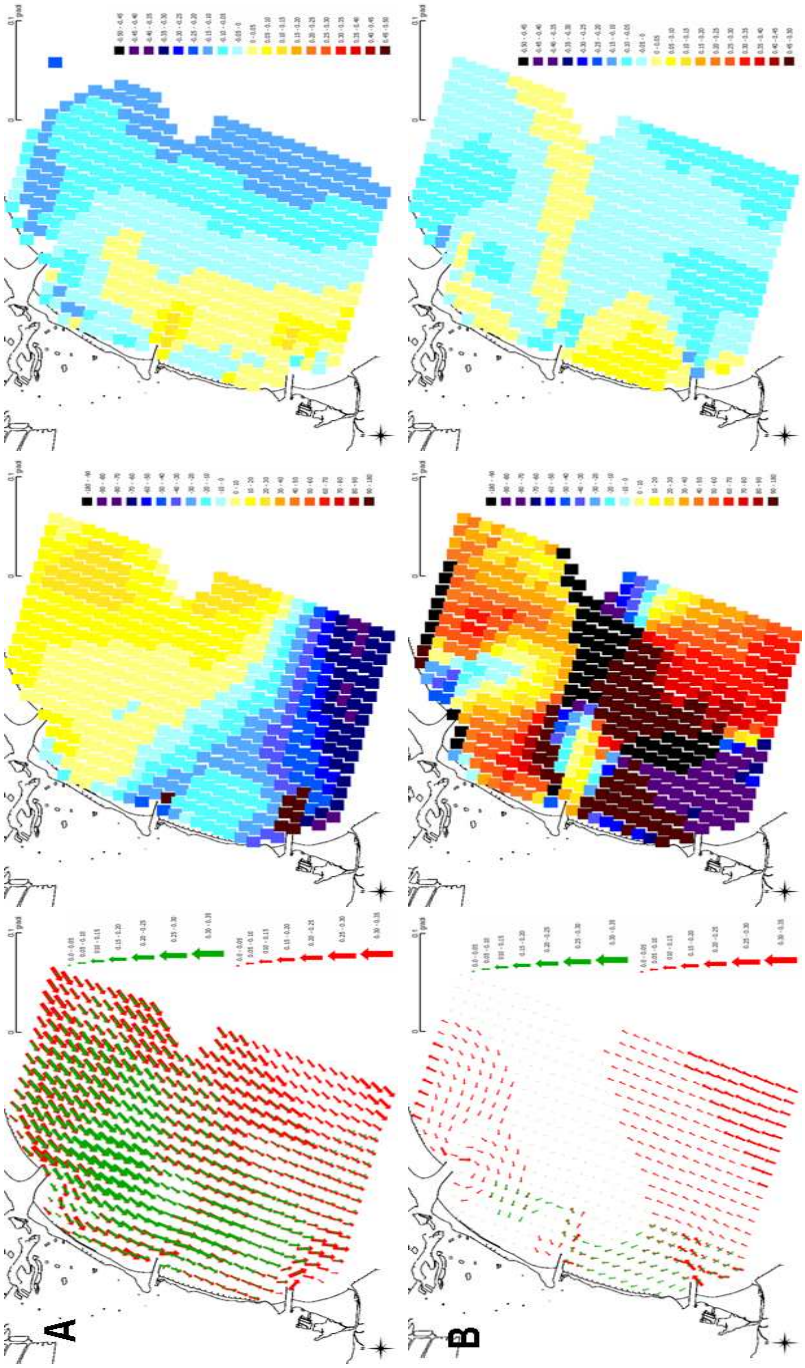

Figure 7.8: Map of averaged detided surface currents for the Bora (A) and Sirocco (B) wind events - comparison between measured HF Radar data (green) and modelled data (red). Direction errors [degrees] and speed errors [m/s] maps are shown in the central and right panels.

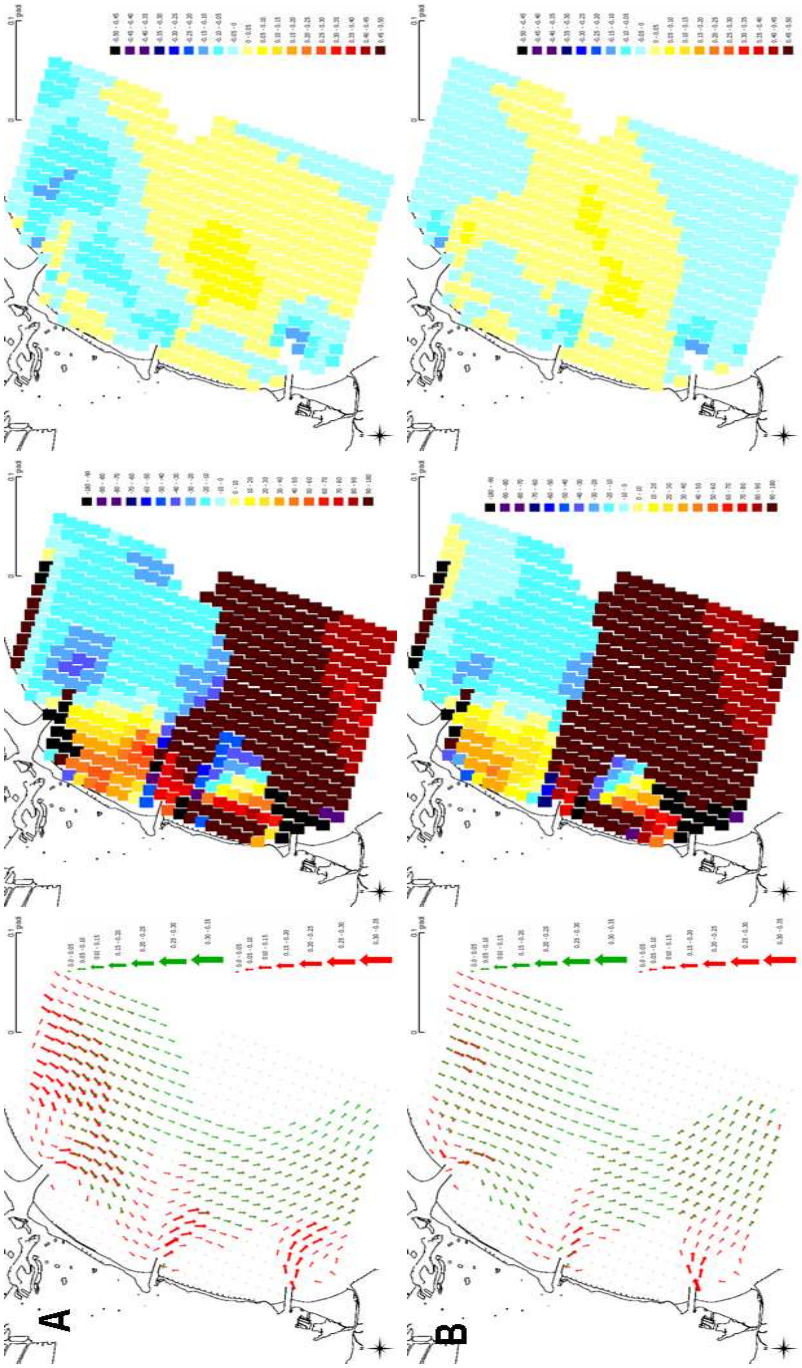

Figure 7.9: Map of averaged detided surface currents for calm (A) and other wind (B) events - comparison between measured HF Radar data (green) and modelled data (red). Direction errors [degrees] and speed errors [m/s] maps are shown in the central and right panels.

Chapter 8

Summary and Conclusions

In this work the main aim was to reproduce by numerical modeling some of the most important hydrodynamic patterns occurring along the coast of the Northern Adriatic Sea and to study the interaction processes between the Venice Lagoon and the open sea.

Untill now, no major studies have been carried out that try to model the exchange mechanisms through the Venice Lagoon inlets. It is also the first work in this area that tries to model the interaction dynamics, running together a model for the lagoon and the Adriatic Sea. The increased spatial resolution achieved in the inlets area permits a realistic study of the interaction processes.

A certain effort has been made in the definition of the state of the art of hydrodynamic modeling in the Adriatic Sea, which is a preferable basin for the processes investigation because of its morphological characteristics and of the main forcings. This overview led to the choice of the most suitable tool for the coastal modeling, identified in the SHYFEM Model.

The need of high spatial resolution and realistic datasets as forcings is stressed, because they strongly impact on the quality of modeling results. Additionally, also the model numerical characteristics have been studied and tested to certify its capability to reproduce the kind of small scale processes which have been investigated in this work.

However, the core of this PhD Thesis has been the numerical modeling of specific processes and temporal ranges and the approach was to proceed from lower to higher complexity in the study. The first simulations have been performed in 2D, limiting the study to barotropic processes to reproduce the discharge rate through the lagoon inlets driven by the action of the tide and

wind (Gačić et al., 2002).

The spatial resolution of the model varied from 30 m inside the Venice Lagoon inlets to 30 km in the middle of the Adriatic Sea, with a transition zone close to the lagoon inlets, characterized by a resolution of 300 m. The open boundary has been chosen as a straight line across the Strait of Otranto on which the tidal SSE is imposed. The model has been calibrated to reproduce the tidal propagation in the Adriatic Sea and in the Venice Lagoon. The SSE along the eastern end of the open boundary line of Otranto and the bottom friction coefficient inside the Venice Lagoon basin were changed during the calibration. For the validation the model results have been compared to measured data of harmonic constants collected in stations located along both the western and the eastern coast of the Adriatic Sea.

For what concerns the tide, the model reproduced the set of harmonic constants for the Diga Sud Lido station for the most energetic tidal constituents (M2, S2 and K1). The results obtained for the other stations close to the Venice Gulf, Falconera, Trieste and Rovinj, were in good agreement with the empirical data. The SSE offshore the Venice Lagoon has been in fact reproduced with an error always lower than 2 cm for the amplitude of the main tides and with a phase difference not higher than 10 degrees. These results are in accordance with the first task of this work, which is the reproduction of the tidal flow through the three lagoon inlets.

After this first step, the water fluxes through the inlets have been computed by the model when tide and wind are forcing the basin. The results have been compared with empirical data of water discharge derived from ADCP measurements collected inside each inlet. The model reproduced the fluxes through the inlets with a good agreement for both of them and an average overestimation less than 2.9 % with a time anticipation of about 20 minutes. The frequency analysis conducted using the FFT both on residual signals of levels and fluxes stressed the capability of the model to reproduce seiches and their effects on the circulation in the interaction areas. Free oscillations were correctly reproduced.

The SHYFEM Model has been already applied to the whole Mediterranean basin to forecast water levels, focusing on the Venetian area (Bajo et al., 2007). The comparison between modeled and measured residual levels time series showed how the coupling of tidal and meteorological forcings, including the surge impact, leads to acceptable results. The success of these simulations on the reproduction both of the SSE, inside and outside the Venice Lagoon, and of the tidal flow, through the lagoon inlets, indicates that the finite element model is performing adequately on the barotropic mode. For the first time the physical processes that drive the interaction between the two

basins were reproduced, as the flux modeling shows. Clearly, the good results reproducing discharges through the inlets are due to the fact that the lagoon is modeled together with the Adriatic Sea. Without the lagoon, the water levels could be certainly reproduced, but not the fluxes between the sea and the lagoon.

The second task of this work was the reproduction of baroclinic processes. 3D runs were required to introduce and study the effects of freshwater, temperature and salinity horizontal gradients and the action of turbulence.

Additionally, the simulations performed introducing ideal forcings, tides and the Bora and Sirocco winds, led to a better understanding about the action of each of them on the study area, both on the horizontal and vertical scale. The secundary effects of tides, shown in the averaged maps of the surface and the second layer, were seen, defining their barotropic action mainly near the inlets. The tidal signal is less that the 20% some kilometers offshore as also seen by measurements (Kovačević et al., 2004).

What concerns results of the idealized winds runs, the Bora acts along the littoral enhancing the geostrophic current and detaching it offshore, parallel to the isobaths. On the other hand the Sirocco causes a change in the direction of coastal currents, from South to North. These 3D runs investigated the coastal vertical structures, defining the limit of wind action below the surface.

The sensitivity analysis was able to define the predominant effect of advection in the sub-mesoscale vortical structures, which are present close to the coast near the three inlets of the lagoon. One of the main results of this work was the confirmation of the model capability to describe small scale processes and the possibility to model the interaction between the lagoon and the open sea, because of the high resolution reached along the littoral. In this way, the model was able to simulate the near coast processes that could not be studied with the HF Radar measurements.

The analysis of different wind fields on the surface circulation defined the main horizontal current structures, clearly identifying the processes connected with winds with low directional variability, such as Bora.

The model obtained also a general description of the coastal current behaviour during the year 2004, showing the barotropic structures occurred during February and the more complex patterns seen in May, with persistent vortical structures due to the presence of many calm wind events.

In the future, a new analysis, introducing higher resolved wind fields as model forcings, could show higher precision in modeling these processes.

The finite element approach used in the SHYFEM Model, with its variable

horizontal resolution, showed to be a suitable tool for the investigation of coastal processes and its implementation in monitoring would become a precious help for the coastal management in the future.

Appendix A

The Arakawa Grids

The problem of what kind of horizontal discretization to apply in ocean models is quite old. From the overview presented in chapter 2 what can be seen is that many models apply one of the possible choices proposed by Arakawa and Lamb (1994). Differently from what can be thought, arranging the computation of all variables in the same grid point presents disadvantages, therefore new solutions are needed.

Arakawa and Lamb (1994) presents five type of grids, identified with letters from A to E.

A grid

the Arakawa A grid is the basic unstaggered grid, in which all the variables are held in the same point Fig. A.1.

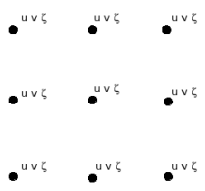

Figure A.1: Arakawa A grid

B grid

The Arakawa B grid computes the velocity variables, zonal and meridional, in the same point and they are semi-staggered Fig. A.2. Usually this kind of grid permits an easier formulation of the Coriolis term and favours the implementation of back-forward scheme, because of the same location of the two velocity components.

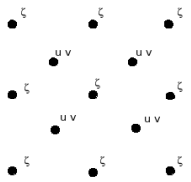

Figure A.2: Arakawa B grid

C grid

The Arakawa C grid is a fully staggered grid where the two components of the velocity and the water levels are computed in different locations Fig. A.3. The C grid is considered more suitable than the other grids for the implementation of semi-implicit time differencing but Coriolis terms need to be averaged in both horizontal directions, risking to reduce the amplitude of these two terms on small scales.

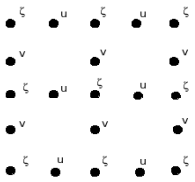

Figure A.3: Arakawa C grid

D grid

Also the Arakawa D grid is a fully staggered grid.

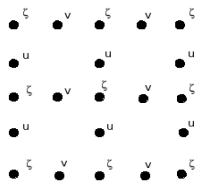

Figure A.4: Arakawa D grid

E grid

The arakawa E grid is a semi staggered grid that looks like the B grid but the locations are rotated through 45 degrees.

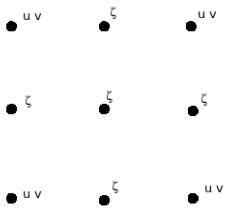

Figure A.5: Arakawa E grid

Appendix B

Turbulence Closure Models

In ocean models, which mostly all assume the hydrostatic approximation, there is the need to parameterize the non-hydrostatic effects. These are considered sub-scale processes which are mainly of convective and turbulent nature (Burchard and Petersen, 1999).

The Navier-Stokes equations can describe the more relevant processes of hydrodynamics but a different approach is needed to deal with the turbulence, due to non-linear instabilities.

B.1 Equations

The Navier-Stokes equation of motion can be written as

$$\partial_t v_i + v_j \partial_j v_i - \nu \partial_{jj} v_i + 2\epsilon_{ijl}\Omega_j v_l = -\frac{\partial_i p}{\rho_0} - \frac{g_i}{\rho_0}\rho \tag{B.1}$$

with v velocity, i j l indices of cartesian system, t time, ρ potential density, ρ_0 reference density, p pressure, ν kinematic viscosity, $\Omega_i = (0, \Omega cos(\Phi), \Omega sin(\Phi))$ rotation and $g_i = (0, 0, g)$ gravitation.

ϵ_{ijl} is the alternating tensor, which changes sign when two indices are switched. Its value is 1 if the indices are sequential (i.e. i=1, j=2, l=3 or i=2, j=3, l=1), -1 if they are not (i.e. i=2,j=1,l=3) and 0 if they are identical.

Following the so called Reynold's decomposition, which defines each variable as composed of a mean field ($\bar{U}$) and a fluctuating one ($\tilde{U}$), knowing that $\langle \tilde{U} \rangle = 0$, the Averaged Reynolds equations can be written

$$\partial_t \bar{v}_i + \bar{v}_j \partial_j \bar{v}_i - \partial_j(\nu \partial_j \bar{v}_i - \langle \tilde{v}_j \tilde{v}_i \rangle) + 2\epsilon_{ijl}\Omega_j \bar{v}_l = -\frac{\partial_i \bar{p}}{\rho_0} - \frac{g_i}{\rho_0}\bar{\rho} \tag{B.2}$$

Multiplying each term of Eq.B.2 for $\bar{v}$ and knowing that $e = \frac{1}{2}\bar{v}^2$, the energy equation can be obtained

$$\partial_t e + \partial_j(\bar{v}_j e + \bar{v}_i \langle \tilde{v}_i \tilde{v}_j \rangle - \nu \partial_j e + \frac{\bar{v}_j \bar{p}}{\rho_0}) = \langle \tilde{v}_i \tilde{v}_j \rangle \partial j v_i - \frac{g\bar{v_3}\bar{\rho}}{\rho_0} - \nu(\partial_j \bar{v}_i)^2 \tag{B.3}$$

Subtracting Eq.B.2 from Eq.B.1, the second moments transport equation can be written

$$\partial_t \langle \tilde{v}_j \tilde{v}_i \rangle + \partial_l(\bar{v}_l \langle \tilde{v}_j \tilde{v}_i \rangle + \langle \tilde{v}_l \tilde{v}_i \tilde{v}_j \rangle - \nu \langle \tilde{v}_j \tilde{v}_i \rangle) \tag{B.4}$$

$$= \overbrace{-\partial_l \bar{v}_i \langle \tilde{v}_l \tilde{v}_j \rangle - \partial_l \bar{v}_j \langle \tilde{v}_l \tilde{v}_i \rangle}^{P_ij} - \overbrace{2\Omega_l(\epsilon_{ilm}\langle \tilde{v}_j \tilde{v}_m \rangle + \epsilon_{jlm}\langle \tilde{v}_i \tilde{v}_m \rangle)}^{\Omega_{ij}}$$

$$- \overbrace{\frac{1}{\rho_0}\{g_i \langle \tilde{v}_j \tilde{\rho} \rangle + g_j \langle \tilde{v}_i \tilde{\rho} \rangle\}}^{B_{ij}} - \overbrace{\frac{1}{\rho_0}(\langle \tilde{v}_i \partial_j \tilde{p} + \tilde{v}_j \partial_i \tilde{p} \rangle)}^{\Pi_{ij}} - \overbrace{2\nu \langle (\partial_l \tilde{v}_j)(\partial_l \tilde{v}_i) \rangle}^{\epsilon_{ij}}$$

where P_{ij} is the shear production, Ω_{ij} the redistribution due to rotation, B_{ij} the buoyancy production, Π_{ij} the pressure strain correlator and ϵ_{ij} the dissipation of the Reynold stress $\langle \tilde{v}_i \tilde{v}_j \rangle$.
In a parallel way of the one presented above, the turbulent kinetic energy equation can be obtained from Eq.B.4, imposing $i = j$ and noting that the TKE can be written as $k = \frac{1}{2}\langle \tilde{v}_i^2 \rangle$

$$\partial_t k + \partial_j(\bar{v}_j + \langle \tilde{v}_j \frac{1}{2}\tilde{v}_i^2 \rangle - \nu \partial_j k + \frac{1}{\rho_0}\langle \tilde{v}_j \tilde{p} \rangle) = \overbrace{-\langle \tilde{v}_j \tilde{v}_i \rangle \partial i \bar{v}_j}^{P} \overbrace{-\frac{g}{\rho_0}\langle \tilde{v}_3 \tilde{\rho} \rangle}^{B} \overbrace{-\nu \langle (\partial_j \tilde{v}_i)^2 \rangle}^{\epsilon} \tag{B.5}$$

with P shear production, B buoyancy production and ϵ dissipation rate of turbulent kinetic energy.
The presented procedure in extracting the above equations is the one-point closure explained in Burchard (2002). In the next section it is explained how the TKE equation and the dissipation rate equation definition is needed to compute a value for the vertical eddy viscosity.

B.2 Turbulence parameterization

The vertical eddy viscosity has to be defined if there is the intent to model the turbulence effects, in order to solve the previous equations with a parameterization , obtaining the velocity scale q and the lenght scale l from them. Many different approaches have been performed to parameterize the turbulent effects. This parameterization can be treated with different approaches, applying an algebraic formulation, 1 equation or 2 equation models.

B.2.1 Algebraic approach

This approach computes the turbulent kinetic energy k and the length l from algebraic relations. The algebraic equation for k is extracted from a simplified form of the transport equation of the turbulent kinetic energy. The equation for the length-scale can have different formulations, each of them generally based on empirical motivations. Algebraic models are a over-simplification in numerous situations (Burchard, 2002).

B.2.2 1 equation models

The computation of k is done with the differential transport equation for the turbulent kinetic energy (Eq.B.4). Once more, even in this case, the length-scale is computed from an empirically or theoretically based relation. Having the value of l, the dissipation rate ϵ is then recalculated by means of

$$l = c_L \frac{k^{3/2}}{\epsilon} \tag{B.6}$$

called Kolmogorov relation, with $c_L = (c_\mu^0)^3/4$ macro length scale for energy-containing eddies.

This is a possible approach and leads to the definition of eddy viscosity ν_t and diffusivity ν_t' as follows

$$\nu_t = c_\nu \frac{k^2}{\epsilon} \qquad \nu_t' = c_\nu' \frac{k^2}{\epsilon} \tag{B.7}$$

It is widely adopted in geophysical models (Burchard, 2002).

B.2.3 2 equation models

In this kind of models, both k and l are computed from the differential transport equations. As it happens in the 1 equation models, k is obtained from the transport equation of the turbulent kinetic energy. Also the length-scale is determined from a differential transport equation. There are different approaches in determining the kind of equation to be used for the length scale computation and this is the main difference between the models presented below. The variable can be obtained from the rate of dissipation, ϵ, or from the product kl (Burchard, 2002).

In the following, basic information about the more used 2 equation models is given. Many discussion raised around the problem of the choice of the right equations to compute the length scale, with, mainly, two different approaches.

Mellor-Yamada model

Mellor and Yamada (1974), as a first step, proposed an algebraic solution for the computation of the macro turbulence length scale. After that, they developed a prognostic transport equation for kL

$$\partial_t(kL) - \partial_z(S_l\sqrt{2k}L\partial_z(kL)) = \frac{L}{2}[E_1P + E_3B - (1 + E_2(\frac{L}{L_z})^2\epsilon)] \qquad \text{(B.8)}$$

with S_l stability function and B_1, E_1, E_2, E_3 parameters (Burchard, 2002). They also introduced a modified TKE equation

$$\partial_t(k) - \partial_z(S_q\sqrt{2k}L\partial_z(k)) = P + B - \epsilon \qquad \text{(B.9)}$$

where S_q, constant stability function, is set to permit a higher entrainment through the density interfaces. The presence of S_q and the absence of the viscous mixing term, are two characterizing aspects of the Mellor-Yamada Model.

k-ϵ model

This is the model applied introducing the GOTM into the SHYFEM structure.

The ϵ equation has to be expressed in a exact form and to achieve this in the terms present on the right hand side of the equation parameters are introduced as closure assumptions taken from theory and observations by calibration. The closed ϵ equation is

$$\partial_t \epsilon - \partial_z((\nu + \frac{\nu_t}{\sigma_\epsilon})\partial_z \epsilon) = \frac{\epsilon}{k}(c_{1\epsilon}P + c_{3\epsilon}B - c_{2\epsilon}\epsilon) \tag{B.10}$$

with $c_{1\epsilon}$,$c_{2\epsilon}$,$c_{3\epsilon}$,σ_ϵ as parameters. If $c_{2\epsilon}$ is calibrated taking in consideration the freely decaying homogeneous turbulence behind a grid the k equation, for long integration times, can be determined as a power law,

$$\frac{k}{k_0} = A(\frac{t}{\tau_0})^d \tag{B.11}$$

d decay rate, A constant parameter, k_0 initial turbulent kinetic energy and τ_0 turbulent time scale. $c_{1\epsilon}$, $c_{3\epsilon}$ and σ_ϵ can be determined in many different ways, here not treated.

What has to be stressed is that, in this case, the equation for small scale turbulence is used to determine the macro length scale and this is one of the central points in the big discussion raised around the physical relevance of different models. Mellor and Yamada (1982) used this argument to support the k-kL model, where there is consistency in the treatment of the macro length scale. On the other hand, Rodi (1987) stressed how the nature of both ϵ and kL equations are fairly empirical and how it is not a matter of physical relevance but, more, of parameterization. No general differences are in the use of one of the two models approach but in the Mellor and Yamada (1974) model, the kL equation needs one more near wall term.

Acknowledgements

I want to gratefully acknowledge my tutor, Dr. Georg Umgiesser, who introduced me in this weird world that is Scientific Research. Thanks for the help and the respect given to someone who is just a beginner.

Thanks to Professor Nadia Pinardi and Professor Antonio Navarra, for the scientific and financial support, both fundamental.

Thanks to Professor Alberto Tomasin, the "Lord of Tides", for the precious time spent discussing about tides, surge and seiches.

Thanks to Dr. John Warner, from USGS, for the discussions on modeling and the great opennes in working on model comparison and thoroughly revising simulation results.

Thanks to Dr. Andrea Cucco, Dr. Christian Ferrarin, Marco Bajo and, particularly, to Francesca De Pascalis and Dr. Michol Ghezzo, which are the colleagues I worked with during these years, for the professional and, above all, personal, support.

Thanks to Dr. Katrin Schroeder because she enlarged my scientific thoughts from the shallow waters to the deep sea...hoping to go far!

Thanks to Dr. Alessandro Sarretta for the sincere support and for the help with GIS and with the emendation of this work.

Thanks to Dr. Vedrana Kovačević and Isaac Mancero Mosquera that provided the HF Radar and that helped me in discussing the criticity of some results.

Thanks for the partial funding to Dr. Cosimo Solidoro.

Thanks to CMCC - Centro Euromediterraneo per i Cambiamenti Climatici, that partially funded this work.

Thanks to INGV for the MFStep data used in this work.

Thanks to CORILA projects 3.2 *Hydrodynamics and morphology of the Venice Lagoon* and 3.5 *Quantity and quality of exchanges between lagoon and sea* that provided the flux data.

Thanks to the Venice Municipality that provided the wind and sea level data.

Bibliography

Arakawa, A. and Lamb, V. R. (1994). Computational Design of the Basic Dynamical Processes of the UCLA General Circulation Model. *Methods of Computational Physics*, 17:173–265.

Artegiani, A., Bregant, D., Paschini, E., Pinardi, N., Raicich, F., and Russo, A. (1997a). The Adriatic Sea General Circulation. Part I: Air-Sea Interaction and Water Mass Structure. *Journal of Physical Oceanography*, 27:1492–1514.

Artegiani, A., Bregant, D., Paschini, E., Pinardi, N., Raicich, F., and Russo, A. (1997b). The Adriatic Sea General Circulation. Part II: baroclinic circulation structure. *Journal of Physical Oceanography*, 27:1515–1532.

Artegiani, A., Gačić, M., Michelato, A., Kovačević, V., Russo, A., Paschini, E., Scarazzato, P., and Smirmic, A. (1993). The Adriatic Sea hydrography and circulation in spring and autumn (1985-1987). *Deep Sea Research*, II(40):1143–1180.

Bajo, M., Zampato, L., Umgiesser, G., Cucco, A., and Canestrelli, P. (2007). A finite element operational model for the storm surge prediction in Venice. *Estuarine, Coastal and Shelf Science*, 75:236–249.

Barron, C. H., Birol Kara, A., Martin, P. J., Rhodes, R. C., and Smedstad, L. F. (2006). Formulation, implementation and examination of vertical coordinate choices in the Global Navy Coastal Ocean Model (NCOM). *Ocean Modelling*, 11:347–375.

Bellafiore, D., Umgiesser, G., and Cucco, A. (2008). Modelling the water exchanges between the Venice Lagoon and the Adriatic Sea. *Ocean Dynamics*, 58:397–413.

Bergamasco, A., Carniel, S., Pastres, R., and Pecenik, G. (1998). A unified approach to the modelling of the Venice Lagoon-Adriatic Sea ecosystem. *Estuarine, Coastal and Shelf Science*, 46:483–492.

Bergamasco, A., Oguz, T., and Malanotte-Rizzoli, P. (1999). Modeling dense water formation and winter circulation in the northern and central Adriatic Sea. *Journal of Marine Systems*, 20:279–300.

Bianchi, F., Ravagnan, E., Acri, F., Bernardi-Aubry, F., Boldrin, A., Camatti, E., Cassin, D., and Turchetto, M. (2004). Variability and fluxes of hydrology, nutrients and particulate matter between the Venice Lagoon and the Adriatic Sea. Preliminary results (years 2001-2002). *Journal of Marine Systems*, 51(v-vi):49–64.

Blumberg, A. F. and Mellor, G. L. (1987). A description of a three-dimensional coastal ocean circulation model. In Heaps, N. S., editor, *Three-dimensional Coastal Ocean Models. Coastal and Estuarine Science*, volume 4, pages 1–16, Washington D.C. American Geophysical Union.

Burchard, H. (2002). *Applied Turbulence Modelling in Marine Waters.* Springer, Berlin Heildelberg.

Burchard, H. and Petersen, O. (1999). Models of turbulence in the marine environment - a comparative study of two equation turbulence models. *Journal of Marine Systems*, 21:29–53.

Castellari, S., Pinardi, N., and Leaman, K. (1998). A model study of the air-sea interactions in the Mediterranean Sea. *Journal of Marine Systems*, 18:89–114.

Cavaleri, L. and Bertotti, L. (1996). In search for the Correct Wind and Wave Fields in a Minor Basin. *Monthly Weather Review*, 125(8):1964–1975.

Cavaleri, L., Piantá, and Iuso, G. (1984). Influence of Sea Structure on the surrounding Wind Field. *Il Nuovo Cimento*, 7C(4):441–446.

Chao, S. and Boicourt, W. C. (1986). Onset of Estuarine Plumes. *Journal of Physical Oceanography*, 16:2137–2149.

Chorin, A. J. (1967). A numerical method for solving incompressible viscous flow problems. *Journal of Computational Physic*, 2:12–26.

Crise, A., Cavazzon, F., Malačić, V., and Querin, S. (2003). Circolazione Indotta dal Vento di Bora nel Golfo di Trieste: Studio Numerico in Condizioni di Stratificazione. In *La difesa idraulica del territorio 2003.*

Cucco, A. and Umgiesser, G. (2005). Modeling the tide induced water exchanges between the Venice Lagoon and the Adriatic Sea. In *Scientific*

Research and Safeguarding of Venice. Proceedings of the Annual Meeting of the CORILA Research Program, 2003 Results, volume III, pages 385–402, Venice, Italy.

Cucco, A. and Umgiesser, G. (2006). Modeling the Venice Lagoon Residence Time. *Ecological Modelling*, 193(1-2):34–51.

Cushman-Roisin, B., Korotenko, K., and Dietrich, D. E. (2005). Simulation and Charaterization of the Adriatic Sea Mesoscale Variability. *Journal of Geophysical Research - Oceans*, Special Adriatic Sea Issue.

Cushman-Roisin, B. and Naimie, C. E. (2002). A 3D-finite element model for the Adriatic tides. *Journal of Marine Systems*, 37(4):279–297.

Fairall, C., Bradley, F. F., Godfrey, J. S., Wick, G. A., and Edson, J. B. (1996). Cool-skin and warm-layer effects on sea surface temperature. *Journal of Geophysical Research - Oceans*, 101:1295–1308.

Ferla, M., Cordella, M., Michielli, L., and Rusconi, A. (2007). Long-term variation on the sea level and the tidal regime in the lagoon of Venice. *Estuarine, Coastal and Shelf Science*, 75:214–222.

Fofonoff, N. P. (1985). Physical properties of seawater: a new salinity scale and equation of state for seawater. *Journal of Geophysical Research - Oceans*, 90(C2):3332–3343.

Foreman, M. G. G. (1978). Manual for tidal currents analysis and prediction. Pacific Marine Science Report 78-6, Institute of Ocean Sciences, Patricia Bay, Sydney, British Columbia.

Foreman, M. G. G. (1996). Manual for tidal heights analysis and prediction. Pacific Marine Science Report 77-10, Institute of Ocean Sciences, Patricia Bay, Sydney, British Columbia.

Franco, P., Jeftić, L., Rizzoli, P. M., Michelato, A., and Orlić, M. (1982). Descriptive model of the Northern Adriatic. *Oceanologica Acta*, 5(3).

Friedrich, H. and Levitus, S. (1972). An approximation of the equation of state for sea water, suitable for numerical ocean models. *Journal of Physical Oceanography*, 2:514–517.

Gatto, P. (1984). Il cordone litoraneo della laguna di Venezia e le cause del suo degrado. *Istituto Veneto di Scienze, Lettere ed Arti - Rapporti e Studi*, IX:163–193.

Gačić, M., Kovačević, V., Mazzoldi, A., Paduan, J. D., Mancero Mosquera, I., Gelsi, G., and Arcari, G. (2002). Measuring Water Exchange between the Venetian Lagoon and the open sea. *Eos, Transaction, American Physical Union*, 83(20).

Gačić, M., Mancero Mosquera, I., Kovačević, V., Mazzoldi, A., Cardin, V., and Gelsi, F. (2004). Temporal variation of water flow between the Venetian lagoon and the open sea. *Journal of Marine Systems*, 51.

Goldmann, A., Rabagliati, R., and Sguazzero, P. (1975). Characteristics of the Tidal Wave in the Lagoon of Venice. Technical Report 47, IBM, Venice Scientific Center.

Haidvogel, D. B., Arango, H. G., Hedstrom, K., Beckmann, A., Malanotte Rizzoli, P., and Shchepetkin, A. F. (2000). Model Evaluation Experiments in the North Atlantic Basin: Simulations in Nonlinear Terrain-Following Coordinates. *Dynamics of Atmospheres and Oceans*, 32:239–281.

Kato, H. and Phillips, O. (1969). On the penetration of a turbulent layer into stratified fluids. *Journal of Fluid Mechanics*, 37:643–655.

Kondo, J. (1975). Air-Sea bulk transfer coefficients in diabatic conditions. *Boundary Layer Meteorol.*, 9:91–112.

Kourafalou, V. (1999). Process studies on the po river plume, north adriatic sea. *Journal of Geophysical Research*, 104(C2):29963–29985.

Kourafalou, V. (2001). River plume development in semi-enclosed Mediterranean regions: North Adriatic and Northwestern Aegean Sea. *Journal of Marine Systems*, 30:181–2005.

Kovačević, V., Gačić, M., Mosquera, I. M., Mazzoldi, A., and Marinetti, S. (2004). Hf radar observation in the northern Adriatic: surface current field in front of the Venetian Lagoon. *Journal of Marine Systems*, 51(1-4):95–122.

Luyten, P., Deleersnijder, E., Ozer, J., and Ruddick, K. (1996). Presentation of a family of turbulence closure models for stratified shallow water flows and preliminary application to the Rhine outflow region. *Continental Shelf Research*, 16(1):101–130.

Luyten, P. J., Jones, J. E., Proctor, R., Tabor, A., Tett, P., and Wild-Allen, K. (1999). COHERENS - a coupled Hydrodynamical-Ecological Model for Regional and Shealf Seas: User Documentation. Report, MUMM.

Malanotte Rizzoli, P. and Bergamasco, A. (1983). The Dynamics of the coastal region of the Northern Adriatic Sea. *Americal Meteorological Society*, 13:1105–1130.

Malačić, V., Viezzoli, D., and Cushman-Roisin, B. (2000). Tidal dynamics in the northern Adriatic Sea. *Journal of Geophysical Research - Oceans*, 105(C11):26,265–26,280.

Mancero Mosquera, I., Gačić, M., Kovačević, V., Mazzoldi, A., Paduan, J. D., and Yari, S. (2007). Surface current patterns in front of the Venetian lagoon and their variability at different wind regimes. In *Scientific Research and Safeguarding of Venice - CORILA Research Programme 2004-2006*, volume VI, pages 441–451, Venice, Italy.

Marinov, D., Norro, A., and Zaldivar, J. M. (2006). Application of COHERENS model for hydrodynamic investigation of Sacca di Goro coastal lagoon (Italian Adriatic Sea). *Ecological Modelling*, 193:52–68.

Marshall, J., Adcroft, A., Hill, C., L., P., and Heisey, C. (1997). A finite-volume, incompressible Navier Stokes model for studies of the ocean on parallel computers. *Journal of Geophysical Research - Oceans*, 102(C3):5753–5766.

Melaku Canu, D., Umgiesser, G., and Solidoro, C. (2001). Short term simulations under winter conditions in the lagoon of Venice: a contribution to the environmental impact assessment of a temporary closure of the inlets. *Ecological Modelling*, 138(1–3):215–230.

Mellor, G. L. (1991). An equation of state for numerical models of ocean and estuaries. *J. Atmos. Oceanic Technol.*, 8:609–611.

Mellor, G. L. and Yamada, T. (1974). A hierarchy of turbulence closure models for planetary boundary layers. *Journal of Atmospheric Science*, 31:1791–1806.

Mellor, G. L. and Yamada, T. (1982). Development of a tubulence closure model for geophysical fluid problems. *Reviews of Geophysics and Space Physics*, 20(4):851–875.

Mosetti, F. (1987). Distribuzione delle maree nei mari italiani. *Bollettino di Oceanologia Teorica ed Applicata*, 5(1):65–72.

Oddo, P. and Pinardi, N. (2008). Lateral open boundary conditions for nested limited area models: A scale selective approach. *Ocean Modelling*, 20:134–156.

Oddo, P., Pinardi, N., and Zavatarelli, M. (2005). A numerical study of the interannual variability of the Adriatic Sea. *Science of the Total Environment*, 353:39–56.

Orlić, M., Gačić, M., and Violette, P. E. L. (1992). The currents and circulation of the Adriatic Sea. *Oceanologica Acta*, 15:109–124.

Paduan, J. D., Gačić, M., Kovačević, V., Mosquera, I. M., and Mazzoldi, A. (2003). Vorticity Pattern Offshore of the Venetian Lagoon from HF Radar Observations. In *Scientific Research and Safeguarding of Venice - CORILA Research Programme 2001-2003*, volume II, pages 361–372, Venice, Italy.

Pasarić, M. and Orlić, M. (2001). Long-term meteorological preconditioning of the North Adriatic coastal floods. *Continental Shelf Research*, 21:263–278.

Pinardi, N., Allen, I., Demirov, E., Mey, P. D., Korres, G., Traon, P. L., Maillard, C., Manzella, G., and Tziavos, C. (2003). The mediterranean ocean forecasting system: first phase of the implementation (1998-2001). *Annales Geophysicae*, 21:1–18.

Pirazzoli, P. and Tomasin, A. (2002). Wind and atmospheric pressure in Venice in the 20th century: a comparative analysis of measurements from the meteorological stations of the Seminario Patriarcale (1900-1955) and the Istituto Cavanis (1959-2000). *Atti dell'Istituto Veneto di Scienze, Lettere ed Arti*, CLX.

Polli, S. (1960). La propagazione delle maree nellÁlto adriatico. *Publications of the Istituto Sperimentale Talassografico - Trieste*, 370.

Polli, S. (1961). La propagazione delle maree nel golfo di Venezia. *Publications of the Istituto Sperimentale Talassografico - Trieste*, 385.

Pullen, J., Doyle, J. D., Hodur, R., Ogston, A., and Book, J. W. (2003). Coupled ocean-atmosphere and nested modeling of the Adriatic Sea during winter and spring 2001. *Journal of Geophysical Research - Oceans*, 108(C1,3320).

Raicich, F. (1994). Note on the flow rates of the Adriatic rivers. Technical Report RF 02, Istituto Sperimentale Talassografico-CNR, Trieste, Italy.

Rasmussen, E. B. (1993). *Three-dimensional hydrodynamic models*, pages 1295–1308. Chapman and Hall, London.

Rochford, P. A. and Martin, P. J. (2001). Boundary conditions in the Navy Coastal Ocean Model. Report nrl/fr/7330-01-9992, Nav. Res. Lab, Stennis Space Cent., Miss.

Rodi, W. (1987). Examples of calculation methods for flow and mixing in stratified fluids. *Journal of Geophysical Research (C5)*, 92:5305–5328.

Sannino, G. M., Barbagli, A., and Artale, V. (2002). Numerical Modeling of the mean exchange through the Strait of Gibiltar. *Journal of Geophysical Research - Oceans*, 107(Ant 3094).

Sciarra, R., Bignami, F., Santoleri, R., and Carniel, S. (2006). The variability of the Adriatic Sea Case 2 waters from SeaWiFS imagery. *submitted to Journal of Geophysical Research - Oceans [In Press]*.

Sherwood, C. R., Carnie, S., Cavaleri, L., Chiggiato, J., Das, H., Doyle, J. D., Harris, C. K., Niedoroda, A. W., Pullen, J., Reed, C. W., Russo, A., Sclavo, M., Signell, R. P., Traykowski, P., and Warner, J. C. (2004). Sediment Dynamics in the Adriatic Sea Investigated with Coupled Models. *Oceanography*, 17(4):58–69.

Signell, R. P., Carniel, S., Cavaleri, L., Chiggiato, J., Doyle, J. D., Pullen, J., and Sclavo, M. (2005). Assessment of wind quality for oceanographic modelling in semi-enclosed basins. *Journal of Marine Systems*, 53:217–233.

Smolarkiewicz, P. K. (1984). A fully multidimensional positive definite sdvection transport algorithm with small implicit diffusion. *Journal of Computational Physics*, 54:325–362.

Smolarkiewicz, P. K. and Clark, T. L. (1986). The multidimensional positive definite sdvection transport algorithm: further development and applications. *Journal of Computational Physics*, 67:396–438.

Tomasin, A. (2005). The software Polifemo for tidal analysis. Technical Note 202, ISMAR-CNR Institute of Marine Science Venice.

Tomasin, A. and Pirazzoli, P. A. (1999). The Seiches in the Adriatic Sea. *Atti dell'Istituto Veneto di Scienze, Lettere ed Arti*, CLVII:299–316.

Umgiesser, G. (2000). Modeling residual currents in the Venice Lagoon. In *Interaction between Estuaries, Coastal Seas and Shealf Seas*, pages 107–124. Terra Scientific Publishing Company (TERRAPUB), Tokyo.

Umgiesser, G. and Bergamasco, A. (1993). A staggered grid finite element model of the Venice Lagoon. In K. Morgan, E. Ofiate, J. P. and Zienkiewicz, O., editors, *Finite Elements in Fluids*, pages 659–668. Pineridge Press.

Umgiesser, G. and Bergamasco, A. (1995). Outline of a primitive equation finite element model. In *Rapporto e Studi*, volume XII, pages 291–320. Istituto Veneto di Scienze, Lettere ed Arti, Venice, Italy.

Umgiesser, G. and Bergamasco, A. (1998). The spreading of the Po plume and the Italian coastal current. In *Physics of Estuaries and Coastal Seas*, pages 267–275. Dronkers and Scheffers (eds), Rotterdam.

Umgiesser, G., Melaku Canu, D., Cucco, A., and Solidoro, C. (2004). A finite element model for the Venice Lagoon. Development, set-up, calibration and validation. *Journal of Marine Systems*, 51:123–145.

Vested, H. J., Berg, P., and Uhrenholdt, T. (1998). Dense water formation in the Northern Adriatic. *Journal of Marine Systems*, 18:135–160.

Williams, R. T. (1981). On the Formulation of Finite-Element Prediction Models. *Monthly Weather Review*, 109:463.

Zampato, L., Canestrelli, P., A.Tomasin, and Zecchetto, S. (2005). A comparison between modelled and observed atmospheric fields over the Adriatic and Tyrrhenian seas. Technical Report 263, ISMAR-CNR, Venezia, Italy.

Zampato, L., Umgiesser, G., and Zecchetto, S. (2007). Sea level forecasting in Venice through high resolution meteorological fields. *Estuarine, Coastal and Shelf Science*, 75:223–235.

Zavatarelli, M. and Pinardi, N. (2003). The Adriatic Sea modelling system: a nested approach. *Annales Geophysicae*, 21:345–364.

Zavatarelli, M., Pinardi, N., Kourafalou, V. H., and Maggiore, A. (2002). Diagnostic and prognostic model studies of the Adriatic Sea general circulation: Seasonal variability. *Journal of Geophysical Research - Oceans*, 107(C1,3004).